



**REanalysis of the TROpospheric chemical composition over the past 40 years
A long-term modelling study of tropospheric chemistry**

**Funded under the 5th EU framework programme
EU-contract EVK2_CT-2002-00170**

Report on the reanalysis simulations

Deliverable D4.4

**S. Szopa ¹, M.G. Schultz ^{2,3}, D. A. Hauglustaine ¹, S. Dalsøren ⁴, T. van Noije ⁵, S. Rast ²,
and N.H. Savage ⁶**

- 1. Laboratoire des Sciences du Climat et de l'Environnement, Gif-sur-Yvette, France**
- 2. Max-Planck-Institute for Meteorology, Hamburg, Germany**
- 3. now at ICG-2, Forschungszentrum Jülich, Jülich, Germany**
- 4. Institute of Geophysics, University of Oslo, Norway**
- 5. Koninklijk Nederlands Meteorologisch Instituut KNMI, The Netherlands**
- 6. Department of chemistry, University of Cambridge, UK**

Table of Contents

1. Introduction	4
2. Participating models	4
3. Input data sets	7
3.1 Meteorological data	7
3.2 Emissions	8
3.2.1 Natural emissions	9
3.2.2 Biomass burning emissions	11
3.2.3 Anthropogenic emissions	12
3.3 Stratospheric boundary conditions	14
3.3.1 Finrose fields produced for RETRO	14
3.3.2 Stratospheric boundary conditions in the tropospheric models	16
4. Analysis of the long-term simulations (ERA-40)	17
4.1 Intercomparison of geographical distributions and vertical cross sections of ozone and precursor concentrations	17
4.1.1 Ozone	17
4.1.2 Carbon Monoxide	19
4.1.3 Hydroxyl radical	20
4.2 Analysis of long-term trends and variability	24
4.2.1 Trend analysis of the LMDz-INCA model	24
4.2.2 ECHAM5-MOZ comparison with MOZAIC data	29
4.2.3 Analysis of surface CO anomalies	31
4.2.4 Synthesis of simulated trends and analysis of inter-model differences	33
5. Conclusions	45
References	47
Annex: Additional analyses performed with earlier model simulations	50
A1. Intercomparison of seasonal signals	50
A2. Comparison with O ₃ ground based measurements	53
A3. Comparison with O ₃ sondes	56
A4. Comparison with CO measurements	56
A5. Comparison with satellite data	57
A6. Budgets and Lifetimes	63

1. Introduction

The RETRO project exploits and synthesizes a wide range of available, but under-utilised, measurements of tropospheric composition using state-of-the-art modelling tools that are available within Europe. In this project, the first comprehensive global long-term tropospheric chemistry integrations covering a time period of 4 decades was performed in order to both reproduce and understand the trends and variability of the tropospheric chemical composition. These simulations were made possible by the availability of the consistent meteorological reanalysis dataset, covering the last 40 years, produced at the European Centre for Medium Range Weather Forecast (ERA-40, ECMWF). This use of the ERA-40 represents the first major exploitation of that data set for atmospheric composition studies and constitutes thus a significant European contribution to investigations of global change.

Work package 4 covers the actual reanalysis of the tropospheric chemical composition over the last 40 years. The five state-of-the-art global models participating in the RETRO project are briefly described in section 2. Three of these models have run the complete 41-year simulations. This study required substantial efforts to prepare the necessary data sets and to run the models for such a long period. In particular, all models used the same emissions of ozone precursors (briefly described in section 3.1; see deliverable D1-6 for details), meteorological input from ERA-40 (described in section 3.2) and stratospheric boundary conditions (section 3.3). In this document, we provide a technical description of the boundary conditions used to perform the simulations.

The long-term model runs were performed chronologically in order to ensure consistency of the results. After completion of the 40-year runs, the model results were processed and archived on the RETRO ftp server ftp://ftp.retro.enes.org/pub/model_results, where they are available for use by the scientific community, by interested stakeholders or by the public. The analysis in these terms for key constituents of the troposphere were performed and evaluated through comparison with data collected under Work Package 2. These results are presented in section 4. There are fewer comparisons with observational data in this report than originally foreseen, because of some errors discovered in the results of all models after the first reanalysis runs. This led to the decision to rerun the long-term simulations, an undertaking which occurred between October 2006 and February 2007. At the time when these simulations were finished, several of the people who had worked on the project were no longer available for additional RETRO work. Therefore, some of the analyses which had been done with the first set of simulations could not be repeated. The results shown in this report are exclusively from the second set of simulations. Additional analyses performed for the first set of model runs are described in the Annex.

2. Participating models

Five state-of-the-art global models were used in the framework of RETRO. Three of these models are off-line Chemistry-Transport-Models (CTMs). They read the needed meteorological fields directly from input files and interpolate these fields onto the model time step. These models are **CTM2** from UiO, **TM4** from KNMI and **pTOMCAT** from UCamb. The two other models are General Circulation Models (GCMs) coupled on-line to chemistry and aerosol models **ECHAM5-MOZ** (aka **MOZECH**) from MPG-IMET and **LMDz-INCA** from LSCE. Table 1 summarizes the general features of these models. The three models which were used for the simulations covering the full ERA40 period are TM4, ECHAM5-MOZ and LMDz-INCA.

The models have horizontal resolutions of 1.8° - 3.75° in longitude and 1.8° - 2.8° in latitude. They include 19-60 vertical levels. The chemical schemes range from simple methane oxidation schemes to full NMHC chemistry. Two of the models also include a full suite of aerosols but this configuration was not used in these simulations due to lack of emission data sets consistent with the gas-phase emissions generated in the project. The total number of tracers range from 27 up to 86. Most of the models have participated in model inter-comparison exercises and evaluation against measurements in the framework of the POET and TRADE-OFF European projects. All five models also ran simulations in the international ACCENT/IPCC Photocomp 2030 intercomparison study (see Dentener et al., 2006; Stevenson et al., 2006; Shindell et al., 2006; van Noije et al., 2006).

One reanalysis simulation covering the period from 1958 to 2000 required a total of 120-480 CPU-days per model for the CTMs or 80-500 CPU-days for each GCM. The amount of file output generated varies from 1680 to 3160 GB per model. These huge amounts of disk space requirements led to the decision to only make monthly mean data available on the RETRO ftp server. More detailed output (3-hourly to daily and including additional fields) can be requested from the authors of this report.

Table 1: Participating models general features

	ECHAM5-MOZ (MOZECH)	LMDz-INCA	TM4	p-TOMCAT	CTM2
Participants	MPG-IMET S. Rast M. Schultz	LSCE S. Szopa D. Hauglustaine	KNMI T. van Noije P. van Velthoven	UCamb N. Savage J. Pyle	UiO S. Dalsoren, J. Sundet, I.S.A. Isaksen
Resolution	2.8x2.8 L31 (up to 10 hPa)	3.75x2.5 L19 (up to 3hPa)	3.0x2.0 L25 (up to 0.48hPa)	2.8x2.8 L31 (up to 10 hPa)	2.8x2.8 L60 (up to 10 hPa)
Total number of species (number of advected tracers)	65 (63)	75 (73) or 89 (87)	37 (22)	60 (42)	61 (51)4
Chemical scheme (number of reactions)	NMHC (135)	NMHC (332)	NMHC (95) Sulphur aerosols	NMHC (131)	NMHC (140) Aerosols
Advection	Lin+Rood 1996	Van-Leer 1977	Russel and Lerner 1981	Prather 1986	Prather 1986
Convection	Tiedtke 1989/Nordeng	Tiedtke 1989	Tiedtke 1989	Tiedtke 1989	Tiedtke 1989
Boundary Layer	1994 Monin Obukhov	LMDz	Holtslag+Boville	Holtslag+Boville	Holtslag
Wallclock time for 1 year simulation	22 h	50h	22h	24h	200 h
Biogenic emissions including NOx	Interactive MEGAN model by Guenther et al. [2006]	ORCHIDEE climatology [Lathiere et al., 2005]	ORCHIDEE climatology [Lathiere et al., 2005]	ORCHIDEE data for 1997 [Lathiere et al., 2005]	POET
Lightning emissions	Interactive [Grewe et al., 2000]	Interactive	Interactive [Meijer et al., 2001]; scaled to 5 Tg N/yr for 1997 (ERA-40)	Interactive	Interactive
Height distribution of biomass burning emissions	Altitude profiles without segregation of vegetation types	no	Altitude profiles with segregation into 3 vegetation types	no	Altitude profiles with segregation into 3 vegetation types
Ocean CO and other VOC emissions	POET (CO, C2H6, C3H8, higher alkanes, C2H4, C3H6)	Erickson and, Taylor (GRL 1992) rescaled such asr CO: 20.0, Isoprene: 0.88, C2H4: 0.688, C3H6: 0., C2H2: 0.20, alkenes: 0.27, CH3COCH3: 12.41Tg.yr-1	POET (CO and CBM-4 categories from C2H6, C3H8, C2H4, C3H6)	POET (CO, C2H6, C3H8)	POET (CO, C2H6, C3H8, higher alkanes, C2H4, C3H6)
Aircraft NOx emissions	Grewe [2003]	Annual total from Grewe [2003] distributed according to ANCAT	Grewe [2003]	Grewe [2003]	Grewe [2003] ?
Stratospheric ozone	Relaxed to stratospheric O ₃ , NO _x , and HNO ₃ down to 200 hPa in extra-tropics and 100 hPa in tropics (10 day time constant)	Stratospheric O ₃ nudged toward climatology above 380K	O ₃ nudged toward climatology above 123 hPa: except 30N–30S, above 60 hPa	O ₃ fixed above 10 hPa based on 2D model	O ₃ , HNO ₃ and NO _x from OsloCTM2 model run with stratospheric chemistry
Key references	<i>Rast et al., in preparation ; Röckner et al. [2003]; Horowitz et al. [2003]</i>	<i>Hauglustaine et al. [2004] Folberth et al. [2006]</i>	<i>van Noije et al. [2004, 2006]</i>	<i>Law et al. [1998] Stockwell et al. [1999]</i>	<i>Sundet [1997]</i>

3. Input data sets

All boundary condition files that were shared between the models were provided in the netcdf data format (see <http://www.unidata.ucar.edu/netcdf>). The meteorological ERA-40 data were processed individually by each model, because the models made use of different meteorological fields (see section 3.1).

3.1 Meteorological data

The fourty years of gridded meteorological data from the ERA-40 reanalysis of the *European Centre for Medium Range Weather Forecast* (ECMWF) needed to perform the comprehensive atmospheric GCM/CTM simulations of this project constitutes a huge amount of data. Each of the models participating in the RETRO project required a different subset of the dataset and uses a different interface for input of these data. Therefore also the file formats of the input data differed. These considerations led to the decision to have each modelling group process the ERA-40 data individually. This was possible, because all groups had access to the ECMWF computer systems with the MARS archive. The data were retrieved in 6-hourly time resolution. Some models retrieved analyzed fields while others used forecast fields. Also, some models retrieved the data in finer resolution than the set-up of their own model necessitates and interpolated the data onto the model grid. Table 3 provides a list of the meteorological variables used by each of the five RETRO models.

Table 3: Meteorological variables of ERA-40 used in the various RETRO models

	ECHAM5- MOZ	LMDz-INCA	TM4	Oslo- CTM2	pTOMCAT
Temperature	X		X	X	X
Specific humidity			X	X	X
Geopotential height			X		
Wind vector (u, v)		X			
Wind divergence	X			X	X
Potential vorticity	X				X
Horizontal mass flux			X		
Convective mass flux			X	X	
Vertical diffusion			X		
LWC			X	X	
IWC			X	X	
Cloud fraction			X	X	
Cloud levels			X	X	
Large-scale precipitation			X	X	
Convective precipitation			X	X	
Aerodynamical resistance			X		
Friction velocity			X		
Temperature 2m			X		
Wind speed 10m					
Surface roughness			X		
Surface pressure			X		X
Sea surface temperature	X	X			
Sea ice cover	X				

During the first year of the project it was discovered that the ERA-40 data set suffered from a couple of inconsistencies in the data assimilation. These resulted in a number of step changes in some meteorological variables when new observational parameters had been introduced in

the ECMWF data assimilation system (in particular TRMM rainfall data). As a consequence, the ERA-40 circulation exhibits too strong meridional overturning and excessive tropical precipitation over the oceans. As we shall see in the discussion of the results, these ERA-40 features make it difficult to reliably distinguish between natural variability and assimilation artefacts. Two examples of this are the time series of natural biogenic VOC emissions and lightning NO_x emissions presented in figures 2 and 3 of the next section. Biogenic VOC emissions are controlled by surface temperature variations and lightning NO_x is determined by convective activity.

3.2 Emissions

Emissions of ozone precursor gases (fossil fuel and industry, biogenic, biomass burning) for the simulated 40-year period were provided directly from workpackage 1 to the participating models. These emissions and their preparation are described in detail in the RETRO report on emissions D1-6 and only a brief summary will be provided here.

The emissions prepared and/or provided in the framework of RETRO have a common horizontal grid of 0.5°x0.5°. The temporal resolution of the data files is monthly. These emissions are then combined and interpolated on the model grid by each modelling team. In particular, each modelling team had to apply their own lumping procedure to combine individual VOC compounds into VOC classes contained in the respective chemical scheme.

As an example for the global distribution of RETRO emissions, figure 1 displays the annual surface emissions of NO_x and CO for the years 1970 and 2000.

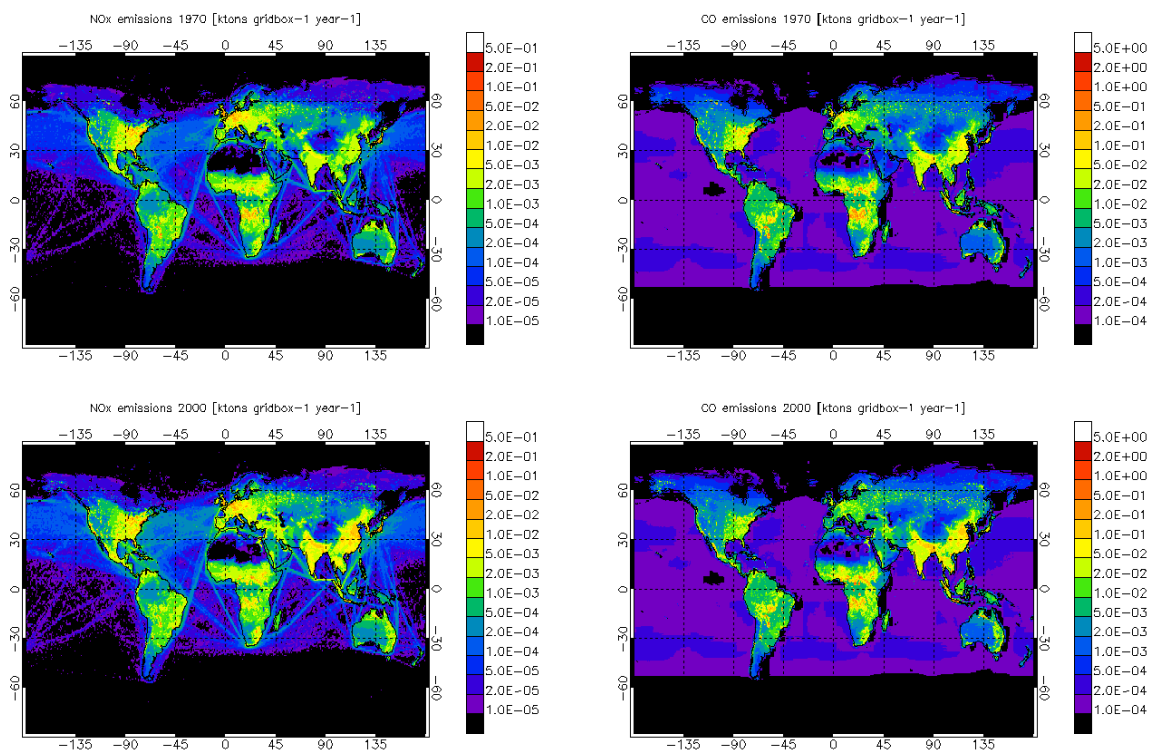


Figure 1: Spatial distribution of NO_x (left) and CO (right) emissions from the RETRO inventory for the years 1970 (top) and 2000 (bottom). These figures contain all RETRO surface emissions (including wild fires and natural sources, but without aircraft and lightning NO_x emissions)

3.2.1 Natural emissions

a. Biogenic emissions

The current state-of-the-art for modelling emissions of isoprene, terpenes, and other volatile organic compounds (VOCs) from terrestrial vegetation is the MEGAN parameterization of *Guenther et al.* [2006]. The release of these compounds is very much species dependent and mainly controlled by the living biomass density, the leaf temperature, and the photosynthetically active radiation (PAR). Isoprene and monoterpene emissions from vegetation are not prescribed for the RETRO project but were left at the individual modeller's discretion. While most models used a prescribed climatology of biogenic emissions, ECHAM5-MOZ computed the biogenic VOC emissions interactively (see Table 1). Biogenic CO and NO_x emissions were prescribed, however. The resulting interannual variability of natural isoprene and monoterpene emissions from ECHAM5-MOZ is shown in Figure 2.

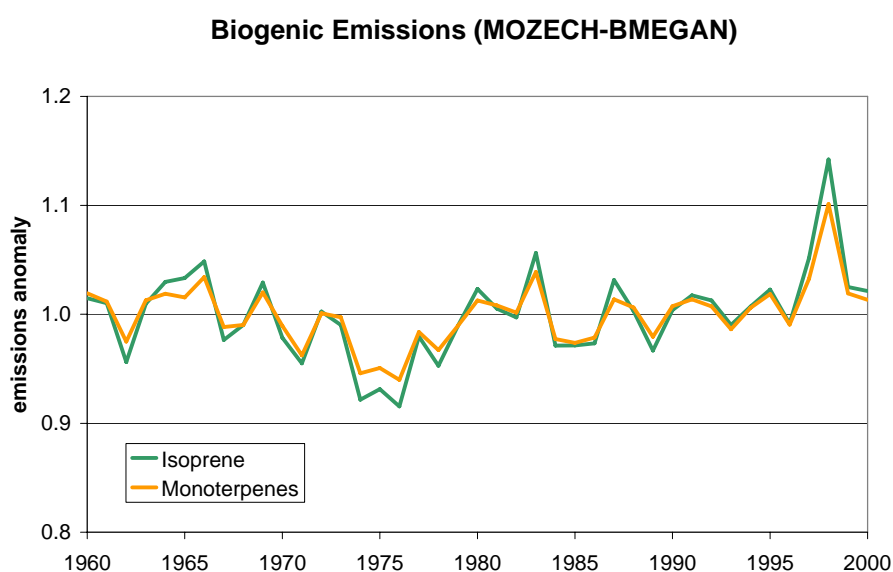


Figure 2: Changes in global annual mean emissions of isoprene and monoterpenes relative to the year 1990 from the ECHAM5-MOZ model using the interactive MEGAN parameterisation of *Guenther et al.*, 2006

For the year 2000, ECHAM5-MOZ calculated global isoprene emissions of 551 Tg and global terpene emissions of 197 Tg. In comparison the data set of *Lathiere et al.*, 2006 (used by LMDz-INCA and TM4) yielded 460 Tg isoprene and 117 Tg terpenes.

b. Lightning emissions

The production of NO from lightning flashes is still a major uncertainty in the global budget of nitrogen oxides in the atmosphere. The models participating in the RETRO simulations used different parameterisations to estimate the lightning flashes based on the occurrence of convection in the model. LMDz-INCA, pTOMCAT and CTM2 used the parameterisation of *Price and Rind* [1992] which is based on convective cloud top heights. TM4 used a scheme based on convective precipitation rates [*Meijer et al.*, 2003] and ECHAM5-MOZ employs a scheme which combines cloud top heights with convective updraught fluxes [*Grewe et al.*, 2001]. The resulting flash densities were converted into NO_x emissions so that between 3 and 5 TgN were produced per year. The scaling factor was kept constant throughout the

simulations. Figure 3 displays the resulting annual NO_x emissions from lightning for the three models running the reanalysis simulations.

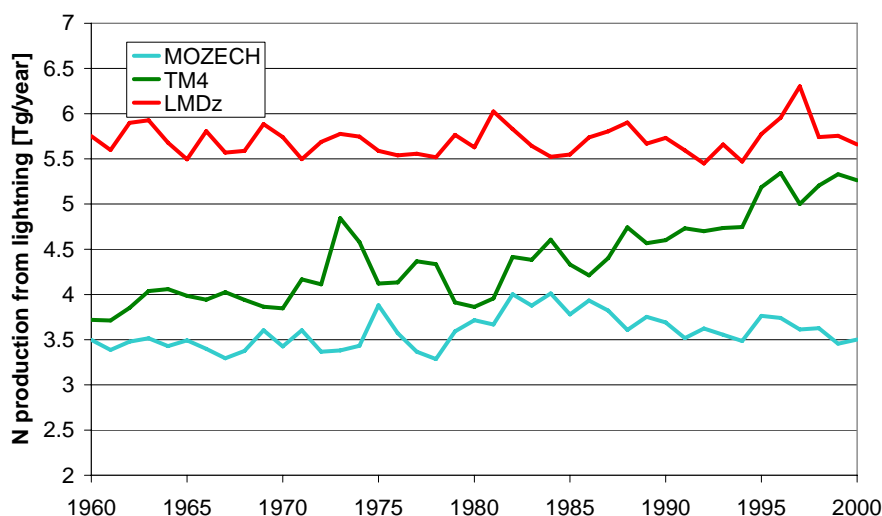


Figure 3: Time series of annual mean NO_x emissions from lightning from the RETRO reanalysis simulations

c. Methane boundary conditions

Within RETRO no explicit study of the global methane budget was made. Reconstructions of CH₄ concentrations over the considered period have been used to constrain the surface concentrations of this gas in the GCMs and for the radiative forcing calculations. Hence, interpolated CMDL measurements of near-surface concentrations are used in the models as boundary conditions. These interpolations, done by MPG-IMET were provided from 1800-2100 (see Figure 4). They were built by computing a global mean trend in three sections: 1800-1970 (using an exponential fit); 1970-1998 (using a 2 order polynomial fit); 1998-2100 (using a linear trend with 5 ppb/year increase). Secondly, the annual mean normalized latitudinal gradient derived from data for 1984-2001 was applied and then, for each latitude, the normalized seasonal cycle derived from the same data was applied. Data for 1800 and 1900 were taken from the IPCC TAR. In LMDz-INCA and ECHAM5-MOZ, a relaxation approach is applied which combines the use of an emissions inventory with the zonal mean surface concentrations. This approach avoids undesired biases in the methane concentration while it accounts for regional differences in boundary layer methane concentrations.

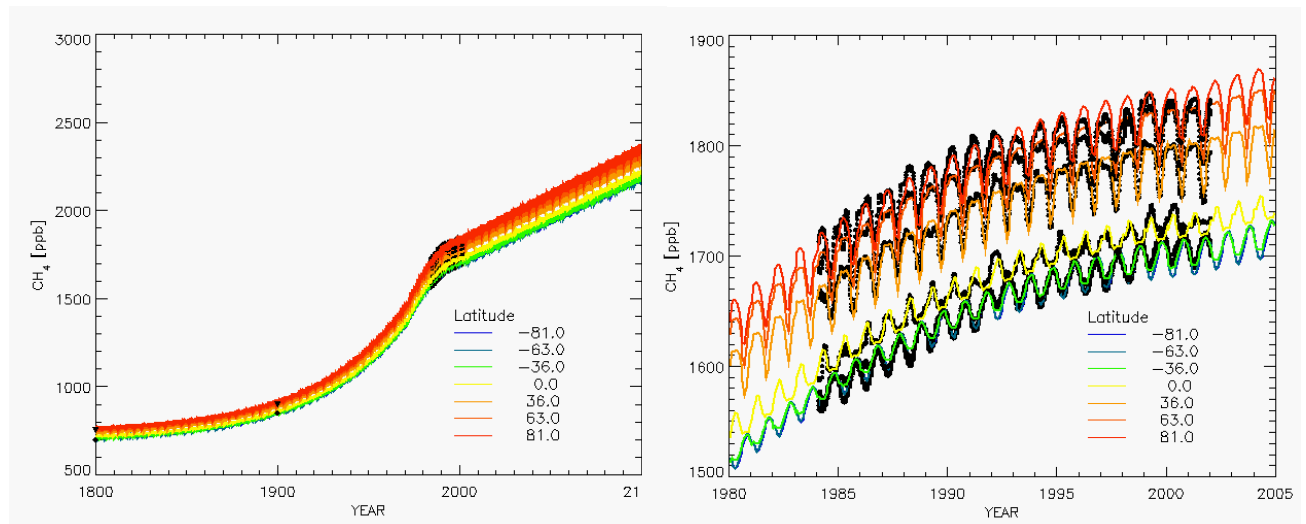


Figure 4: Evolution of latitudinal trends of methane used to constrain the models as boundary conditions

d. Oceanic emissions

While oceanic emissions are generally small compared to present-day terrestrial sources, they may have a sizeable impact on the global budgets of a number of ozone and aerosol precursors, such as DMS, C₂H₄, C₃H₆, acetone, halogens, and possibly CO and H₂. Given the scarcity of new data sets available to improve the knowledge about these processes, no new inventory was provided within RETRO. Most of the models used the POET fluxes for this source except the LMDz-INCA model which was forced with the distribution of Erickson and Taylor 1992 whereas the total fluxes are from Bates et al.

3.2.2 Biomass burning emissions

Fires represent a very important source of trace gases in many world regions and they often control the interannual variability of emissions. The RETRO inventory of open vegetation fires is described in detail in a manuscript under review at Global Biogeochemical Cycles (Schultz et al., 2007) which is reproduced as Annex in deliverable D1-6. The inventory is based on a composite approach using information from many different reports and journal articles together with satellite information on burned areas and active fires and a predictive model for fire occurrence and fire spread. Figure 5 shows the temporal evolution and interannual variability of the RETRO fire emissions segregated by region. Many exceptional large fire events are captured by this inventory, but it must be stated that the uncertainties remain large and some speculation remains in particular for early years.

The RETRO fire inventory has been thoroughly compared with other available emission inventories and was found to agree well with the version 2 of the Global Fire Emissions Database (GFED) [van der Werf et al., 2006]. Future modelling studies which aim to extend the RETRO simulations into more recent years could therefore use a combination of RETRO data and GFED2 data without introducing a strong artificial variability signal.

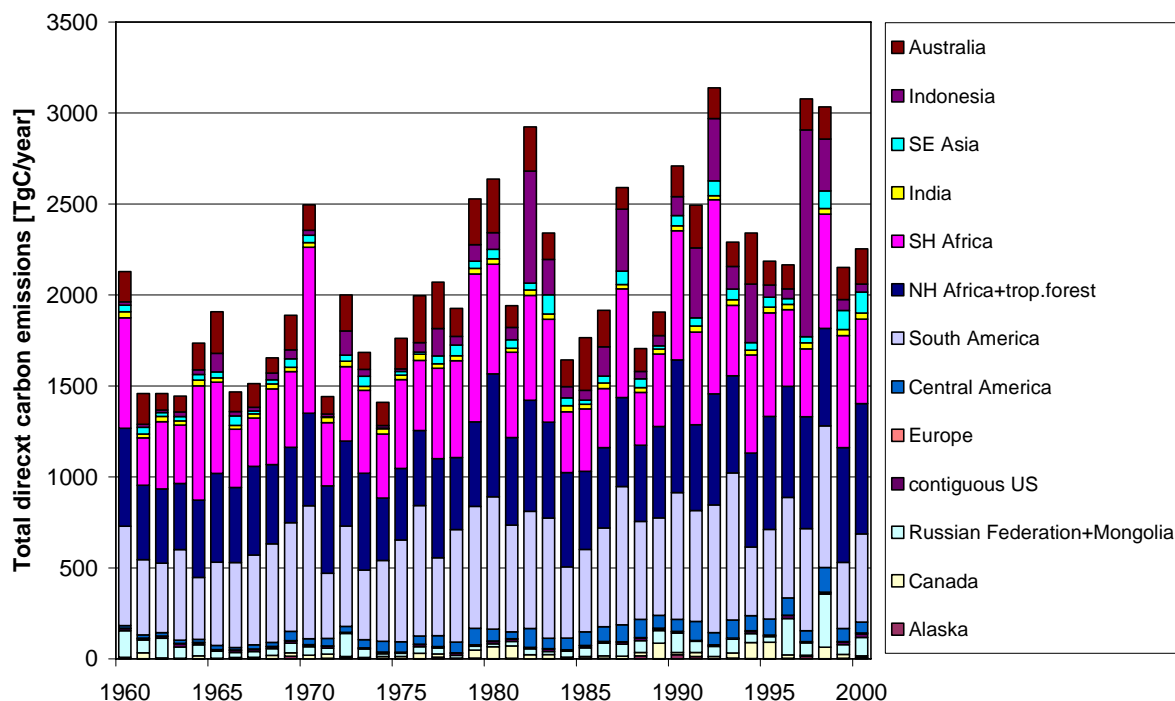


Figure 5: Estimated total direct carbon emissions from wildland fires (i.e. excluding carbon release after degradation of remaining organic matter) for the 40-year period of RETRO.

3.2.3 Anthropogenic emissions

The emission datasets and the methods used to produce them are fully described in the D1-6 report. This section summarizes the main features of these datasets.

As of yet, no formal uncertainty estimates have been performed, but we believe that the emissions provided are correct within 30% globally (regional deviations may be substantially larger).

a. Anthropogenic activities (except shipping and aircraft)

The RETRO activities with respect to fossil fuel emissions were provided by the TEAM model (TNO Emission Assessment Model, see http://www.air.sk/tno/retro_pictures/index.php). The TEAM model is a tool to generate anthropogenic emission data from various pollutants considering: (i) the type of activity, (ii) the period of emission, (iii) the technology applied.

Ten different sectors according to the LOTOS groups (see Table 2) are considered. The data contain emissions from structural activities (incidental emissions from e.g. volcanoes, disasters, military actions or huge vegetation fires are not included).

The data sets are provided as annual netcdf files with monthly mean emissions. RETRO concentrated on the production of emissions data for NO_x, CO and 25 volatile organic compounds or compound classes (alcohols, ethane, propane, butanes, pentanes, hexanes & higher alkanes, ethene, propene, ethyne, isoprene, monoterpenes, other alk(adi)enes & alkynes, benzene, toluene, xylene, trimethylbenzenes, other aromatics, esters, ethers, methanal, other alkanals, ketones, acids, and others). Figure 6 shows the NO_x emissions as a function of time for OECD (Organisation for Economic Co-operation and Development) member countries over the last four decades. Due to inconsistencies in the reported activity

data of several countries, a smoothing procedure had to be applied regionally, so that a homogeneous time series could be created (see deliverable D1-6 for details).

Table 2: Description of the emission sectors used for the anthropogenic emissions in RETRO (LOTOS sector definitions)

Lotus Group Number	Lotus Group Description
1	Power generation
2	Residential, commercial and other combustion
3	Industrial combustion
4	Industrial processes
5	Extraction distribution of fossil fuels
6	Solvent use
7	Road transport
8	Other mobile sources
9	Waste treatment and disposal
10	Agriculture and Landuse change

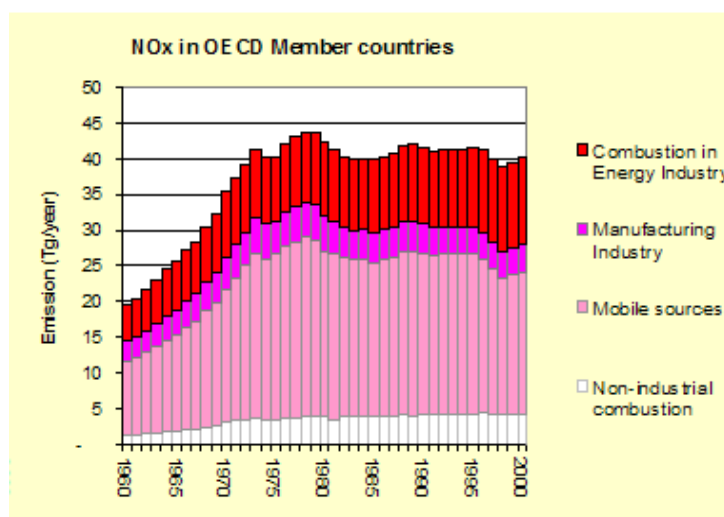


Figure 6: Evolution of the NOx emissions in OECD member countries

b. Aircraft emissions

Aircraft emissions were provided by V. Grewe from the ANCAT 2001 study on a monthly basis from 1960 to 2030 with a resolution of $3.75^{\circ} \times 3.75^{\circ}$ for 7 altitude levels and the gridded emissions were merged into one single file for each compound and year. LMDz-INCA used a different emissions data set from the TRADEOFF project and scaled the annual total to the emissions from the RETRO data set to account for the long-term trend.

c. Ship emissions

For international shipping, the data were made available by the University of Oslo group. The original data set (VERITAS inventory of international ship traffic emissions) was compiled for the year 2001 and is described in Endresen et al., 2003. This data set was scaled with a globally uniform scaling factor derived from bunker fuel sales statistics in order to estimate the historic trends. We realize that this method is rather crude and may not reflect important changes in emission factors over time, but at present there is no other information available to

obtain reliable, regionally aggregated ship emission trends. The international shipping emissions do not have a seasonal variation, but they are provided here as monthly mean data in order to facilitate handling.

The VOC split of ship emissions was done according to Endresen et al., 2003.

3.3 Stratospheric boundary conditions

At the time when the RETRO project began, there was no model available to satisfactorily simulate chemistry and transport in both the troposphere and the stratosphere within one consistent framework and for the long term integrations envisaged within RETRO. Therefore, the tropospheric GCMs and CTMs employed in this project needed to be supplied with stratospheric ozone column data and lower stratospheric ozone and nitrogen oxide (NO_y) concentrations in order to reproduce changes in the penetration of UV radiation into the troposphere and in the stratosphere-troposphere exchange of ozone and NO_y. In order to define the stratospheric boundary conditions for the tropospheric models, a 41-year simulation driven by ERA-40 data was performed with the FinROSE model of FMI. The resulting lower stratospheric ozone concentrations and total ozone columns were archived on the RETRO ftp server and evaluated with some ozone sonde data.

3.3.1 Finrose fields produced for RETRO

A stratospheric simulation covering the complete ERA-40 time period from September 1957 to August 2002 was done with the FinROSE chemistry-transport model (Damski 2005) using the 6 hourly analysis data. The simulations were run by the FMI with a horizontal grid resolution of 10x5 deg (long-lat) at 24 levels up to 0.1 hPa (ca. 65km). The ozone data set contains ozone mixing ratio as 3D monthly mean fields produced from daily average model output together with the surface pressure.

The FinROSE-CTM is based on the NCAR Rose model (e.g. Brasseur et al., 1997). The FinROSE-CTM is a 3D grid point model using a flux-form semi-Lagrange transport scheme (Lin and Rood, 1996). The model features detailed middle atmospheric chemistry together with a detailed parameterisation for heterogeneous processing on/in liquid binary aerosols and PSCs, including PSC sedimentation and a NAT-rock parameterisation. The chemistry scheme includes 27 long-lived species/families, and 14 species in photochemical equilibrium with about 120 gas-phase reactions, 10 heterogeneous reactions and 37 photodissociation processes. The rate constants used for the chemical kinetics are according to the recommendations given in JPL 2000/2002 (Sander et al. 2002). Photolysis rates are derived from a look-up table depending on solar zenith angle, ozone column and altitude. The look-up tables have been compiled using PHODIS-radiative transfer model (e.g. Kylling et al 1997). The chemical rate equations are solved by considering a chemical equilibrium state for short-lived species and a semi-implicit scheme is used for the integration of the long-lived species.

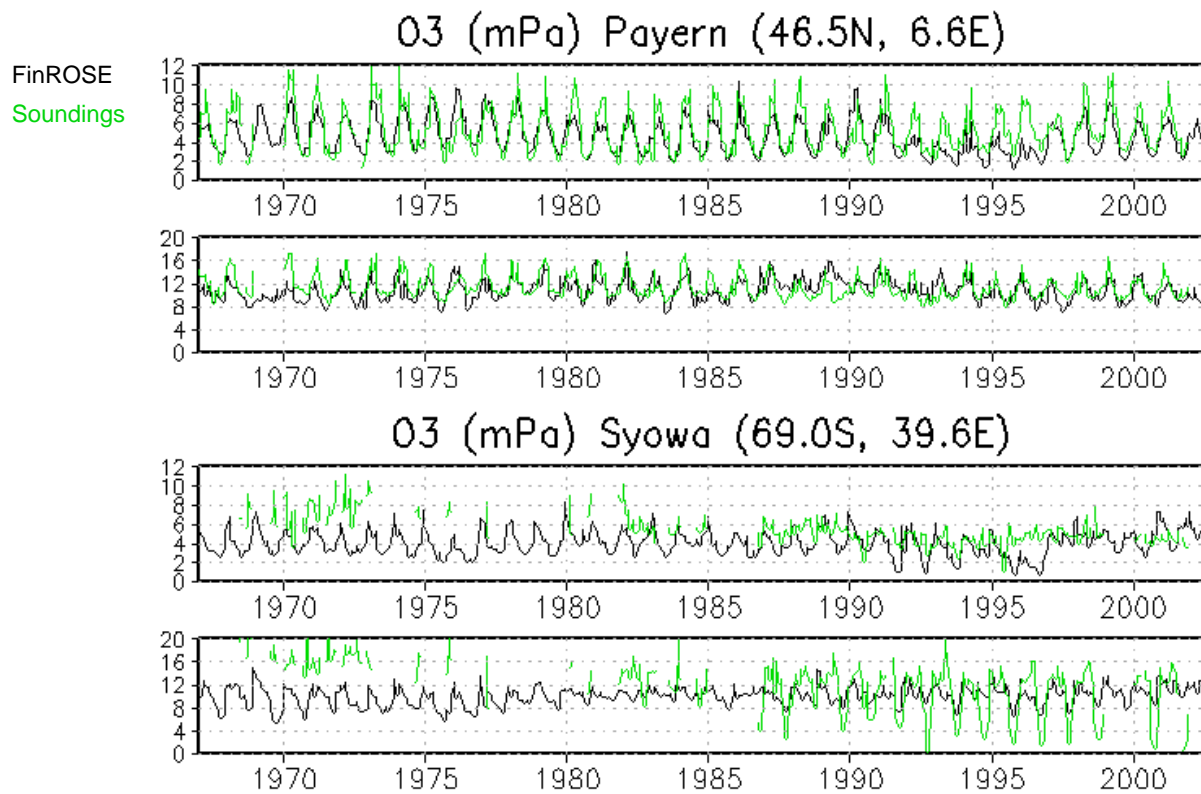


Figure 7: Ozone partial pressure monthly mean time series for Payern and Syowa at 177 and 67 hPa levels

Based on comparisons with ozone soundings (Figure 7), satellite and climatology data the ozone distribution and variability seem reasonable, at least in a qualitative sense. However, some shortcomings are evident. Excessive total ozone values (650DU) were observed at high northern latitudes in the winter and early spring (high ozone levels in the UT/LS region). The reason for this artefact was a distortion of the vertical profiles caused by noise in the ERA-40 wind fields. The ozone column in the tropics is too thin, which is likely due to the strong upwelling in the tropics. The variation (min-max) in ozone was less in the model results compared to e.g. ozone soundings. The smoothing effect was likely due to the fairly modest resolution. The strong meridional circulation in the ERA-40 data can be seen as in the stratospheric age-of-air, which in the FinROSE run does only slightly exceed 2 years (Figure 8). The age-of-air decreases by a few months going from the 1960s to the 70s, which indicates a change of circulation in the meteorological data. This shows up e.g. as an increase in Arctic total ozone between the 1960s and 70s.

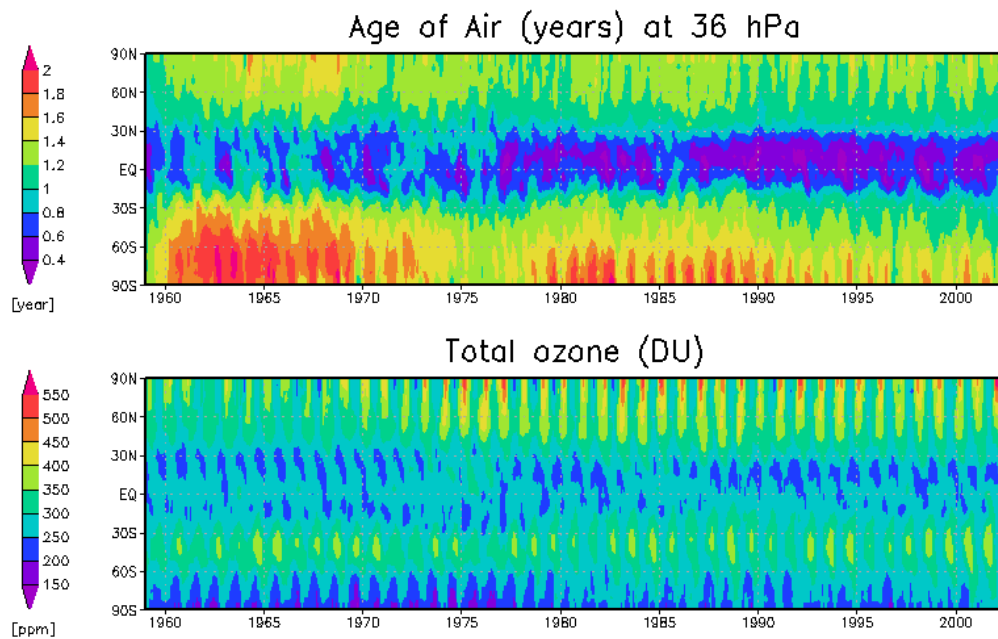


Figure 8: FinROSE CTM monthly mean age-of-air at 36 hPa and total ozone column in Dobson units

3.3.2 Stratospheric boundary conditions in the tropospheric models

Two of the three models participating in the RETRO reanalysis simulations employed a time-dependent stratospheric boundary condition for ozone, while ECHAM5-MOZ ran with a constant climatology. While the first reanalysis run made use of the FinROSE stratospheric ozone fields, results from another model were used for the second run, because this model appeared to produce less artefacts with the ERA-40 meteorology. The new ozone fields from a SLIMCAT simulation (Tian and Chipperfield 2005) were provided by UCamb and interpolated to the respective model resolutions of the LMDz-INCA and TM4 model.

The ability of SLIMCAT to simulate the fields and processes that are important for determining the ozone distribution in the recent past is assessed by comparisons with measurements and other model results in Eyring et al. (2006).

4. Analysis of the long-term simulations (ERA-40)

The long-term reanalysis simulations were performed by 3 of the 5 RETRO models (ECHAM5-MOZ, LMDz-INCA, TM4). UiO performed time slice simulations for specific years with the CTM2 model and UCamb focused on the late nineties with pTOMCAT simulations. The reanalysis simulations had to be repeated after some initial analysis showed a number of shortcomings in the results of all three models. The second reanalysis simulations also contained improved emission data sets (version 2 of the anthropogenic and biomass burning inventories with corrections for the seasonal cycle of the former and improved parameterisations of the latter). Note that no simulations with these improved emissions were made with the UiO CTM2 or UCamb pTOMCAT model.

The monthly mean concentration fields from all three reanalysis models are stored on the RETRO ftp server in ftp://ftp.retro.enes.org/pub/model_results. A wide variety of plots based on these simulations can be viewed on the RETRO web interface: http://nansen.ipsl.jussieu.fr/cgi-bin/AEROCOM/retro/retro_annualrs.pl.

In the following the analysis of the reanalysis simulations is described. There is only little evaluation with observational data and no thorough discussion of the global budgets and chemical lifetimes of species, because no time was available to perform these analyses. Annex 1 contains some extra analyses performed with the first version of the reanalysis simulations and we will discuss the quality of the new simulations based on those evaluations and the observed changes in the model results.

4.1 Intercomparison of geographical distributions and vertical cross sections of ozone and precursor concentrations

First of all, we present a qualitative comparison between the results of the 3 reanalysis models.

4.1.1 Ozone

Figure 9 displays the surface ozone mixing ratio simulated in 1960 and 2000 by LMDz-INCA, TM4, and ECHAM5-MOZ for the July-August-September seasonal mean. For both 1960 and 2000, ECHAM5-MOZ simulates the highest ozone surface levels over precursor source regions as well as background areas whereas the LMDz-INCA model shows the lowest ozone values. As expected, surface ozone concentrations significantly increased over northern industrialised areas between 1960 and 2000. In the LMDz-INCA simulation, this increase is in the 10 to 15 ppbv order over Europe (with a maximum over Mediterranean sea) and United States. The highest absolute increases are observed over Middle East and East China where it reaches up 20ppbv. Over North Atlantic Ocean, the summer seasonal values are increased by about 8 to 12 ppbv whereas over Pacific Ocean this increase does not exceed 8 ppbv. In the Southern hemisphere, the magnitude of the ozone changes is much weaker (a few ppbvs) except over the Guinean Gulf where an 18 ppbv decrease is observed between 1960 and 2000 due to a positive anomaly of biomass burning emissions in south Africa in 1960. Figure 10 illustrates the zonal mean ozone mixing ratios in 1960 and 2000 and confirms the relative magnitude of simulated ozone in the three models. The midlatitudinal increase in the northern hemisphere takes place over the whole height of the troposphere.

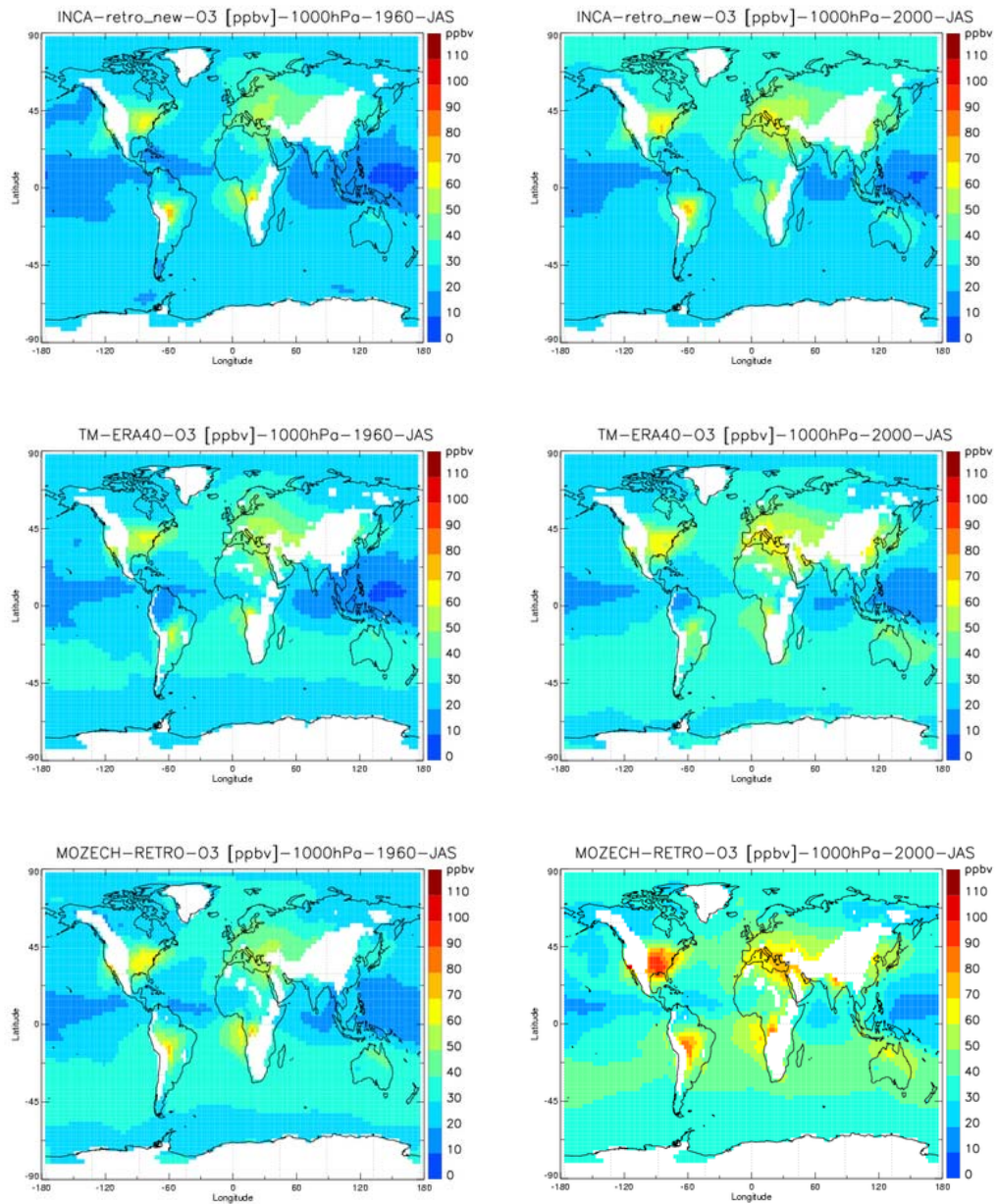


Figure 9: Summertime surface ozone mixing ratio (interpolated to 1000hPa) in 1960 (left column) and 2000 (right column) simulated by LMD_zINCA, TM4 and ECHAM5-MOZ (MOZECH)

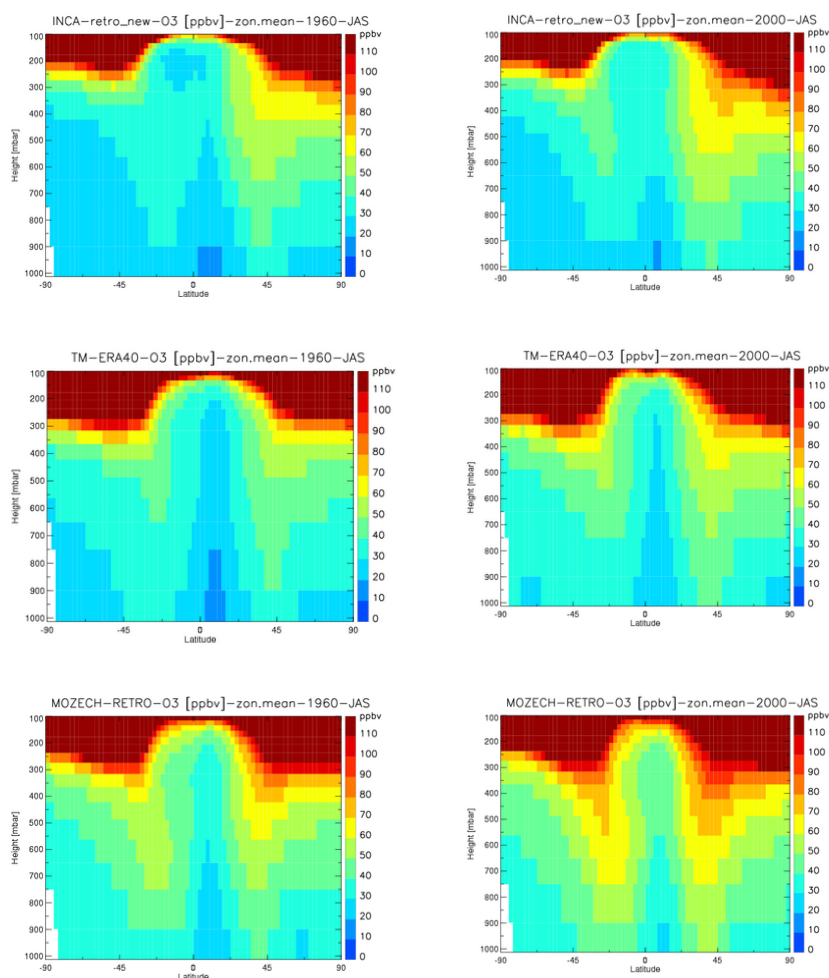


Figure 10: Summertime zonal mean ozone mixing ratios in 1960 (left column) and 2000 (right column) simulated by LMDz-INCA, TM4 and ECHAM5-MOZ

4.1.2 Carbon Monoxide

The surface CO mixing ratios computed by the 3 global models for 1960 and 2000 are more scattered than for ozone (Figure 11). The surface CO mixing ratios simulated by ECHAM5-MOZ are significantly greater than those of the other models in 1960 and 2000.

Over the remote oceans (far from continental outflow), at 45°N, the ranges of CO values are 40 to 70ppbv for LMDz-INCA, 60 to 80ppb for TM4 and 60 to 100ppbv for ECHAM5-MOZ in 1960. The mean values over the Atlantic Ocean are slightly greater than those over the Pacific Ocean both in 1960 and 2000. In the southern hemisphere, far from sources (e.g. -30 to -90 °S), LMDz-INCA and TM4 simulate mean values in the 40-60ppb range for 1960, while ECHAM5-MOZ produces concentrations in the 50-70ppbv range. In 2000, the background concentrations increased by about 10 ppbv in all models.

Over the continental areas of the northern hemisphere, the highest CO concentrations in summer, are observed in the eastern part of United States where the seasonal mixing ratios exceed 150ppbv. Over Europe, the mean seasonal values simulated are in the 80-150ppbv range (except ECHAM5-MOZ which simulates maximum values exceeding 150ppb). At

these latitudes, the range of mean summertime surface CO is not changed between 1960 and 2000 but a slight horizontal extension of the highest levels is observed in the LMDz-INCA and ECHAM5-MOZ simulations. One important feature in the Northern hemisphere is observed over Asia where the concentrations were close to the background level in 1960 and now reach similar seasonal values as in other polluted northern hemisphere areas. In the Southern hemisphere, the emissions of CO are mainly due to biomass burning over Amazonia, central Africa, Indonesia and North of Australia. No significant changes in CO are observed over these areas between 1960 and 2000, but any possible trend signal could well be masked by the large interannual variability of the biomass burning emissions (see Figure 5 in section 3.2.2).

Looking at the zonal mean CO concentrations (Figure 12), one can see that in the southern hemisphere, maximum CO zonal means are found close to the equator between 900 and 800hPa whereas in the northern hemisphere highest values are located in the first altitude level (1000-900hPa) around 45° N. ECHAM5-MOZ is different from the other models since it shows higher maximum in terms of intensity as well as spatial repartition with CO zonal means exceeding 90ppbv over middle and high northern latitudes from 1000hPa to 500hPa. The increase in CO between 1960 and 2000 takes place over the whole troposphere.

4.1.3 Hydroxyl radical

Figures 13 and 14 present the surface OH mixing ratios and the zonal means in summer for 1960 and 2000, respectively. The highest OH levels arise in the tropics due to the strongest intensity of sunlight and the availability of moisture in this region. In all three models, the shape of the summer seasonal and zonal mean agrees well with the climatology of Spivakovsky et al. (2000) for July. The maximum zonal mean is observed at around 30°N but with vertical gradients between 1000 and 800hPa more or less simulated depending on the models. The trend between 1960 and 2000 is unclear with a slight increase around 30°N in the LMDz-INCA and TM4 simulations and no significant change in the ECHAM5-MOZ simulation. The lowest zonal means are observed at high latitudes and are almost unchanged between 1960 and 2000. At the surface, the highest values are generally encountered over the continents except over tropical forests where low OH levels are found due to intense emissions of biogenic VOC which react rapidly with OH.

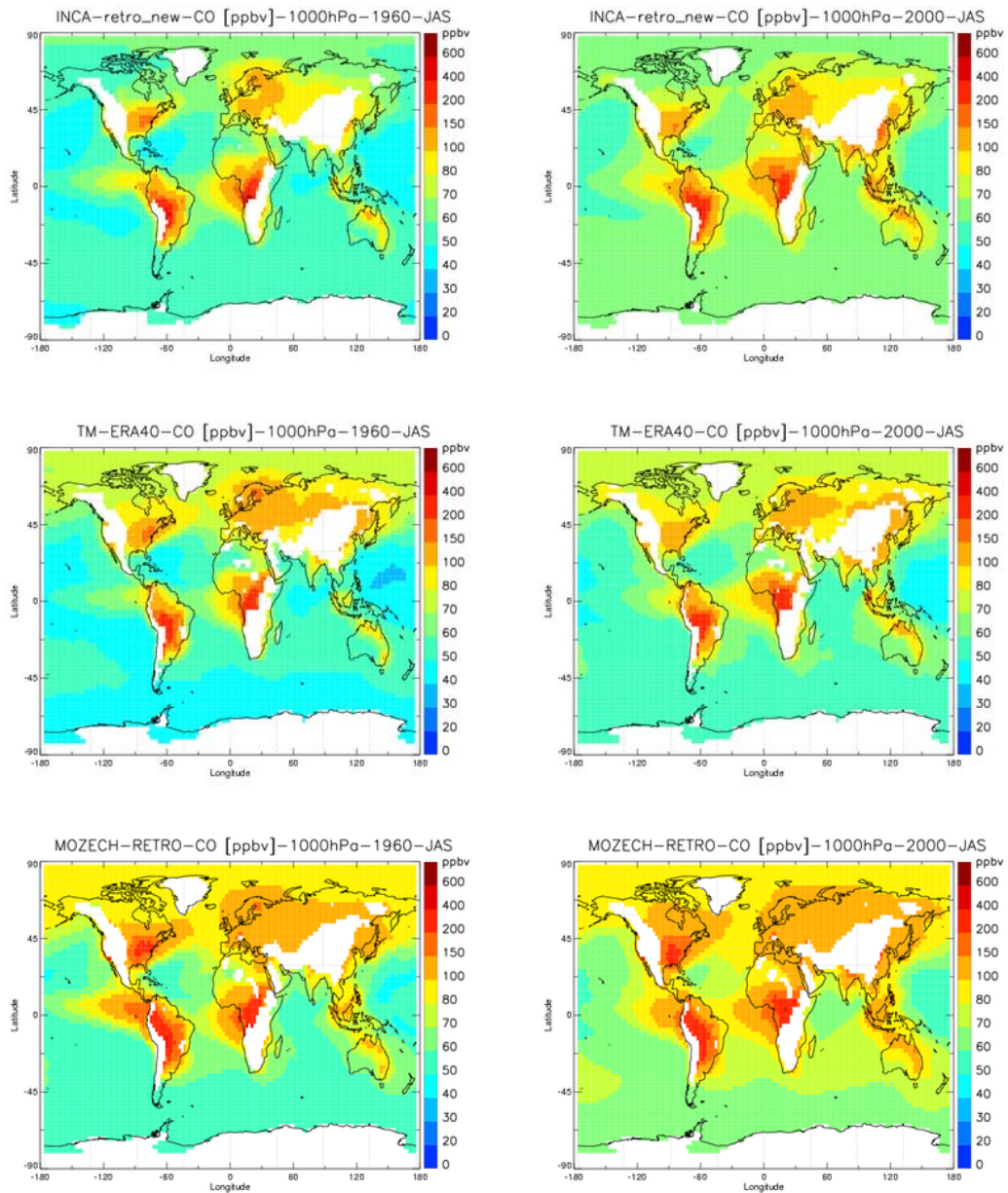


Figure 11: Summertime surface carbon monoxide mixing ratios (interpolated to 1000hPa) in 1960 (left column) and 2000 (right column) simulated by LMDzINCA, TM4 and ECHAM5-MOZ (MOZECH)

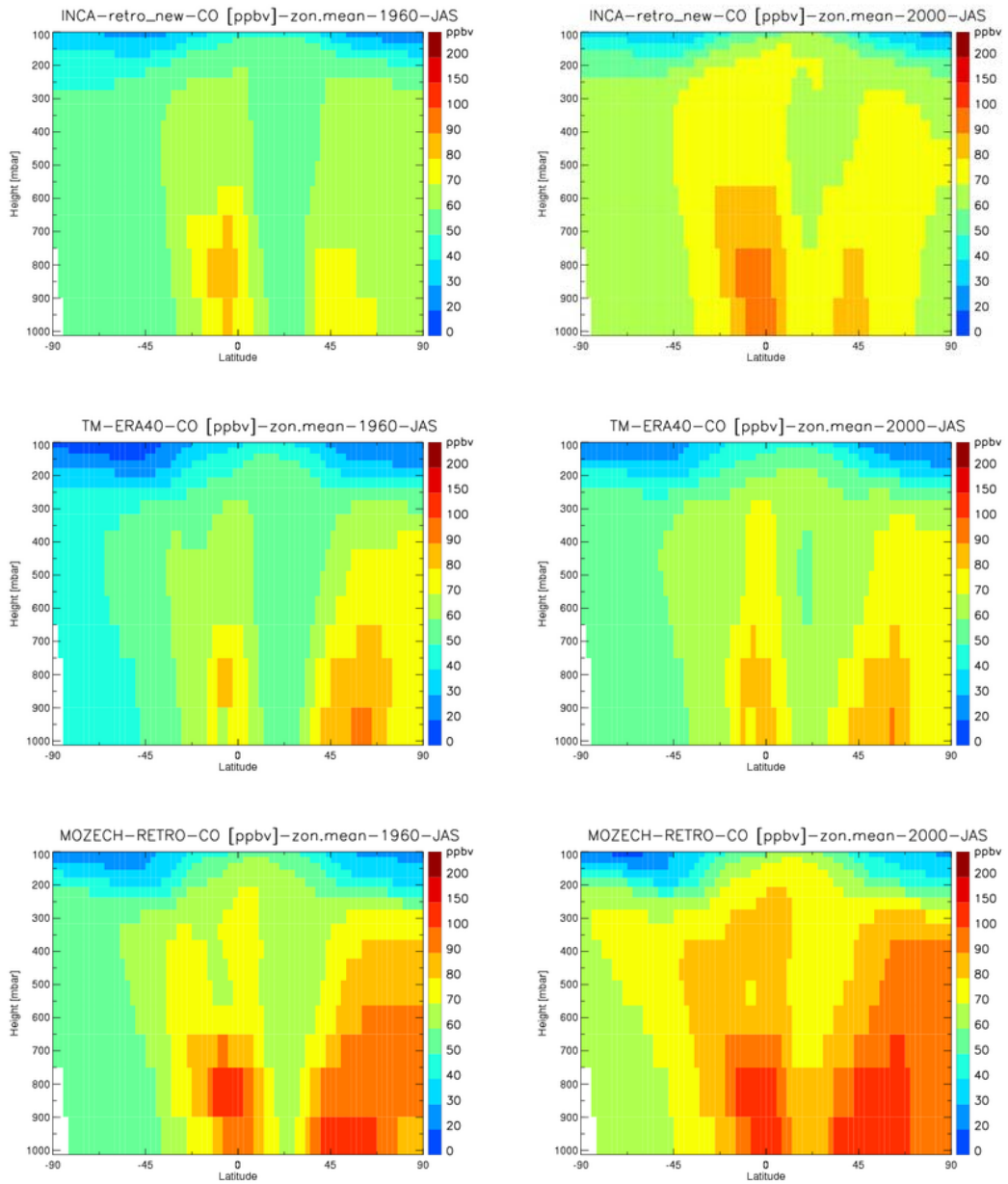


Figure 12: Summertime zonal mean carbon monoxide mixing ratio in 1960 (left column) and 2000 (right column) simulated by LMDzINCA, TM4 and ECHAM5-MOZ (MOZECH)

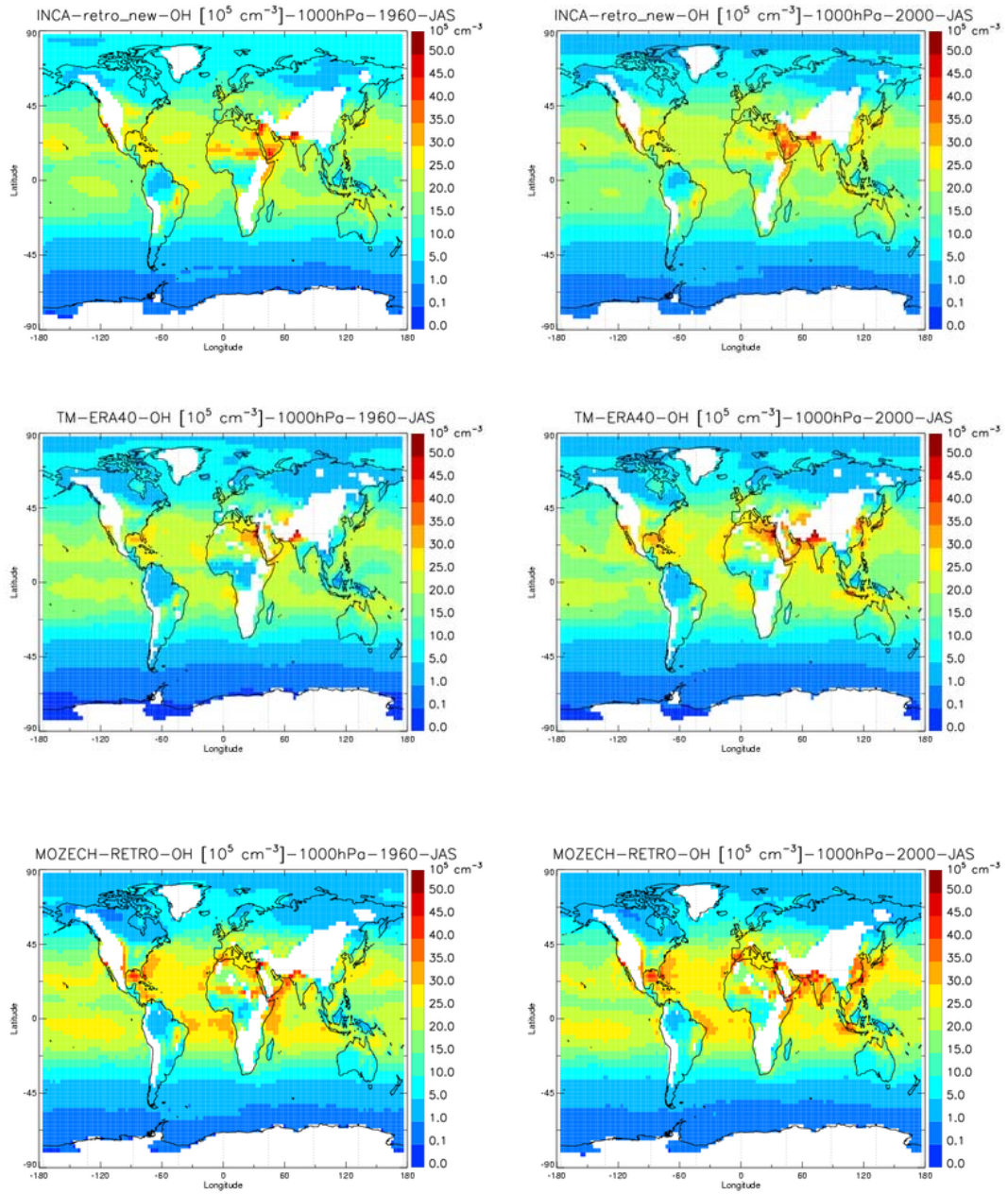


Figure 13: Summertime surface hydroxyl radical mixing ratio (interpolated to 1000hPa) in 1960 (left column) and 2000 (right column) simulated by LMDzINCA, TM, and ECHAM5-MOZ (MOZECH)

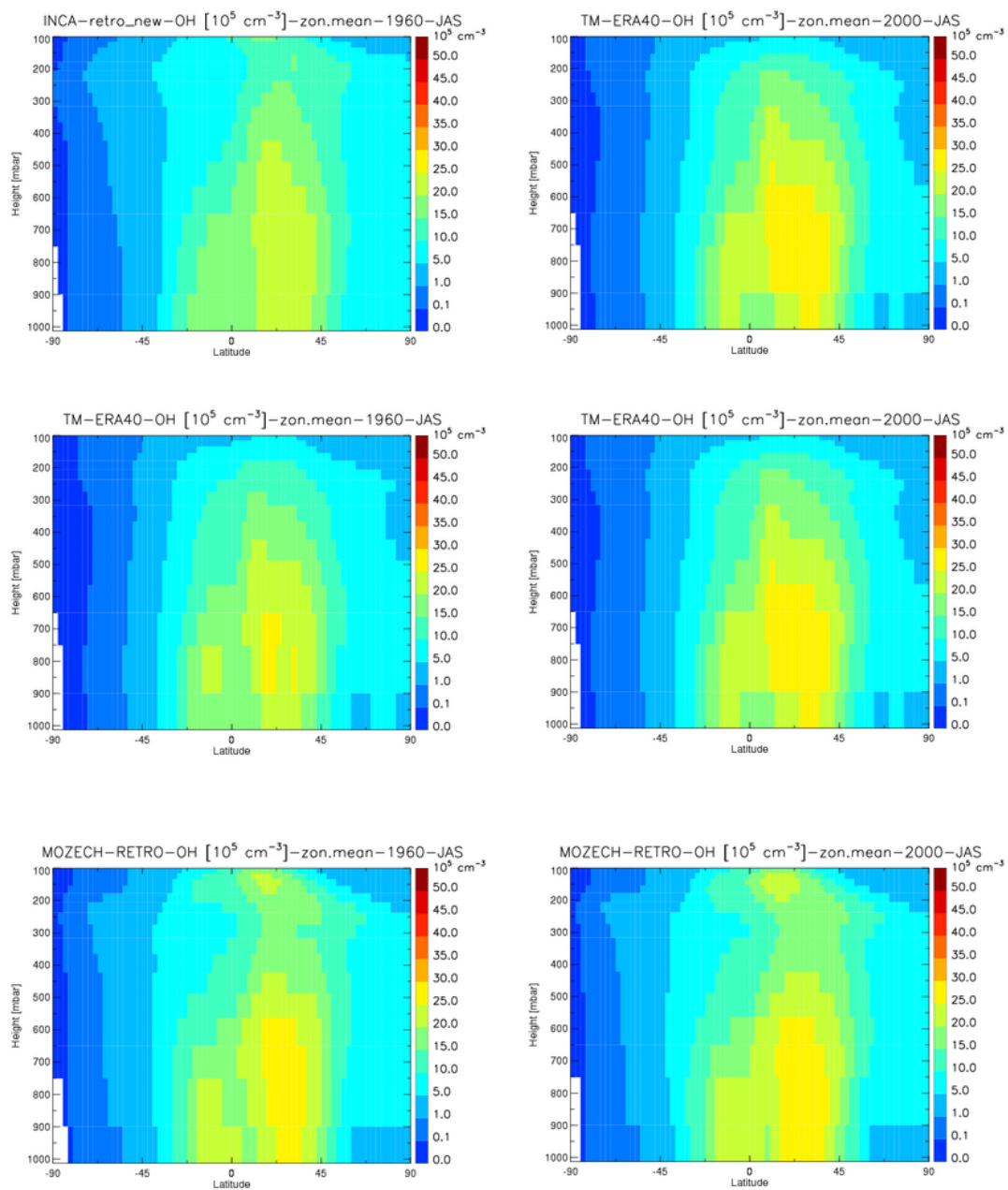


Figure 14: Summertime zonal mean hydroxyl radical mixing ratios in 1960 (left column) and 2000 (right column) simulated by LMDz-INCA, TM and ECHAM5-MOZ (MOZECH)

4.2 Analysis of long-term trends and variability

4.2.1 Trend analysis of the LMDz-INCA model

The evolution of the zonal surface ozone mixing ratios over the whole 40 years, as simulated by the LMDz-INCA model is depicted in Figure 15. The main feature is an increase of zonal mean ozone in the northern hemisphere. This feature is maximum at $\sim 45^\circ\text{N}$ with maximum exceeding 45ppbv (for monthly zonal mean) after about 1970 instead of 40-45ppbv in the early 1960s. Regarding the annual minima at these mid latitudes of the northern hemisphere,

they have also significantly increased compared with the 1960's levels. Since about 1975 the annual minimum ozone levels are equivalent in magnitude to the maximum values of the 1960s. Another key characteristic is that this increase took mainly place during the 1970s. Thereafter, both minimum and maximum levels remained rather constant. In the southern hemisphere, a slight increase of maximum values is simulated around 30°S.

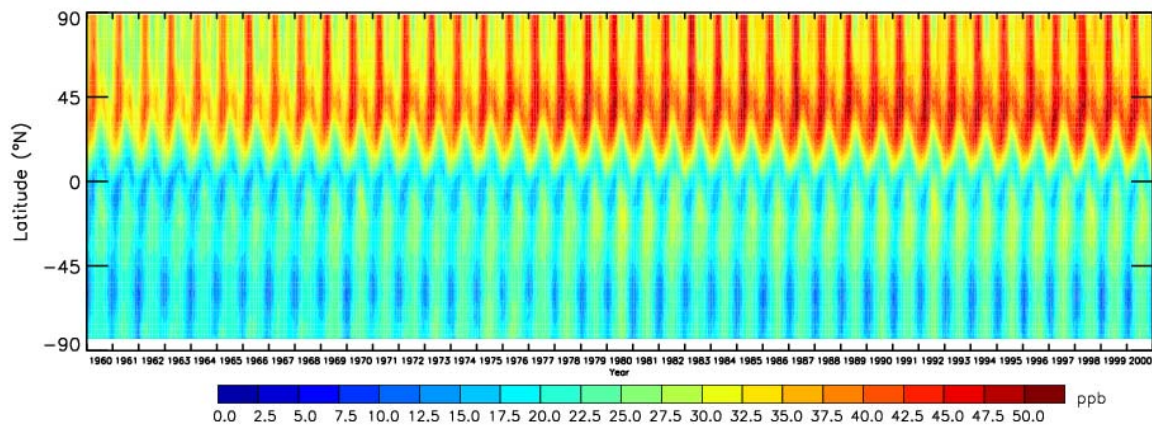


Figure 15: Temporal evolution of the zonal mean surface ozone concentrations simulated by LMDz-INCA

Using the ten highest daily values of surface ozone per year, trends were computed for each decade (Figure 16). The general increase of maximum ozone concentrations at the end of the 1960s and 1970s is confirmed by this figure. In the 1980s, the positive trend is conserved mainly over Europe, India and North-Eastern USA but an overall decrease is simulated over the oceans. During the 1990's, the maximum ozone continued to increase in NE-USA, and over Asia. The features in the southern hemisphere are more heterogeneous and no significant trend appears. The trend signals exhibit a large spatial and temporal heterogeneity. This provides an explanation for the difficulties to derive robust trend estimates from measurements of surface concentrations alone. Furthermore, ozone minima and maxima show significantly different features and have to be separated to deduce reliable tendencies. However, Figure 17 confirms an overall increase of maximum values and, to a lesser extent of minimum values when considering the whole period.

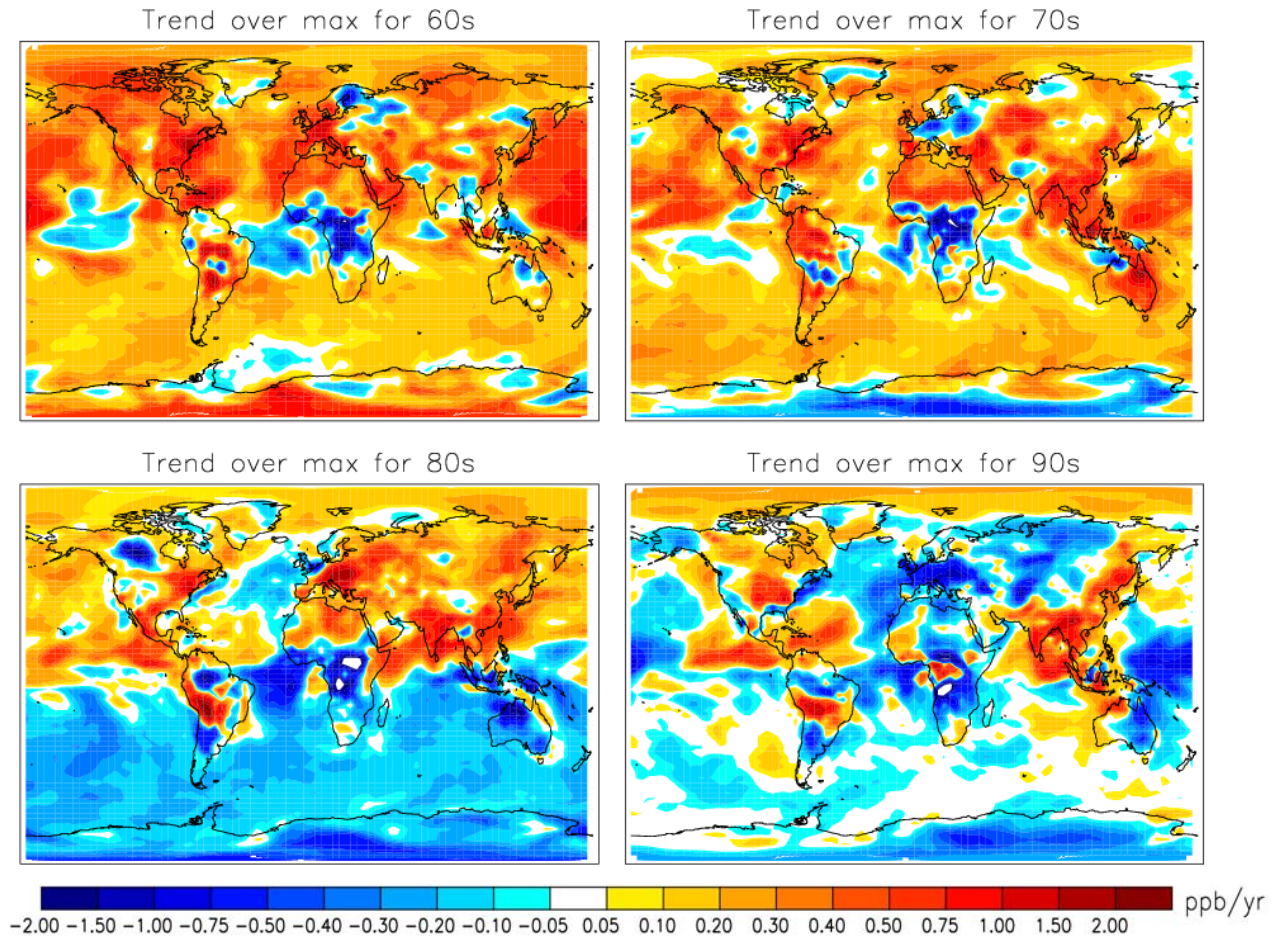
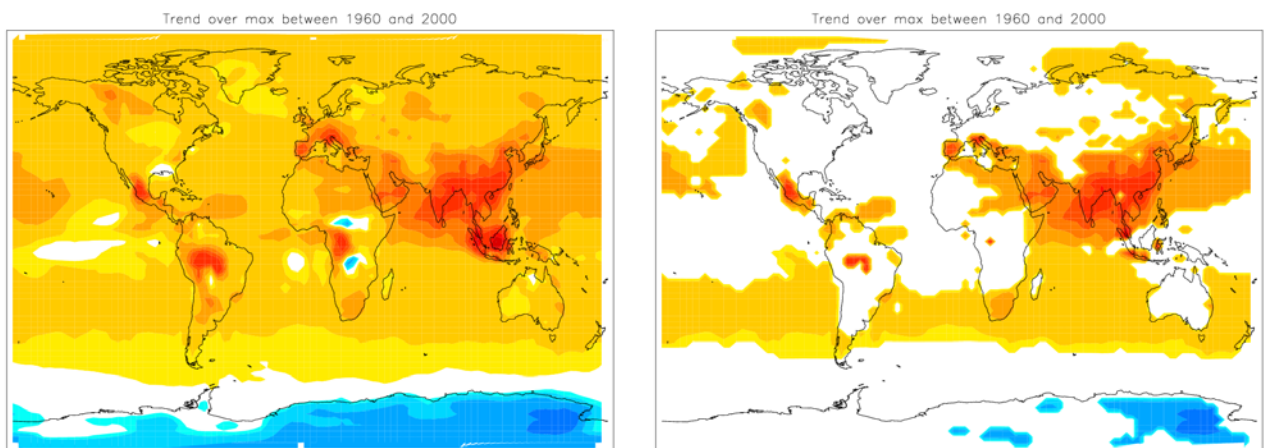


Figure 16 : Spatial pattern of decadal maximum surface ozone trends (computed using the ten highest daily values per year) separated by decades. Results from the LMDz-INCA model.



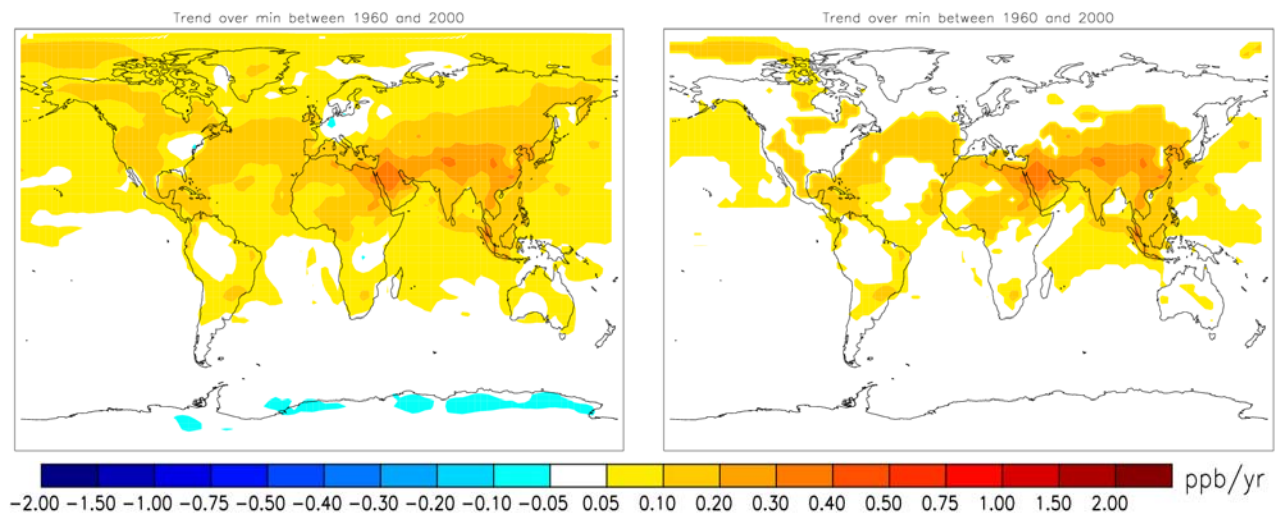


Figure 17 : Spatial pattern of trends in maximum (top) and minimum (bottom) surface ozone concentrations (computed using the ten highest daily values per year) for the entire 41-year period. The right column shows the same data but only for regions where the R^2 correlation coefficient is greater 0.4. Results from the LMDz-INCA model.

Figure 18 shows the decadal trend patterns for the ten highest and the ten lowest surface ozone mixing ratios of each individual year at eight locations in the world as simulated by the LMDz-INCA model. At continental locations (c, f, h) the maximum values are scattered in a 10 ppb range whereas the minimum values are less spread out. While no or only little trend is observed for the minimum values, the maximum values show a clear increase between 1960 and 2000 for all continental locations. This increase is most pronounced for the point located on the coast of the South Asian sea with respective rates of 0.36, 0.77 0.67 0.47ppb per year for the sixties, seventies, eighties and nineties.

In the North Atlantic, close to the European coast (location e), the maximum values show an increase in the 1960's ($0.43 \text{ ppb}\cdot\text{year}^{-1}$) and 1970's ($0.42 \text{ ppb}\cdot\text{year}^{-1}$) and a slight decrease in the 1980's ($-0.06 \text{ ppb}\cdot\text{year}^{-1}$) and 1990's ($-0.48 \text{ ppb}\cdot\text{year}^{-1}$). In contrast, the minimum values show a slight increase throughout the whole period. In the North Pacific (location a), both minimum and maximum values show a continuous increase over time. The Southern ocean locations (b, d, g) exhibit more or less constant mixing ratios after about 1970.

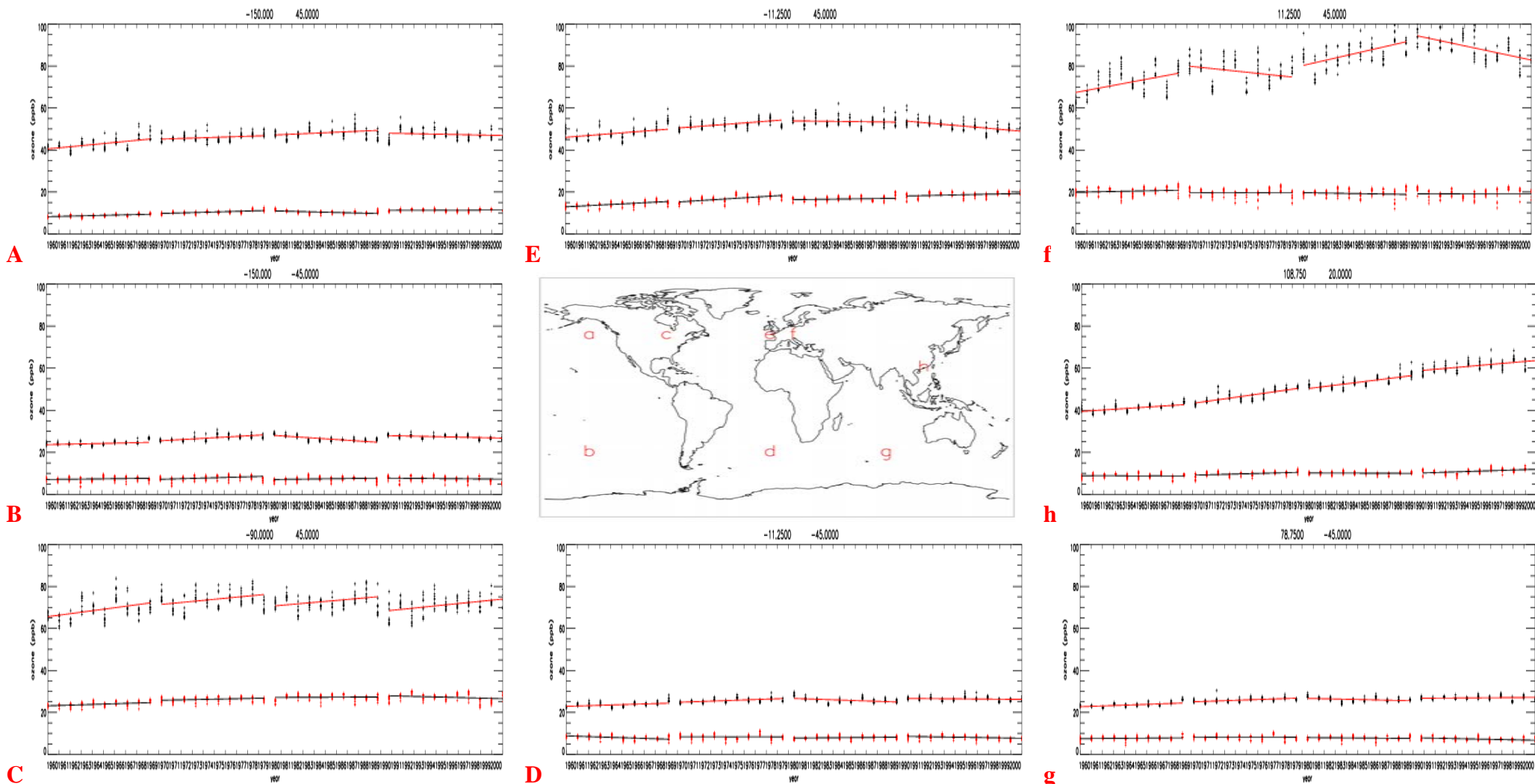


Figure 18: Decadal trends of surface ozone maxima and minima from the LMDz-INCA simulation at selected locations

4.2.2 ECHAM5-MOZ comparison with MOZAIC data

The ozone concentrations of the 1990s simulated by ECHAM5-MOZ were compared with measurements from the MOZAIC programme at several altitudes. For this analysis monthly mean values were used and the aircraft data were sampled from the vertical profiles of MOZAIC flights (upon departure and arrival of the airplanes) across a pressure range similar to the vertical extent of the model grid box. Time series plots were produced for all MOZAIC airports. Here we show only a couple of examples for which sufficient observational data were available and to characterize different world regions.

Figure 19 displays the comparison for the two central European airports of Brussels and Frankfurt. In both cases the seasonal and interannual variability of the ozone mixing ratio is captured rather well by the model. In the middle and upper troposphere ECHAM5-MOZ exhibits a high bias of up to 30 ppb at 500 hPa (level 17). The simulated values in the boundary layer (level 28) and in the lower stratosphere (level 10) agree well with the observations. Note that the stratospheric values are controlled by the prescribed ozone climatology and variations are due to different circulation patterns alone. The variability of stratospheric concentrations is much larger than the simulated variability. Interestingly, this does not appear to have an effect on the concentrations in the upper troposphere or below, where the observed and simulated variability agree very well.

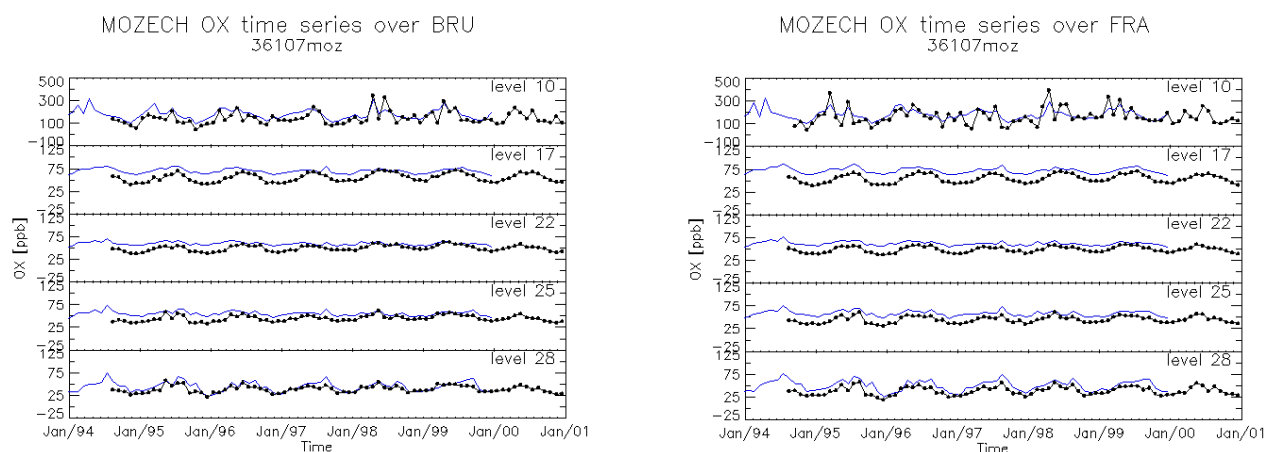


Figure 19: Time series of monthly mean ozone mixing ratios at selected altitudes over Brussels (left) and Frankfurt (right). MOZAIC flight data are shown as filled circles and the ECHAM5-MOZ results as solid blue line. The model levels correspond to the following pressure levels: level 10 = 240 hPa, level 17 = 500 hPa, level 22 = 720 hPa, level 25 = 850 hPa, level 28 = 960 hPa

Figure 20 shows the same analysis for four North American airports. Again, ECHAM5-MOZ captures the seasonal and interannual variability of the observations rather well and exhibits a high bias in the upper and middle troposphere. Note that the seasonal variability of the stratospheric concentrations is much larger over North America than over Europe. This difference is well reproduced by the model. In contrast to the European observations, ECHAM5-MOZ also exhibits a high bias in the North American boundary layer. This is particularly pronounced for the East coast airport New York and in the summer. The annual

maximum concentrations also occur about 2 months later in the model than in the observations. So far the reason for this discrepancy is unclear.

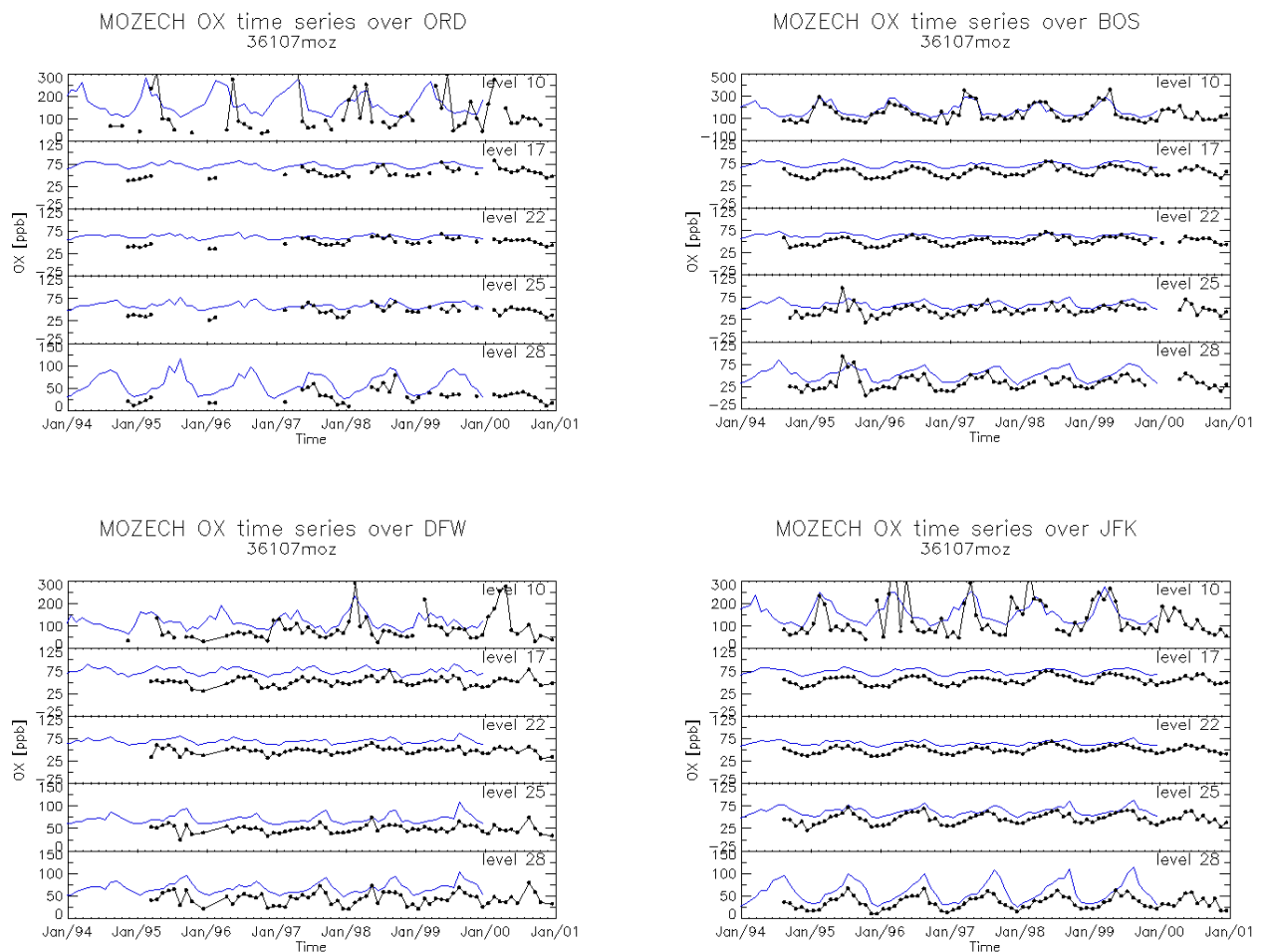


Figure 20: As figure 19 but for the four North American airports Chicago (ORD), Boston (BOS), Dallas (DFW) and New York (JFK)

In Figure 21, the model results are compared with MOZAIC data for the airports of Tokyo and Johannesburg. For these airports fewer observations are available, but some conclusions can be drawn anyhow. In the middle and upper troposphere over Tokyo the same high bias is found as for the European and North American locations. Again the seasonal and interannual variability is generally captured well, although the low concentrations in the middle and lower troposphere during the summer monsoon in 1996 and to some extent also in 1999 are not reproduced. In the boundary layer, the model shows a high bias for summertime values but captures the wintertime concentrations very well. There are not enough data available to evaluate the stratospheric variability signal over Tokyo.

Over Johannesburg, the variability is captured well at all levels, but here the model shows a high bias also in the stratospheric level (model level 10).

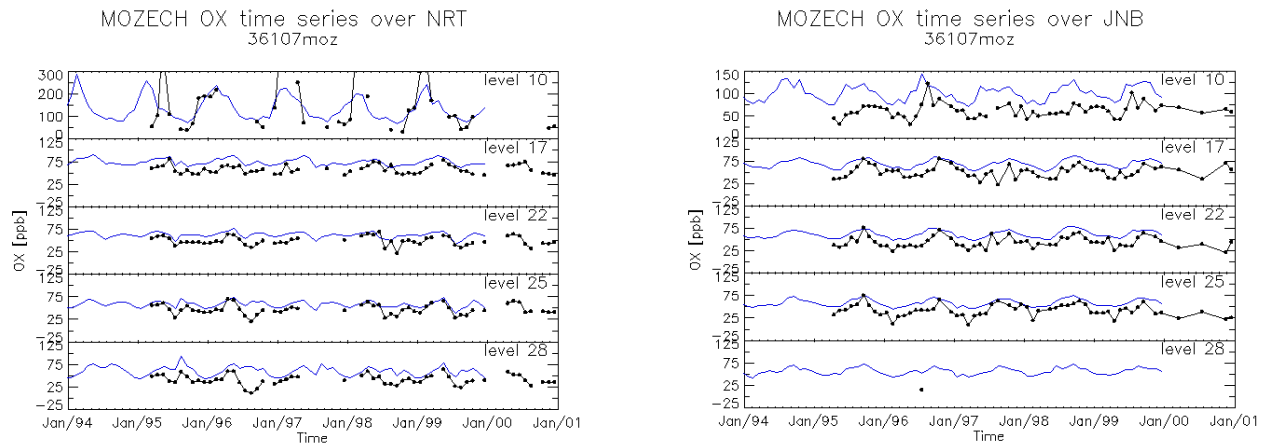


Figure 21: As figure 19 but for the airports of Tokyo (NRT, left) and Johannesburg (JNB, right)

4.2.3 Analysis of surface CO anomalies

As discussed in section 4.1, the three RETRO reanalysis simulations yield significantly different concentration levels of carbon monoxide. In general the models have a tendency to underestimate the surface CO concentrations, in particular in the northern hemisphere winter and at high latitude locations (not shown). Summertime values of ECHAM5-MOZ and surface concentrations in the southern hemisphere agree very well (see Rast et al., manuscript in preparation). Note that the CO concentrations of all models should have increased in comparison to earlier simulation results shown in the Annex (section A1) due to the revised emission inventories.

In this section, we investigate the anomaly patterns of CO concentrations at selected NOAA-ESRL station sites. For this purpose, we compute 12-months running averages of the observational data and the model results and display the monthly anomaly as the difference of the monthly mean concentration in one year and the multi-annual mean value of the same month. In this way, any bias is removed from the analysis and the interannual variability patterns emerge.

Figure 22 shows the anomaly plots for 7 NOAA-ESRL sampling locations ordered by latitude from north to south. It is evident, that most of the time the three models show very similar anomalies and they agree rather well with the observed anomaly patterns. In particular, the models capture the strong decline of carbon monoxide levels in the northern hemisphere after 1990 and the strong enhancement of CO in tropical and subtropical latitudes in 1997 (due to the Indonesian forest fires of that year). The models also qualitatively reproduce the strongly enhanced CO concentrations in the northern hemisphere in 1998, but they underestimate this enhancement by about a factor of two. This signal is caused by excessive boreal forest burning in 1998. The paper describing the RETRO fire inventory by Schultz et al. (2007) discusses this episode and states that fire emissions in boreal regions may be underestimated if the amount of soil organic carbon that is burned is larger than assumed. The anomaly analysis presented here indicates that this is indeed the case.

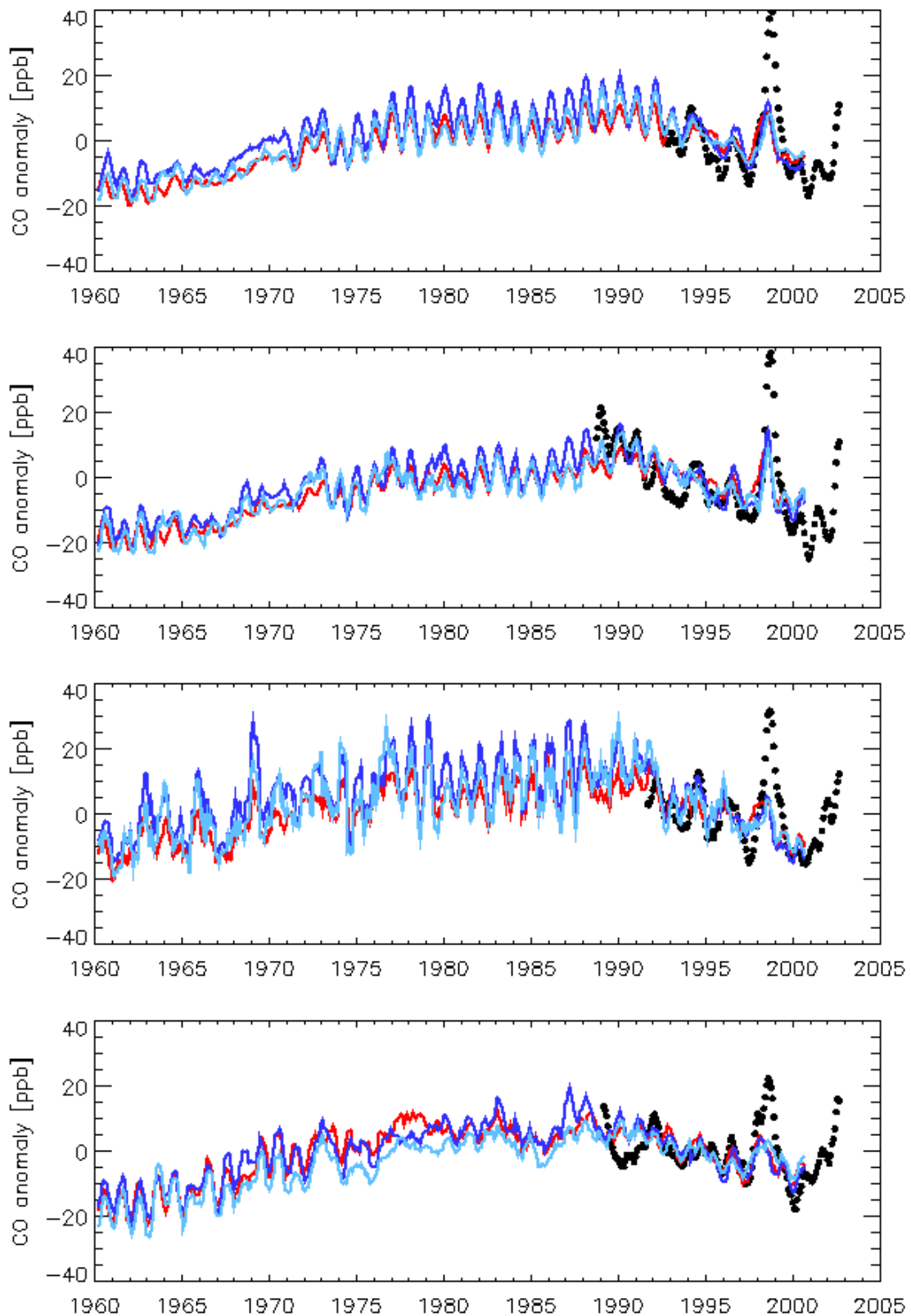


Figure 22: Monthly mean anomaly plots of CO concentrations at selected NOAA-ESRL sampling locations. The data have been smoothed before plotting (explanation see text). The stations are from top to bottom: Alert, Canada; Barrow, Alaska; Mace Head, Ireland; Niwot Ridge, USA. On the next page the same plots are shown for Mauna Loa, Hawaii; Ascension Island; and Cape Grim, Australia. Black bullets: observations, red line: LMDz-INCA, dark blue line: TM4, light blue line: ECHAM5-MOZ

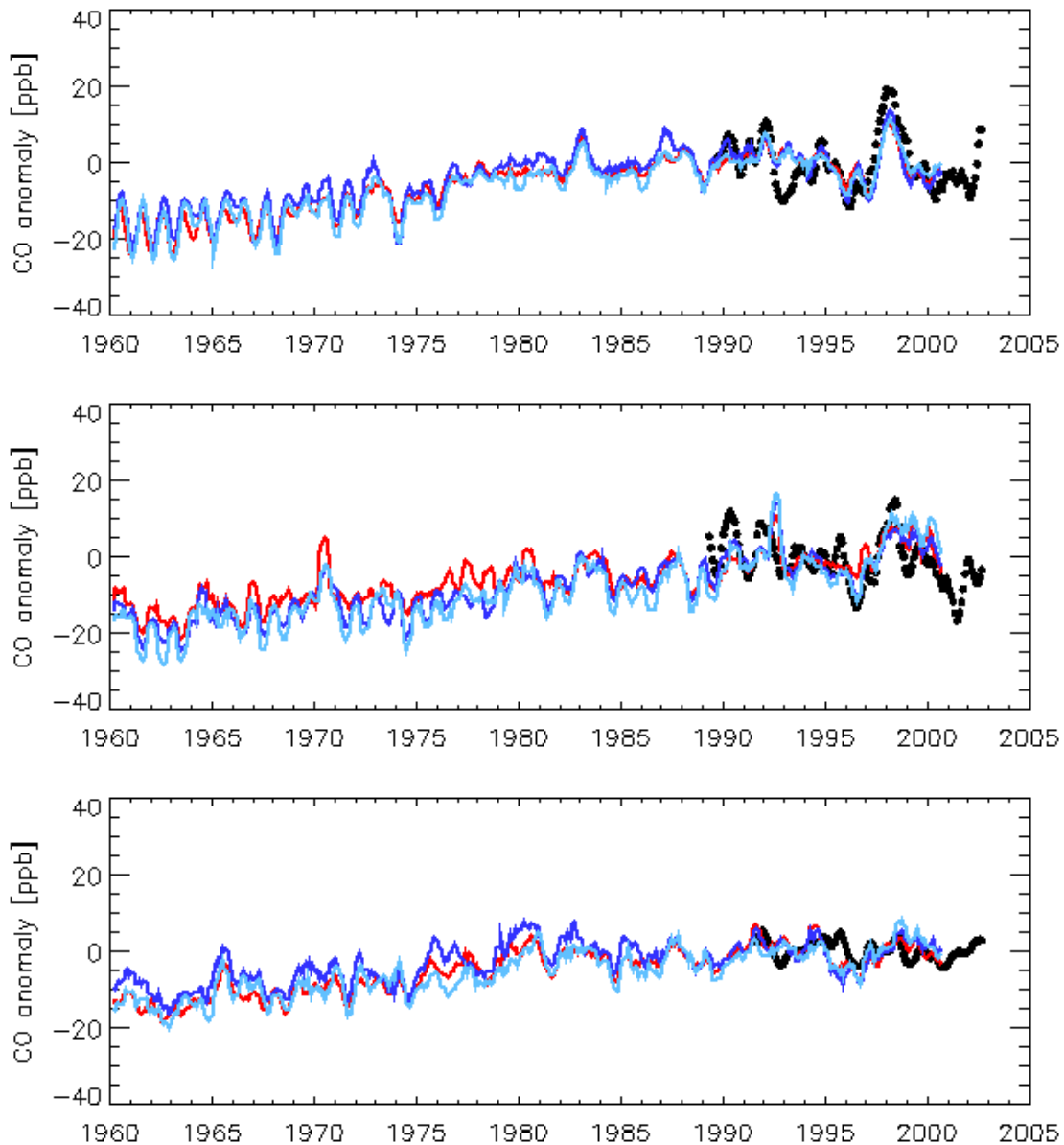


Figure 22, continued

The high latitude stations displayed in Figure 22 (Alert and Barrow) show an interesting feature in the anomaly time series: while all models generate a very regular seasonal pattern between 1972 and 1992, the pattern is much less regular during the other years. Until now, no explanation has been found for this behaviour.

4.2.4 Synthesis of simulated trends and analysis of inter-model differences

CO

The analyses presented so far were for the most part based on surface concentrations. Because of the different vertical and horizontal resolutions of the models, these comparisons may not always reflect real uncertainties which are due to incomplete knowledge of processes or parameter values. For the following discussions we therefore integrate over larger areas and across several model levels. This should give a more robust estimate of model trend and

variability patterns. If we find good consistency between the model averaged quantities we might put some confidence in the realism of the simulations. However, in some cases the consistency will also be caused by the use of identical boundary conditions for all models or by similarities in the adaptation of the ERA-40 meteorological data (use of wind vectors versus divergence and vorticity, or the use of the ERA-40 surface pressure fields).

We begin with wintertime (Figure 23) and summertime (Figure 24) trends in the boundary layer CO concentrations over Europe, North America and East Asia. The three regions were defined with rectangular boundaries as follows:

Europe: 0° E – 30° E
 North America: 120° W – 60° W
 East Asia: 110° E – 140° E

Each region was divided in four latitude bands of ten degrees width: 25° N-35° N, 35° N-45° N, 45° N-55° N, and 55° N-65° N. Vertically, we distinguish between the boundary layer(0-1 km altitude), the middle troposphere (4-8 km) and the upper troposphere (8-12 km).

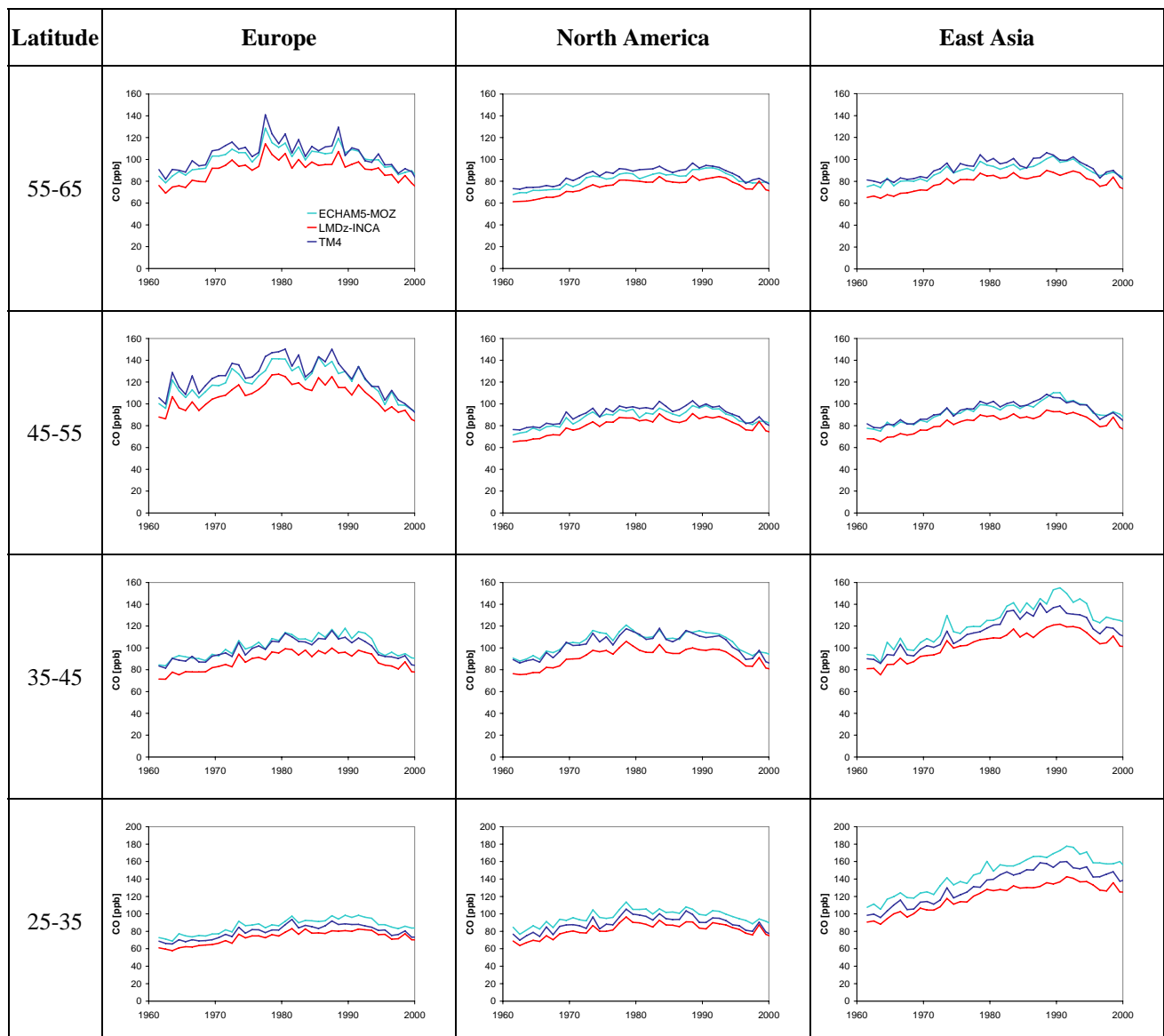


Figure 23: Time series of wintertime boundary layer CO concentrations simulated by the three RETRO reanalysis models. For details on the region definitions, see text. Note the different scale for the southernmost latitude band.

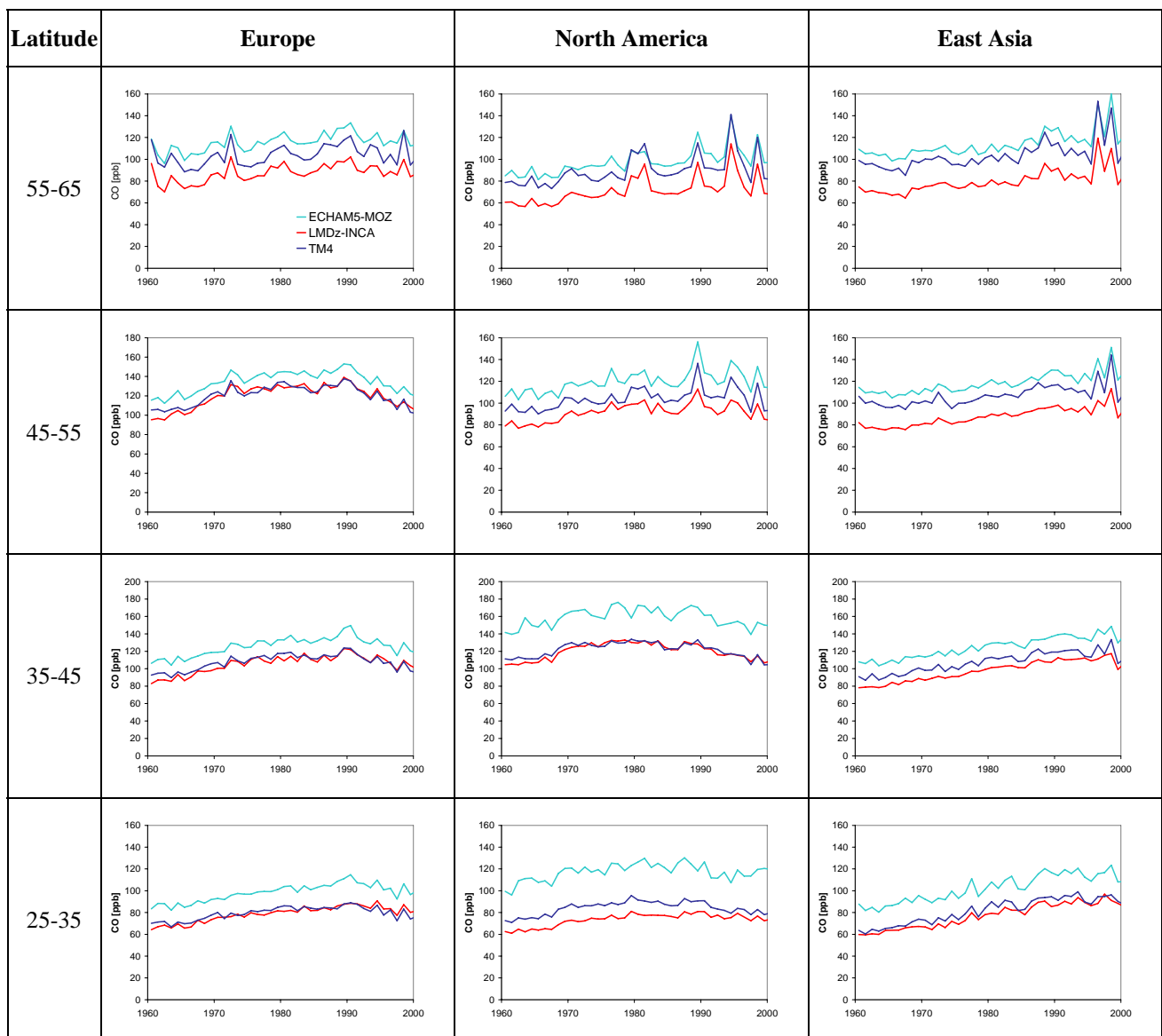


Figure 24: As Figure 23, but for summertime boundary layer CO concentrations. Note the different scale for the latitude band 35°N-45°N

In most regions, the three models show very good consistency in terms of the general trend pattern and the interannual variability of the seasonally averaged boundary layer CO concentrations (Figures 23 and 24). Absolute concentrations – particularly in summer – differ by up to 40 ppb (20-30%), but the shape of the curves is very similar. LMDz-INCA typically produces the lowest CO concentrations. In winter, ECHAM5-MOZ and TM4 mostly have rather similar values (except for the lower latitude bands over East Asia), and they are about 10-20 ppb higher than those of LMDz-INCA. In summer, the differences between LMDz-INCA and TM4 are usually similar (sometimes even smaller), but ECHAM5-MOZ exhibits much higher concentrations than the other two models (20-40 ppb more; most pronounced in the lower latitude bands over North America and East Asia). Independent analysis of passive tracer experiments performed in the framework of the task force on hemispheric transport of air pollution (TFHTAP) multi-model simulations shows that ECHAM5-MOZ generates the most stable boundary layer of several models during summertime. Therefore, pollutant

species accumulate in the boundary layer and are less efficiently ventilated than in other models. As a secondary effect, these higher pollutant levels also reduce OH concentrations so that the lifetime of the species is extended (although ECHAM5-MOZ still yields relatively short lifetimes overall).

Wintertime CO concentrations are mostly controlled by the surface emissions and horizontal transport. These properties seem to be represented in a consistent manner in the three models. The wintertime concentrations first increase in all regions by 20-40 ppb between 1960 and 1990 (in some regions the maximum is very broad and peak concentrations are reached earlier). After 1990, a general decline of boundary layer CO is simulated. This decline is strongest over Europe. Between 45° N and 55° N, simulated CO concentrations in the year 2000 are even lower than those in 1960. In most other regions, the year 2000 concentrations are similar to the 1960 values. Only in East Asia, south of 45° N, the simulated decline is weaker and the year 2000 values remain above the values of 1960. This general decline of boundary layer CO during the 1990s is consistent with observations (see Figure 22 and Novelli et al., 2003). It should be noted, however, that the uncertainties of the emissions data, particularly for East Asia, is large, and there have been tremendous changes occurring in this region after the late 1990s, which may not be adequately reflected in the RETRO emissions data sets. Observations from recent field campaigns indicate an increase in East Asian CO emissions of almost 50% since the year 2000 (D. J. Jacob, personal communication, 2007). The investigation of the effect of this increase on other regions is urgently needed but beyond the scope of the RETRO project.

The summertime concentrations generally show similar trend patterns as the wintertime values, but the change is typically less pronounced. In particular the decline after 1990 is almost absent in the most northern latitudes (55° N-65° N) and over East Asia. Nowhere do the boundary layer CO concentrations in summer fall below the values of 1960 as they did in winter.

The interannual variability of boundary layer CO is most pronounced in the northern latitude bands in summer and over Europe in winter. A lot of this interannual variability is caused by boreal forest fires which were especially strong in 1996 and 1998 (see Figure 5 in section 3.2.2).

Figure 25 below depicts similar time series for the summertime CO concentrations over Europe, North America and East Asia in the free troposphere. Again, the three models show very consistent behaviour, and the absolute concentrations are also in rather good agreement. The trends of the free tropospheric CO concentrations show some similarity to those in the boundary layer, but one can see less of a decrease after 1990. The ratio of CO concentrations in the free troposphere versus those in the boundary layer gives some indication of the intensity of vertical mixing in the individual models. These ratios are summarized for the summertime CO mixing ratios of the 1960s and the 1990s in Table 3. LMDz-INCA generally has an atmosphere that is more thoroughly mixed (ratios above 0.8) than the other two models, which have ratios that are typically around 0.7. A similar evaluation for the ratio of 8-12 km concentrations over boundary layer concentrations yields very similar results with an overall decrease in the ratios by 10% for ECHAM5-MOZ and TM4, whereas the ratios of LMDz-INCA remain virtually the same. The change of the vertical exchange ratio over time is generally smaller than the inter-model differences, but there appears to be a small but significant increase in this ratio over North America, and a noticeable decrease over East Asia. Whether this is real or an artefact introduced by the ERA-40 data remains an open question.

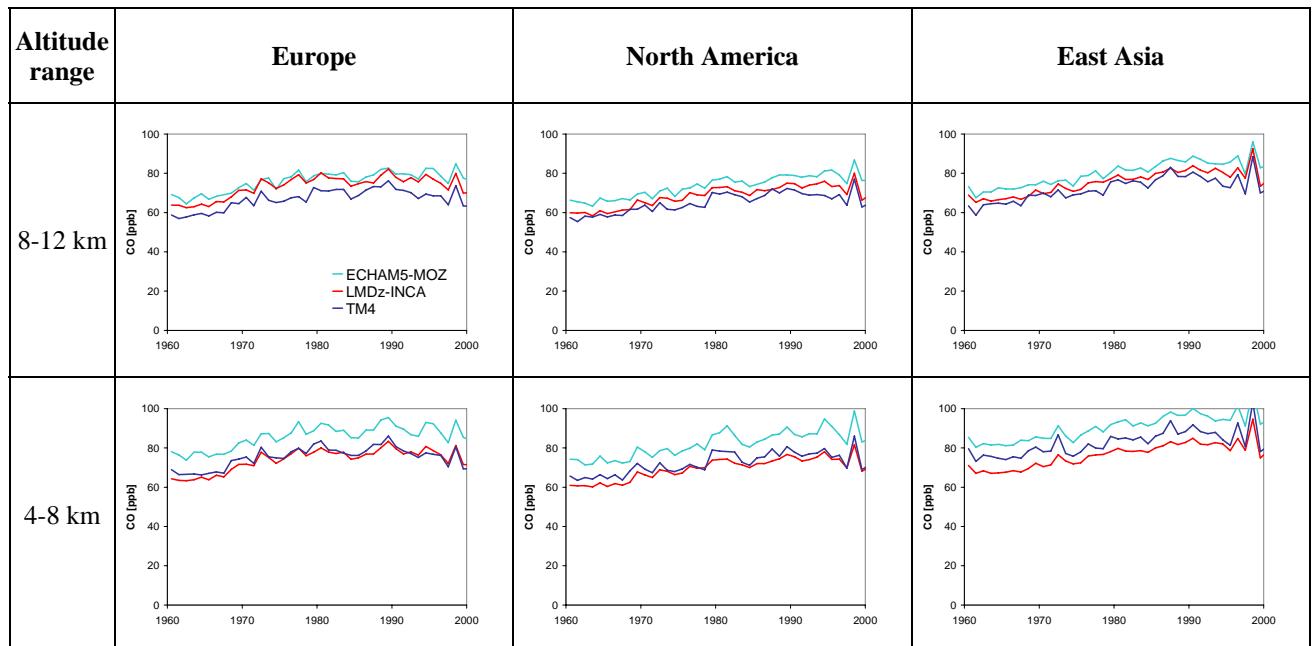


Figure 25: Time series of summertime CO concentrations in the latitude band 45°N - 55°N between 8 and 12 km altitude (top) and between 4 and 8 km altitude (bottom) simulated by the three RETRO reanalysis models. For details on the region definitions, see text.

Table3: Ratio of summertime CO mixing ratios in the free troposphere (4-8 km) over the respective mixing ratios in the boundary layer from the three RETRO models averaged over the 1960s and over the 1990s and across all latitude bands described in the text

Model	Europe		North America		East Asia	
	1960s	1990s	1960s	1990s	1960s	1990s
ECHAM5-MOZ	0.68	0.70	0.67	0.71	0.75	0.73
LMDz-INCA	0.73	0.74	0.79	0.81	0.88	0.82
TM4	0.68	0.69	0.70	0.73	0.79	0.74

Figure 26 summarizes the analysis of the simulated CO concentrations over Europe. It shows the latitudinal gradients of CO in the three altitude regimes shown in Figures 24 and 25 and for three decadal mean periods during the 41-year RETRO interval. While the models show generally consistent behaviour (as already diagnosed above), there are some differences in particular with respect to the gradient between 50°N and 60°N . LMDz-INCA exhibits the steepest gradient in the boundary layer and TM4 has the lowest gradient. LMDz-INCA is the only model that shows lower concentrations north of 55°N in the free troposphere, while the other models have either constant or slightly higher concentrations in this latitude region.

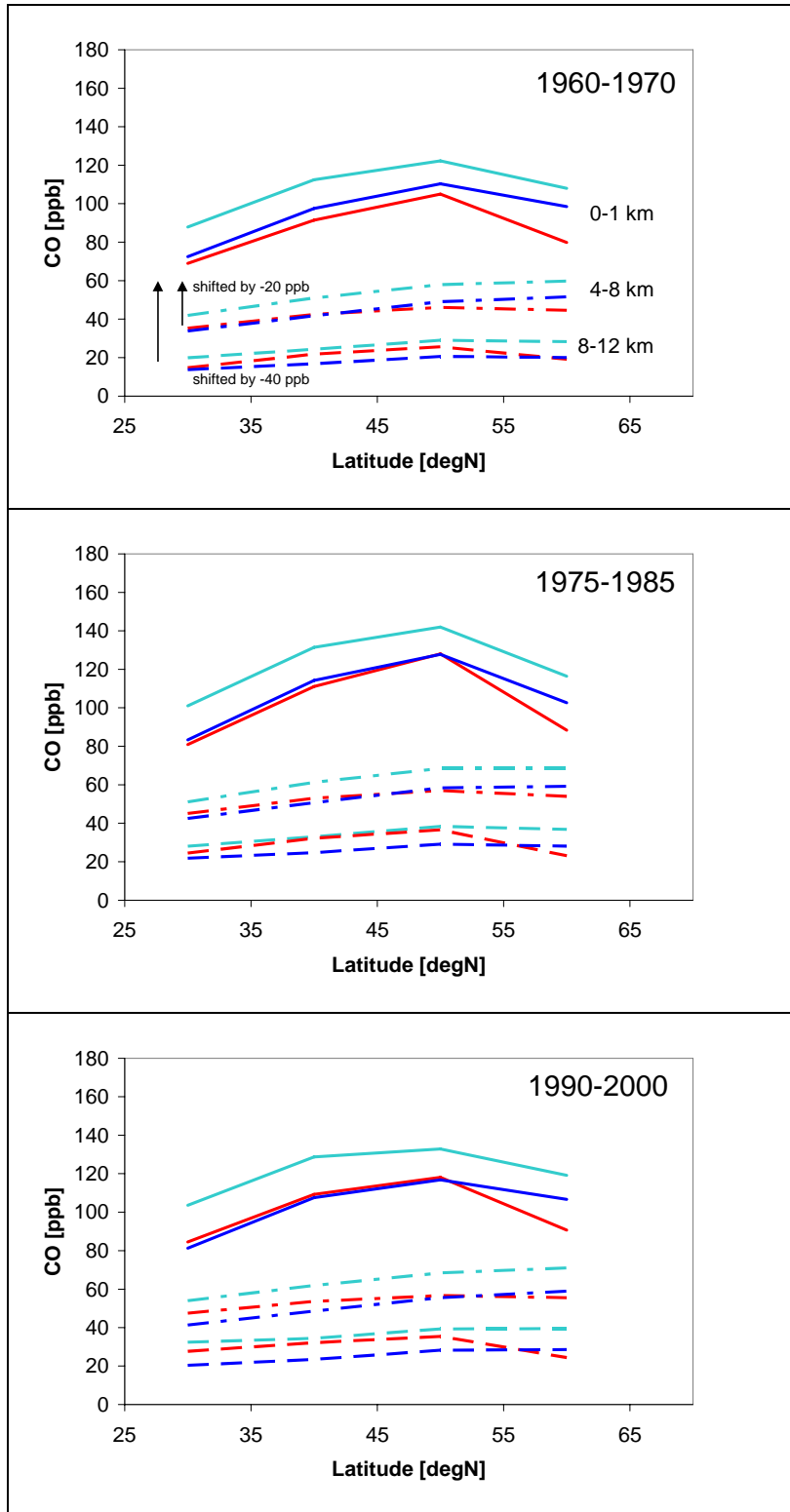


Figure 26: Latitudinal distributions of summertime CO concentrations over Europe averaged over three 11-year periods and in three altitude regimes. Red lines: LMDz-INCA, light blue lines: ECHAM5-MOZ, dark blue lines: TM4. Note that the lines for 4-8 km have been shifted by -20 ppb and those for 8-12 km by -40 ppb for clarity.

Ozone

Like the simulation of CO in the boundary layer, the computed concentrations of ozone in the wintertime boundary layer also show some consistency (Figure 27). In particular the two general circulation models ECHAM5-MOZ and LMDz-INCA run in parallel for almost all regions and throughout the 41-year RETRO period. The chemistry transport model TM4 exhibits more variability (especially before 1980) and it doesn't always co-vary with the other two models.

All models simulate a general increase in the wintertime boundary layer ozone concentrations over all three regions and in all latitude bands. This increase varies between 3 and 8 ppb between the years 1960 and 2000 (12-25%). Most of the increase occurred between 1960 and 1970. Thereafter the large interannual variability makes it difficult to reliably determine a robust trend signal. The weakest increase is observed in the northernmost latitudes over Europe and East Asia, the strongest trend signal can be found in the lowest latitude band over East Asia.

Figure 28 shows the corresponding analysis for summertime boundary layer ozone concentrations. Interestingly, the models often show even better consistency in these time series than for the wintertime data (please note the different y-axis scales, however). On the other hand, the spread between the absolute concentrations is much larger in some regions, especially over North America in the southernmost latitudes. Typically, ECHAM5-MOZ and TM4 follow each other quite closely, whereas LMDz-INCA often yields somewhat lower concentrations. Three exceptions are the latitude band 45-55 °N over Europe, where ECHAM5-MOZ and LMDz-INCA are closer together, the latitude band 35-45 °N over North America, where LMDz-INCA and TM4 are closer (and ECHAM5-MOZ exhibits a much higher variability than the other two models) and the latitude band 25-35 °N over North America, where TM4 falls in the middle between the other two models.

Again, all models simulate increasing ozone concentrations over time in practically all regions. This summertime increase typically lasted longer than the increase in winter: In the lower and mid-latitudes over Europe and North America the slope begins to flatten between 1985 and 1990, while East Asia exhibits a continuous rise in the boundary layer ozone concentrations according to the models.

The interannual variability of the summertime boundary layer ozone concentrations is generally less than the variability in winter. One noteworthy exception is the strong signal from boreal forest fires observed in the northern latitudes over East Asia and to some extent also over North America.

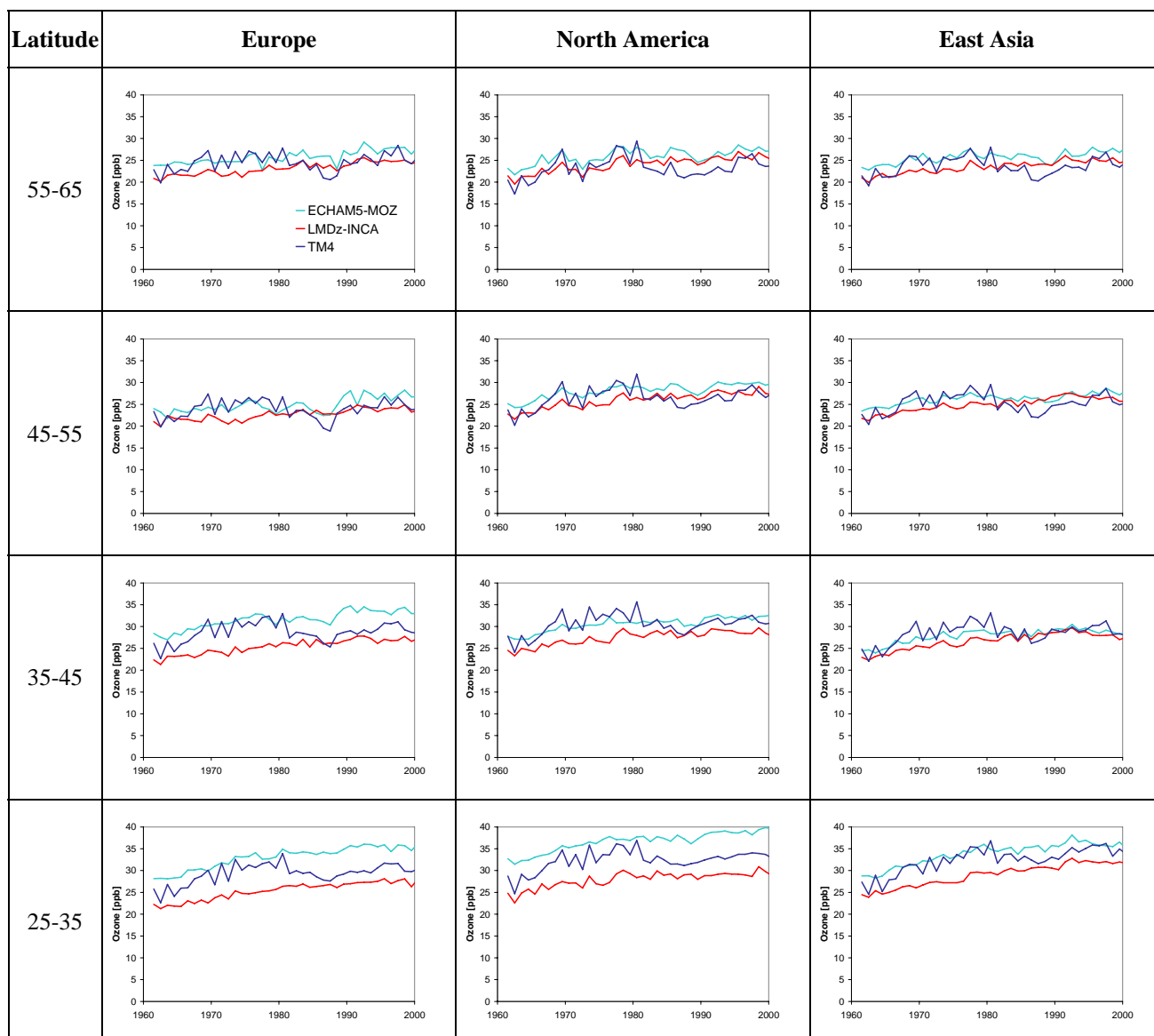


Figure 27: Time series of wintertime boundary layer ozone concentrations simulated by the three RETRO reanalysis models. For details on the region definitions, see text

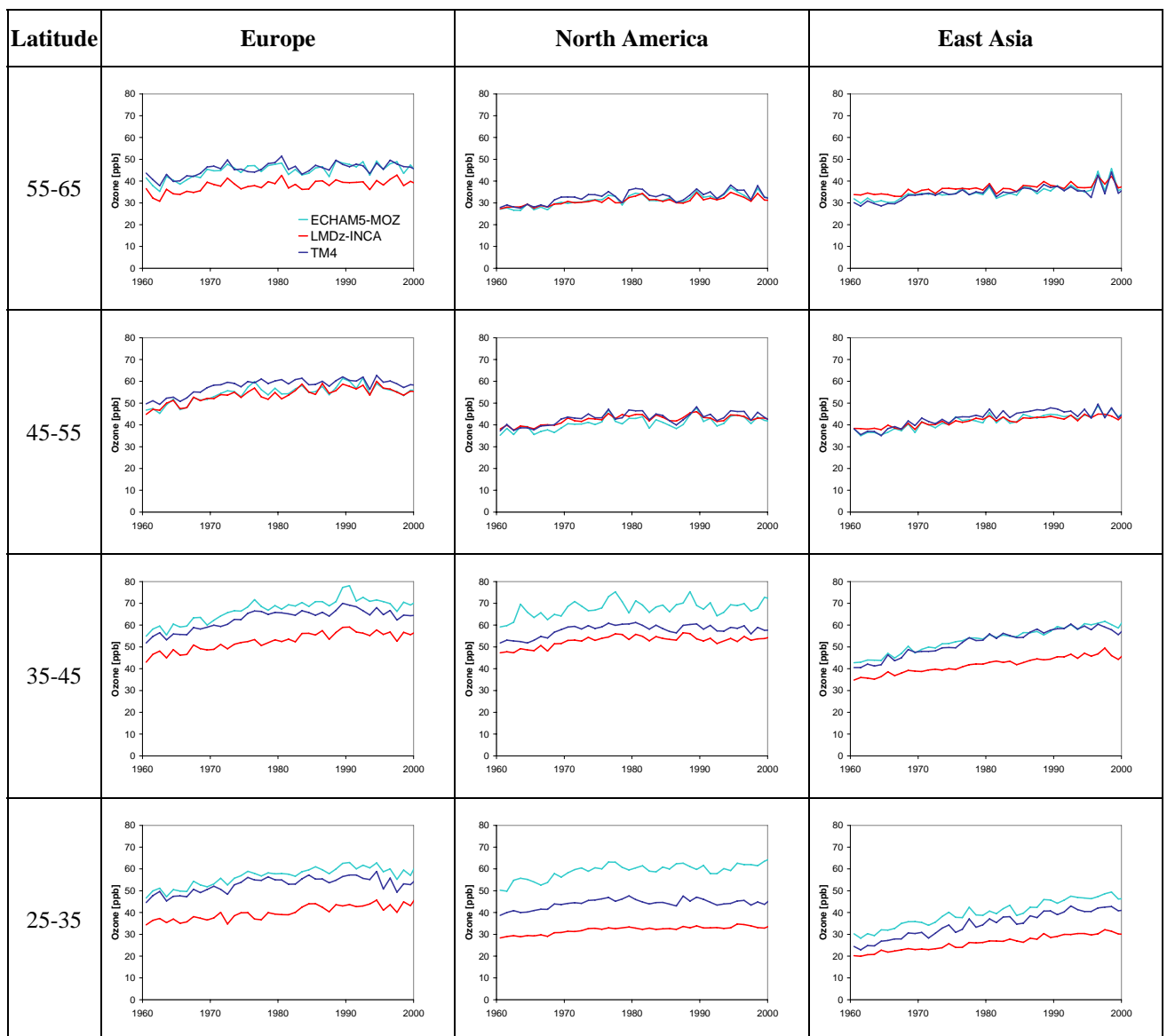


Figure 28: As Figure 27, but for summertime boundary layer ozone concentrations

Figure 29 (on the next page) summarizes the decadal mean trends in the boundary layer summertime ozone concentration over Europe as calculated by the three individual models. All models show the highest ozone concentrations in the 35-45 °N band and the lowest concentrations at northern latitudes. Also, all models yield higher ozone concentrations in the decade of the 1990s than during the 1960s. However, while ECHAM5-MOZ and TM4 generate very similar concentrations for the period 1975-1985 as for 1990-2000, the LMDz-INCA model shows a continuous increase. In LMDz-INCA the concentrations in the latitude band 45-55 °N are almost identical to those at 35-45 °N, while the other two models yield lower concentrations at 45-55 °N, resembling more the concentrations between 25 °N and 35 °N. The spread between the models ranges from about 15 ppb or 35% (lower latitudes in the 1960s) to almost 20 ppb or 20% (lower mid-latitudes around 1980).

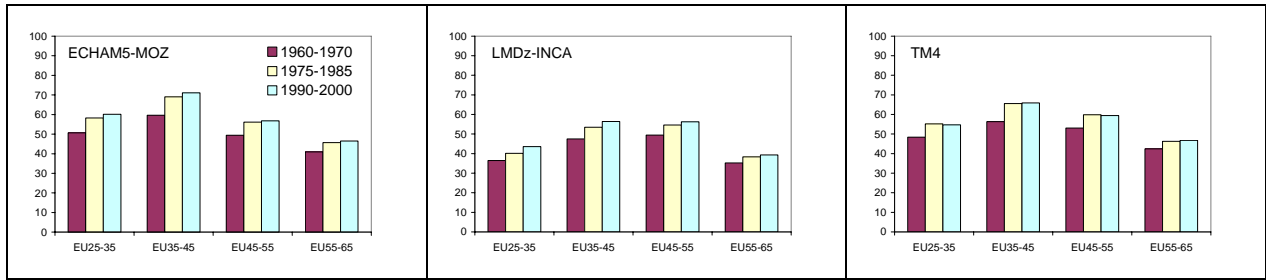


Figure 29: Decadal mean concentrations of boundary layer (0-1 km) ozone over Europe as simulated by the three individual models. The data are presented for the four latitude bands defined in the text

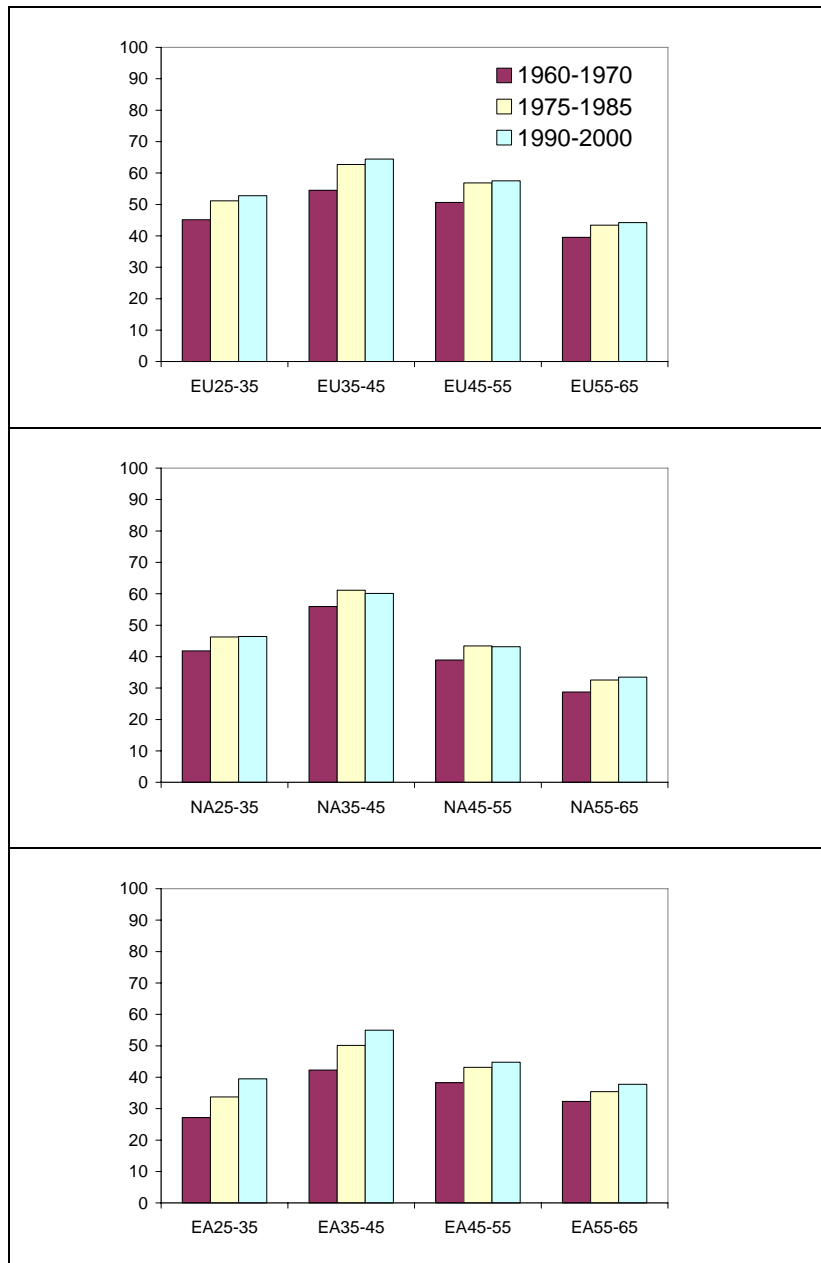


Figure 30: Decadal mean concentrations of boundary layer (0-1 km) ozone over Europe (top), North America (center) and East Asia (bottom) as derived from the mean results of the three individual models

Past experience has shown that the ensemble mean model result normally generates the most robust estimate of atmospheric state variables. Figure 30 therefore displays the mean-model trends for summertime boundary layer ozone for all the regions described above. According to our simulations the highest ozone values are found in the Mediterranean latitudes over Europe and ozone concentrations have increased by more than 10 ppb in this region since the 1960s. Central Europe and the northern part of the United States (including in particular the East coast urban agglomerations of New York and Washington) exhibit the second-highest ozone concentrations and experienced a similar rise over time. Up to the year 2000, the simulated boundary layer ozone concentrations over East Asia remained somewhat lower than over Europe and North America, but this region experiences the strongest increase, in particular in the latitude band 35-45 °N, where the values in the 1990s have come close to those over central Europe or the United States.

Future studies using the RETRO simulation results will have to carefully assess the quality of the mean-model results by comparing them to independent observational data sets. Here we only present a short analysis of data from the Global Atmosphere Watch (GAW) station Hohenpeissenberg in comparison with the ECHAM5-MOZ results. Ozone concentrations at Hohenpeissenberg were measured since the 1970s, and the data set therefore provides a valuable benchmark for the model simulations. The measurement station is located on a mountain top and is occasionally influenced by boundary layer air, but it also samples air from the free troposphere. In order to minimize spurious trend signals due to sampling artefacts, we performed separate evaluations for summertime and wintertime data and for daytime (well mixed boundary layer) and night-time (stable boundary layer) situations. The model results were sampled in the grid box that is closest to the measurement site and at the pressure level where temperature observations matched the simulated (ERA-40) temperatures best.

Figure 31 shows the temporal trend of the daytime and night-time ozone concentrations at Hohenpeissenberg from the model and from the observations. The winter trend is shown in the top panel and the summertime trend in the bottom panel. The mean wintertime concentrations in the model are in reasonable agreement with the observations. The simulated values agree excellently with the measured values for the early 1970s. Thereafter, the observations show a steady and significant increase, which is absent from the model simulation. There is only a very small difference between the daytime and night-time data in the observations, whereas the model has a larger diurnal cycle. Some features of the interannual variability are reproduced by the model (e.g. the peak concentrations in the year 1990), but the overall correlation is rather poor. Further sensitivity runs are needed to find out the reasons for these differences. Our speculation is that the interannual differences are largely driven by the ERA-40 meteorology, whereas the discrepancy in the long-term trend may be due to errors in the emission data or biases in the model parameterisations (e.g. underestimated impact of long-range transport or unaccounted changes in the exchange between the stratosphere and the troposphere).

In summer the simulated ozone concentrations in ECHAM5-MOZ are generally higher than the observed values. The difference is approximately 10 ppb for the late 1990s. Linking this to the analysis of ozone trends from all three models (Figure 28), the evaluation with the Hohenpeissenberg data indicates that the concentrations of LMDz-INCA are closest to reality for this time period. Similar to the wintertime situation, the model tends to produce a rather flat curve after 1975 or so, whereas the measurements show a constant increase in time, interrupted by outstanding peaks in 1993 (not captured by the model) and 2003 (beyond the RETRO period). This indicates that some source of the European ozone trend is missing from the RETRO boundary conditions.

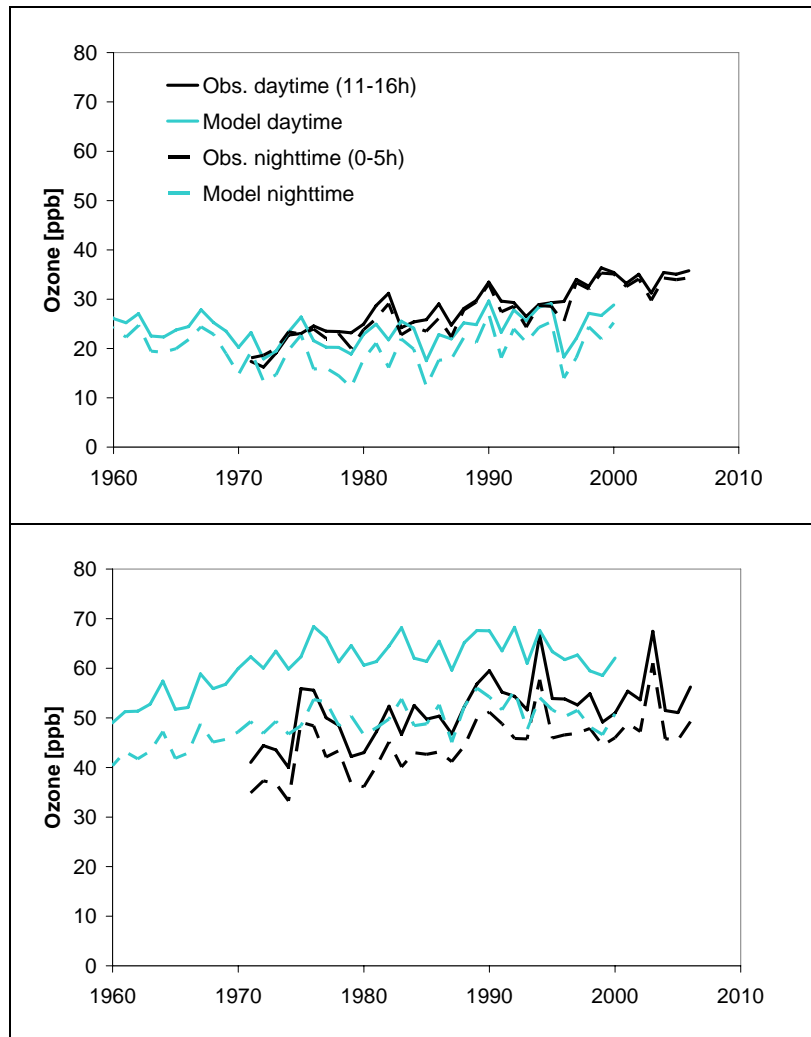


Figure 31: Comparison of wintertime (top) and summertime (bottom) ozone concentrations for the GAW station Hohenpeissenberg (11.0 E, 47.8 N, 977 m asl). The measurements are hourly averages, while the data from the ECHAM5-MOZ simulation are 3-hourly values representative for 20 minutes each. Observational data courtesy Stefan Gilge and Harald Flentje, DWD

In Figure 32, we compare the correlation between the seasonal mean temperature and the seasonal mean ozone concentrations at Hohenpeissenberg. Unfortunately, the observed temperature record available to us ranges only from 1995 to 2005 so that a 1:1 comparison is presently impossible. Generally, the observational data has a lower spread than the model results and shows almost no correlation between ozone and temperature, whereas the model yields a reasonably strong correlation. This may be caused by a few outlier data points where average temperatures around 17 °C were recorded. We excluded the extreme value of the year 2003 (mean temperature above 18.5 °C) from the fit of the observational data. If this point had been included, the slope of the fit to the measurements would be very similar to the model slope. Clearly this analysis should be repeated when the full temperature record from the Hohenpeissenberg station becomes available.

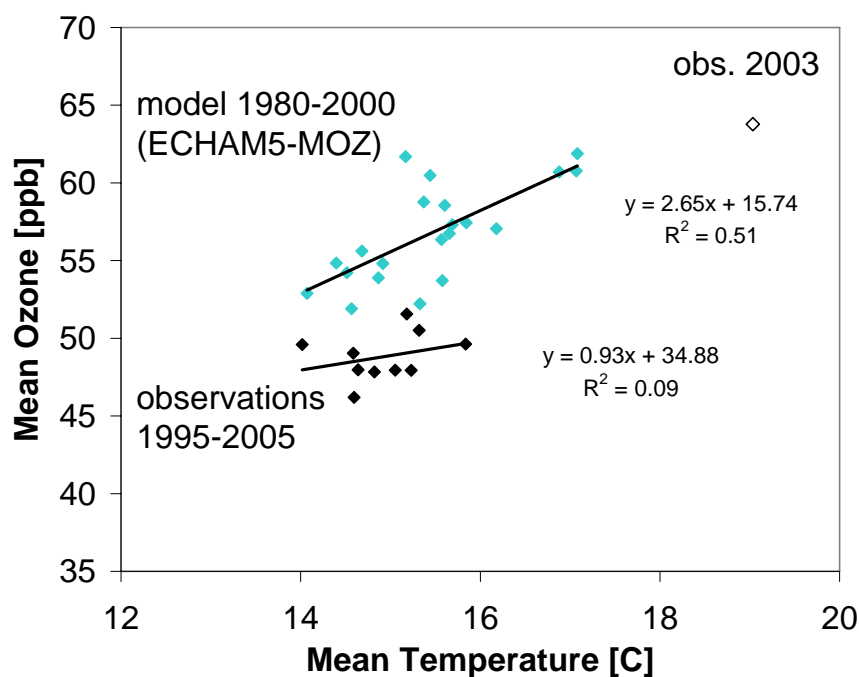


Figure 32: Correlation between seasonal mean summertime temperatures and ozone concentrations for the GAW station Hohenpeissenberg. Note that the observational data and the model results cover different time periods. The exceptional values of the summer 2003 were excluded from the linear fit of the observational data. Data courtesy Stefan Gilge and Harald Flentje, DWD

5. Conclusions

In the RETRO project, the first comprehensive global long-term tropospheric chemistry integrations covering a time period of 4 decades were performed with the objective to both reproduce and understand the trends and variability of the tropospheric chemical composition. These simulations, based on ERA-40 meteorological data, were made possible thanks to the development of original and consistent emission datasets (RETRO work package 1) tailor-made to incorporate long term trends in anthropogenic emissions as well as the interannual variability of large global sources such as biomass burning.

Three state-of-the-art global atmospheric chemistry models were used to achieve the reanalysis of the tropospheric chemical composition over the last 40 years. Two of the models are general circulation models (ECHAM5-MOZ, LMDz-INCA), while the third one is a chemistry transport model (TM4). In addition, two other CTMs (CTM2 and p-TOMCAT) were used to simulate time slices for specific years and to investigate variability patterns in the late 1990s.

The long-term simulations formed the central part of the RETRO project. Unfortunately their start was delayed, because of unforeseen difficulties in generating the required emission data sets. Once completed, the simulations were analysed and evaluated with several observational data sets. The ability of the models to reproduce seasonal cycle of ozone, carbon monoxide and nitrogen dioxide was investigated using ground based stations (WOUDC, CMDL, EMEP), ozone sonde data as well as satellite measurements. In the course of this analysis

errors were detected in all three model simulations which mandated a rerun of the simulations. The results from these final runs are described in this report together with the set-up of the experiments.

The three models show very good consistency in terms of the interannual variability and trend patterns, but the absolute concentrations of carbon monoxide, ozone and the hydroxyl radical differ substantially (up to 30% in certain regions). According to the LMDz-INCA model, maximum surface ozone concentrations increased by 0.8 ppb/year or more in Central America, Southern Europe and South and East Asia between 1960 and the year 2000. The trend in summertime mean ozone concentrations in the boundary layer is somewhat smaller. All three models predict an increase between 5 and 15 ppb over Europe, North America and East Asia south of 55° N for the time period 1960-2000.

The simulated interannual ozone variability patterns during the 1990s compare well with data from the MOZAIC aircraft sampling programme and CO concentrations agree with monthly mean variability patterns derived from the NOAA ESRL Cooperative Sampling Network. A comparison of the ECHAM5-MOZ results with a long-term ozone record from the Global Atmosphere Watch station Hohenpeissenberg indicates however, that some factors leading to a general increase in the observed ozone concentrations are absent from the model simulations. A similar conclusion was reached based on an analysis of mountain site measurements at Jungfraujoch and Zugspitze and comparison with earlier model results (C. Ordóñez, unpublished manuscript; see also Annex A3).

Over Europe, the decadal mean simulated summertime boundary layer ozone concentrations increased by about 10 ppb in the Mediterranean region (latitude band 35°-45° N) and by 4-7 ppb north of 45° N between the 1960s and 1990s. This corresponds to a relative change of 18.2% (16.8-19.1% range in the individual models) in the Mediterranean region, 13.5 % (12.0-14.8%) from 45° N to 55° N and 11.8% (10.1-13.7%) from 55° N to 65° N. These results are remarkably consistent between the models. Taking into account the results from the comparison with mountain stations described above, these trends may yet underestimate the real changes in boundary layer ozone.

According to the model simulations, the largest increase in ozone concentrations over Europe and North America occurred between 1960 and 1970. Thereafter, the curves flatten out, but despite a wealth of measures to curb regional air pollution beginning during the 1980s, there are no indications of a general decrease in ozone concentrations. This is consistent with earlier findings that peak ozone concentrations in pollution episodes may have declined, but the so-called background concentrations continue to rise (see EUROTRAC Synthesis report, 2003). In fact, the recent summers of 2003 and 2006 exhibited a number of ozone episodes which rival those in the 1980s and 1990s. Due to the lack of time, no further sensitivity runs could be performed which might have shed some light on the reasons for the increasing background trend and for the apparent underestimation of this trend in the models. Current hypotheses are: (i) errors in the prescribed precursor emission trends, (ii) changes in the transport patterns and stratosphere-troposphere exchange of ozone or (iii) a substantial role of changing methane concentrations.

The strongest increase in boundary layer ozone trends is simulated for the East Asian region. While the ozone concentrations here were only about 2/3 of the values in Europe and North America in the 1960s, they have reached comparable levels during the 1990s. This problem has become even more pressing over the past few years due to the rapid economic growth in China. Comparisons of NO₂ emission trends over China with tropospheric NO₂ columns observed from space (see RETRO deliverable D1-6) indicate that the RETRO inventory severely underestimates the strong recent increase in ozone precursor emissions after 1996.

References

- Arellano AF, Kasibhatla PS, Giglio L, van der Werf GR, Randerson JT (2004) Top-down estimates of global CO sources using MOPITT measurements *Geophys. Res. Lett.* 31 (1): Art. No. L01104.
- Brasseur, G.P., X.X. Tie, P.J. Rasch, F. Lefevre (1997), A three-dimensional simulation of the Antarctic ozone hole: Impact of anthropogenic chlorine on the lower stratosphere and upper troposphere, *J. Geophys. Res.*, 102 (D7): 8909-8930.
- Brunner, D., J. Staehelin, H. L. Rogers, M. O. Köhler, J. A. Pyle, D. Hauglustaine, L. Jourdain, T. K. Berntsen, M. Gauss, I. S. A. Isaksen, E. Meijer, P. van Velthoven, G. Pitari, E. Mancini, V. Grewe, R. Sausen, An Evaluation of the Performance of Chemistry Transport Models by Comparison with Research Aircraft Observations. Part 1: Concepts and overall Model Performance, submitted to *Atmos. Chem. Phys.*, 2003.
- Dameris, et al. (2005), Long-term changes and variability in a transient simulation with a chemistry-climate model employing realistic forcing, *Atmos. Chem. Phys.*, 5, 2121-2145.
- Erickson, D. J. and Taylor, J. A. (1992), 3-D Tropospheric CO Modeling: the possible influence of the Ocean, *Geophys. Res. Lett.*, vol. 19, no 19, pp. 1955 - 1958
- Eyring, V., et al. (2006), Assessment of temperature, trace species, and ozone in chemistry-climate model simulations of the recent past, *J. Geophys. Res.*, 111, D22308, doi:10.1029/2006JD007327.
- Fishman J., J. M. Hoell Jr., R. D. Bendura, R. J. McNeal, V. W. J. H. Kirchhoff, NASA GTE TRACE A Experiment (September-October 1992): Overview, *J. Geophys. Res.* 101 (D19), p. 23,865-23,879, 1996.
- Folberth, G., D.A. Hauglustaine, J.Lathière, and F.Brocheton (2005), Impact of biogenic hydrocarbons on tropospheric chemistry: results from a global chemistry-climate model, *Atmos. Chem. Phys. Dis.*, 5, 1680-7375/acpd/2005-5-10517.
- Fortuin, J.P.F., and H. Kelder (1998), An ozone climatology based on ozonesonde and satellite measurements, *J. Geophys. Res.*, 103(D24), 31,709-31,734.
- Gettelman, A., J. R. Holton, and K. H. Rosenlof (1997), Mass fluxes of O₃, CH₄, N₂O and CF₂Cl₂ in the lower stratosphere calculated from observational data, *J. Geophys. Res.* 102, 19,149-19,159,.
- Guenther, A., C. N. Hewitt, T. Pierce, B. Lamb, P. Harley, and R. Fall, A global model of natural volatile organic compound emissions, *J. Geophys. Res.*, 100, 8873-8892, 1995.
- Hauglustaine, D. A., F. Hourdin, L. Jourdain, M.-A. Filiberti, S. Walters, and J.-F. Lamarque (2003), Interactive chemistry in the Laboratoire de Météorologie Dynamique general circulation model: description and background tropospheric chemistry evaluation, *J. Geophys. Res.*, D4 doi:10.1029/2003JD003,957.
- Horowitz, L. W., et al. (2003), A global simulation of tropospheric ozone and related tracers: Description and evaluation of MOZART, version 2, *J. Geophys. Res.*, 108(D24), 4784, doi:10.1029/2002JD002853.
- Kylling, A., Albold, A., and Seckmeyer, G. (1997), Transmittance of a cloud is wavelength – dependent in the UV-range: Physical interpretation, *Geophys. Res. Lett.*, 24(4), 397–400.

- Lathiere, J., D. A. Hauglustaine, A. Friend, N. DeNoblet-Ducoudre, N. Viovy, and G. Folberth (2005), Impact of climate variability and land use changes on biogenic volatile organic compound emissions, *Atmos. Chem. Phys.*
- Law, K. S., P. H. Plantevin, D. E. Shallcross, H. L. Rogers, J. A. Pyle, C. Grouhel, V. Thouret, and A. Marenco (1998), Evaluation of modeled O₃ using Measurement of Ozone by Airbus In-Service Aircraft (MOZAIC) data, *J. Geophys. Res.*, 103, 25721-25737.
- Lin, S.-J., and R. B. Rood (1996), Multidimensional flux-form semi-Lagrangian transport schemes, *Mon. Weather Rev.*, 124, 2046–2070.
- Nordeng, T. E. (1994), Extended versions of the convective parameterization scheme at ECMWF and their impact on the mean and transient activity of the model in the tropics, Tech. Memo. 206, Eur. Cent. Medium-Range Weather Forecasts, Reading, U. K.
- Novelli, P. et al., CO trends from the NOAA Cooperative Sampling Network, *IGAC Newsletter*, 2003.
- Pétron G., C. Granier, B. Khattatov, V. Yudin, J. F. Lamarque, L. Emmons, J. Gille, D. Edwards, Monthly CO surface sources inventory based on the 2000-2001 MOPITT satellite data, *Geophys. Res. Lett.*, Vol. 31, L21107, doi:10.1029/2004GL020560, 2004.
- Prather, M. J. (1986), Numerical advection by conservation of second-order moments, *J. Geophys. Res.*, 91, 6671–6681.
- Price, C., and D. Rind, A simple lightning parameterization for calculating global lightning distributions, *J. Geophys. Res.*, 97, 9919-9933, 1992.
- Röckner, E., et al. (2003), The atmospheric general circulation model ECHAM 5. Part I: Model description, Rep. 349, Max Planck Inst. for Meteorol., Hamburg, Germany. (Available at http://mpi-web.dkrz.de/de/web/science/a_reports_archive.php?actual=2003#)
- Russell, G. L., and J. A. Lerner (1981), A new finite-differencing scheme for the tracer transport equation, *J. Appl. Meteorol.*, 20, 1483–1498.
- Sander, S. P., et al. (2003), Chemical kinetics and photochemical data for use in stratospheric modeling, evaluation 14, *JPL Publ.* 02-25.
- Schultz M.G., A. Heil, J.J. Hoelzemann, A. Spessa, K. Thonicke, J. Goldammer, A. C. Held, and J. M. C. Pereira, Global Emissions from Wildland Fires from 1960 to 2000, submitted to *Glob. Biogeochem. Cycl.*, 2007.
- Sinha P., L. Jaeglé, P. V. Hobbs, Q. Liang, Transport of biomass burning emissions from Southern Africa, *J. Geophys. Res.* 109, D20204, doi:10.1029/2004JD005044, 2004.
- Spivakovsky, C. M., et al. (2000), Three-dimensional climatological distribution of tropospheric OH: Update and evaluation, *J. Geophys. Res.*, 105(D7), 8931–8980.
- Stockwell, D. Z., C. Giannakopoulos, P. H. Plantevin, G. D. Carver, M. P. Chipperfield, K. S. Law, J. A. Pyle, D. E. Shallcross, and K. Y. Wang (1999), Modelling NO_x from lightning and its impact on global chemical fields, *Atmos. Environ.*, 33, 4477-4493.
- Streets, D. G., K. F. Yarber, J.-H. Woo, and G. R. Carmichael, Biomass burning in Asia: Annual and seasonal estimates and atmospheric emissions, *Global Biogeochem. Cycles*, 17(4), 1099, doi:10.1029/2003GB002040, 2003.
- Sundet, J. K. (1997), Model studies with a 3-D global CTM using ECMWF data, Ph.D. thesis., Dep. of Geophys., Univ. of Oslo, Oslo.

Tian, W.S., M.P. Chipperfield (2005), A new coupled chemistry-climate model for the stratosphere: The importance of coupling for future O₃-climate predictions, *Q. Roy. Met. Soc.*, 131 (605): 281-303.

Tiedtke, M. (1989), A comprehensive mass flux scheme for cumulus parameterization in large-scale models, *Mon. Weather Rev.*, 117, 1779–1800.

Tian, W., and M. P. Chipperfield (2005), A new coupled chemistry-climate model for the stratosphere: The importance of coupling for future O₃-climate predictions, *Q. J. R. Meteorol. Soc.*, 131, 281-304.

van Leer, B. (1977), Toward the ultimate conservative difference scheme. Part IV: A new approach to numerical convection, *J. Comput. Phys.*, 23, 276–299.

van Noije, T.P.C., A. Segers, and P.F.J. van Velthoven (2006), Time series of the stratosphere-troposphere exchange of ozone simulated with reanalyzed and operational forecast data, *J. Geophys. Res.*, 111, D03301, doi:10.1029/2005JD006081.

van Noije, T.P.C., H.J. Eskes, M. van Weele, and P.F.J. van Velthoven (2004), Implications of the enhanced Brewer-Dobson circulation in European Centre for Medium-Range Weather Forecasts reanalysis ERA-40 for the stratosphere-troposphere exchange of ozone in global chemistry transport models, *J. Geophys. Res.*, 109, D19308, doi:10.1029/2004JD004586.

Van Aardenne, J. A., F. J. Dentener, J. G. J. Olivier, C. G. M. Klein Goldewijk, and J. Lelieveld (2001), A 1x1 degree resolution data set of historical anthropogenic trace gas emissions for the period 1890-1990, *Global Biogeochem. Cycles*, 15, 909_929.

Yienger, J. J., and H. Levy II (1995), Empirical model of global soil-biogenic NO_x emissions, *J. Geophys. Res.*, 100, 11,447-11,464,.

Annex: Additional analyses performed with earlier model simulations

A1. Intercomparison of seasonal signals

In this section comparisons between the seasonal cycles simulated by the models and CMDL data were done for O₃ and CO for 1997. These preliminary simulations were performed during the test phase prior to the availability of RETRO emissions. The simulations were done with the POET emissions.

Surface Ozone - CMDL

There appears to be strong evidence for the impact of halogen chemistry on the Barrow observations with springtime concentrations being well below the range of all model calculations. The raw hourly data contain many periods when zero concentrations of ozone are observed and this is consistent with previous observations (e.g. Bottenheim et al, 2002) which have explained this as a result of a rapid increase in Bromine concentrations. As none of the models contain these chemical reactions they are unable to reproduce these very low ozone events and so the monthly means are too high.

It is not possible to say that any one model shows clearly better results than all others. The models generally capture the seasonal cycle of the observations although at almost all sites the concentrations in p-TOMCAT are much too high. The ozone peak in July/August at Mauna Loa seen in ECHAM5-MOZ and Oslo CTM is not observed in either the other models or the measurements. There does not appear to be a consistent picture of model performance with a model that does well at one station (e.g. p-TOMCAT at Samoa) doing very badly at another (e.g. at Barrow). However in general LMDZ, TM4 and p-TOMCAT seem to give the best results at these stations for ozone.

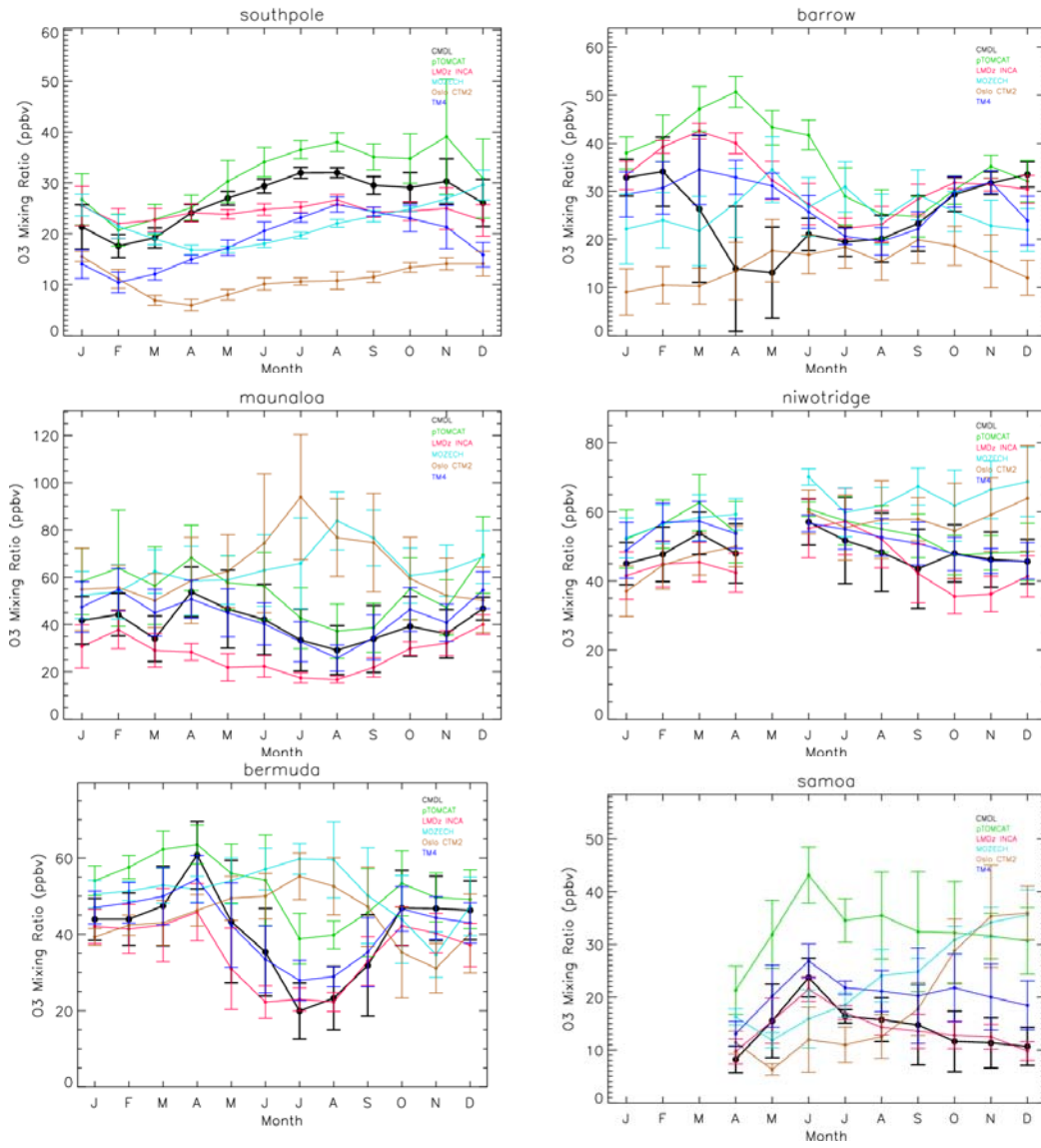


Figure A1: Model comparison to surface ozone data for 1997

Carbon Monoxide - CMDL

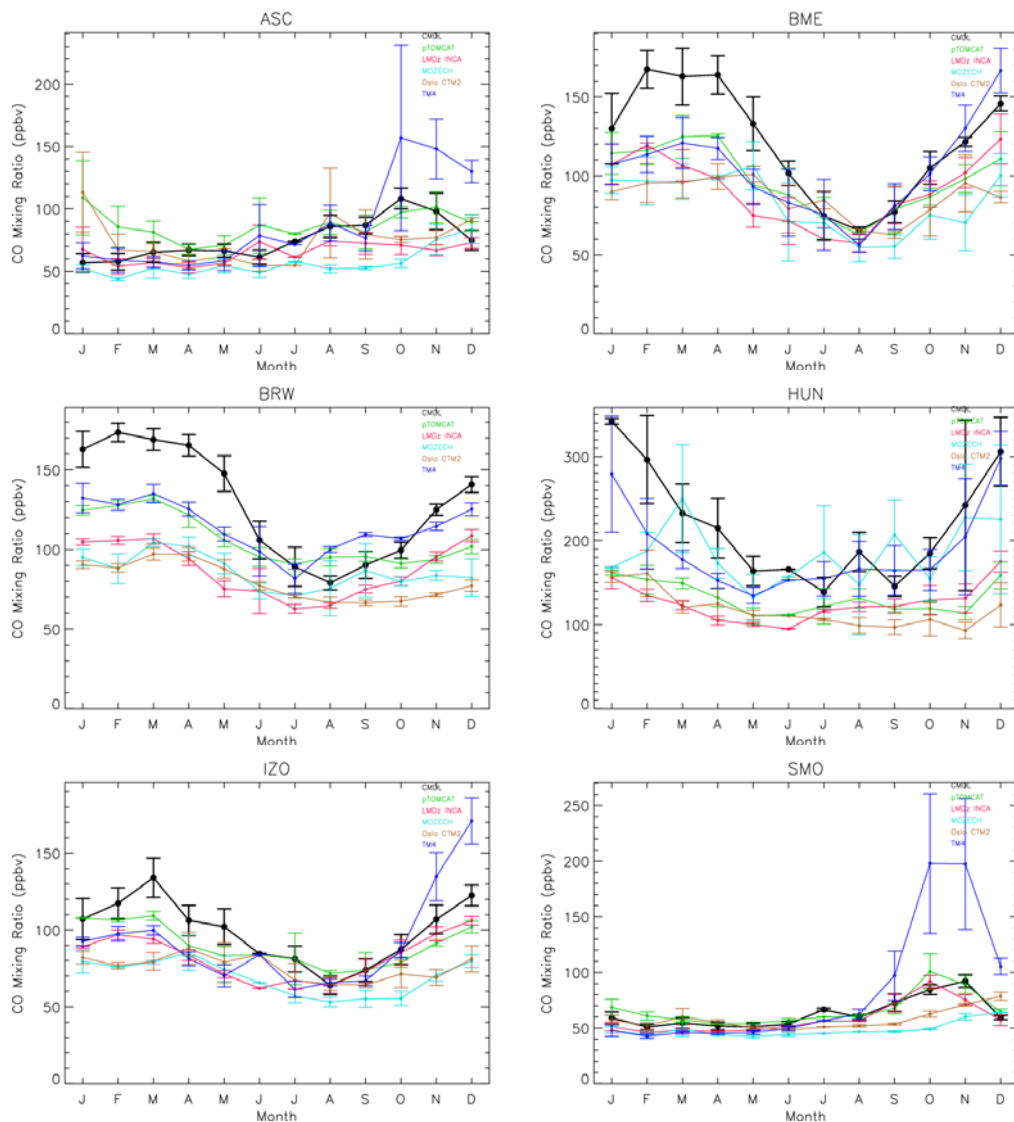


Figure A2: CO concentrations at selected CMDL sites for 1997

It can be seen from these plots that although the models generally reproduce well the general timing of the seasonal cycles, there is a large range in the modelled concentrations and at large number of sites the model concentrations are all consistently smaller than the observations. The most dramatic signal is the response to large biomass burning in Indonesia seen in the TM model at the Samoa (SMO) site. This is discussed in more detail in D3-4.CO concentrations in TM are in general higher than the other models but at many sites still do not have concentrations as large as in the observations. The exception to this seems to be in the latter months of the year when at some southern hemisphere sites TM does have much larger CO concentrations probably due to the influence of the fires.

Evolution of the O₃ seasonal cycle

Figures A3 and A4 show the evolution of the lowest and highest monthly means for the first year of each decade. These results were obtained by LMDz-INCA with the V2 emission dataset. In the Southern hemisphere, the minimum monthly means appear to have been almost unchanged during the 40 years whereas the highest monthly means have slightly increased over oceans during the sixties. Concerning the Northern hemisphere, the minimum values as well as the maximum have strongly increased during the sixties and seventies over both

oceans and continents. During the eighties and nineties, minimum monthly means continued to increase over Asia and, in a lesser extent, over United States. Maximum values are almost unchanged after 1980 except over southern oceans where a slight decrease is simulated. The annual minimum does not show any decrease and even continues to increase over Atlantic Ocean.

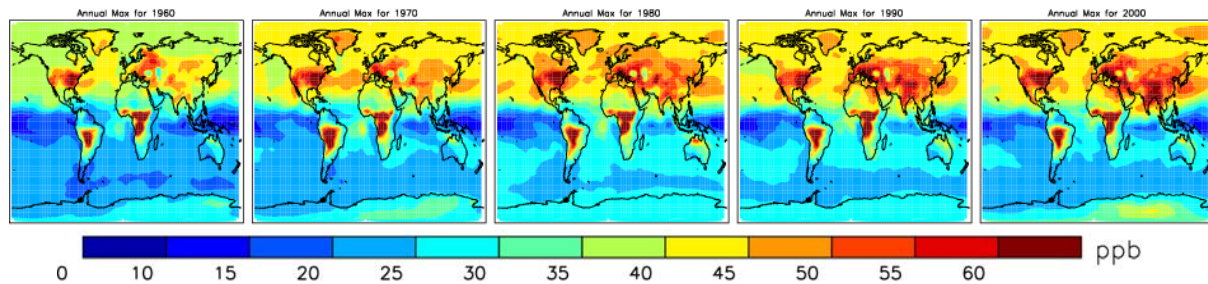


Figure A3: Annual highest monthly surface O_3 mean for 1960, 1970, 1980, 1990 and 2000 simulated with LMDz-INCA

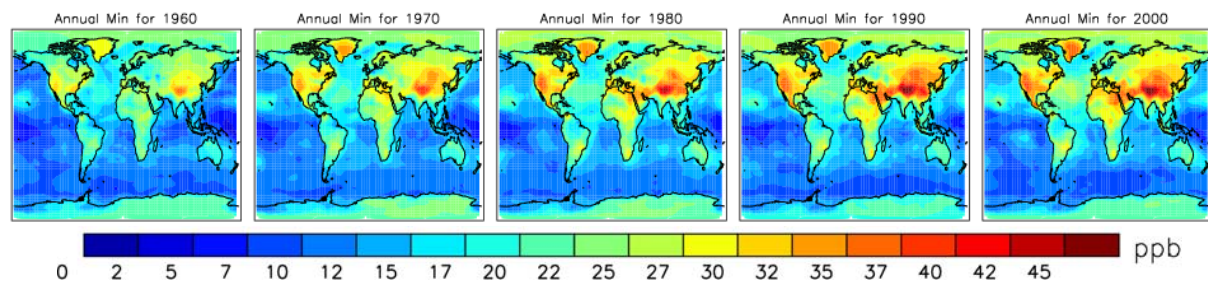


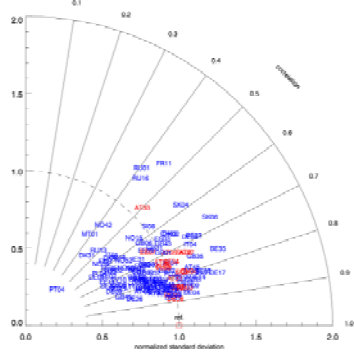
Figure A4: Annual lowest monthly surface O_3 mean for 1960, 1970, 1980, 1990 and 2000 simulated with LMDz-INCA

A2. Comparison with O_3 ground based measurements

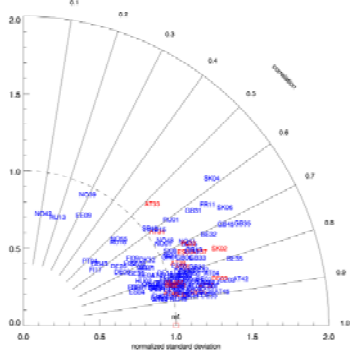
In order to check the ability of the different 3D global models involved in RETRO to reproduce the seasonal variations of the European surface ozone, their results for the nineties (based on V1 emissions) were compared by LSCE with the European EMEP data.

The measurements as well as the model results are averaged with a three day rolling mean in order to remove the high frequency variations. Figure A5 summarizes, with Taylor diagrams, the correlation and normalized standard deviations (i.e. $\sigma_{\text{mod}}/\sigma_{\text{obs}}$) obtained, at each EMEP stations, for each of the 5 models for the year 1997. For this year, the LMDz-INCA model seems to have the lowest dispersion of the points indicating in particular its ability to reproduce the standard deviation of the ozone observations. The results of the UiO, ECHAM5-MOZ and TM4 models are also fairly good whereas the TOMCAT results are quite scattered with some poor correlations at several stations.

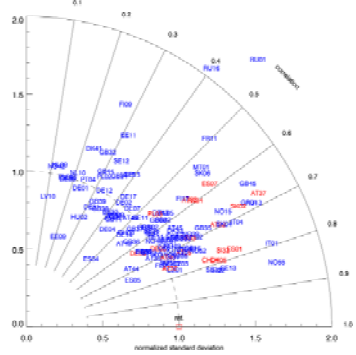
LMDz-INCA



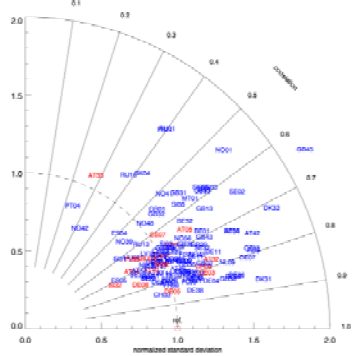
UiO



TOMCAT



ECHAM5-MOZ



TM4

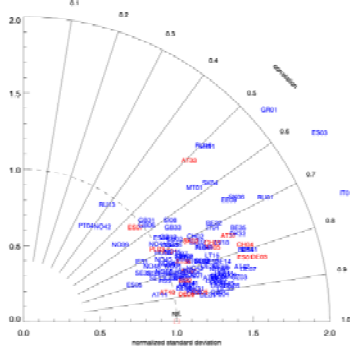


Figure A5: Taylor diagrams for 1997 with 3-day time filtered ozone mixing.

For a more quantitative analysis, the statistical results, averaged over the EMEP stations, for each year are displayed in the Table A1

Table A1: Summary statistics of the comparison with EMEP data for whole years of the nineties with 3-day time filtered ozone mixing ratios.

Criteria for good results highlighting						
	<10ppb	[0,9 ; 1,1]	>0,7			
Uio	Abs bias (ppb)	$\sigma_{\text{mod}}/\sigma_{\text{obs}}$	Correlation	Threshold 20%	Threshold 30%	
1996	7,39	0,94	0,69	0,49	0,67	
1997	6,74	1,06	0,77	0,53	0,70	
1999	7,30	0,99	0,67	0,52	0,71	
2000	6,87	0,97	0,69	0,53	0,71	
ECHAM5-MOZ	bias_abs	sdv_mod/std_obs	Correlation	Threshold 20%	Threshold 30%	
1990	12,68	1,19	0,72	0,24	0,36	
1991	11,84	1,20	0,68	0,28	0,42	
1992	13,16	1,06	0,73	0,25	0,37	
1993	12,45	1,16	0,73	0,28	0,41	
1994	12,23	1,10	0,72	0,29	0,43	
1995	11,93	1,17	0,67	0,31	0,45	
1996	11,11	1,11	0,68	0,34	0,48	
1997	11,08	1,13	0,70	0,34	0,48	
1998	10,62	1,14	0,69	0,36	0,52	
1999	10,59	1,11	0,66	0,38	0,54	
2000	11,85	1,14	0,68	0,32	0,46	
TOMCAT	bias_abs	sdv_mod/std_obs	Correlation	Threshold 20%	Threshold 30%	
1997	15,72	1,14	0,56	0,23	0,34	
1998	15,63	1,31	0,52	0,24	0,35	
1999	16,03	1,35	0,54	0,23	0,35	
2000	15,77	1,18	0,52	0,22	0,33	
INCA	bias_abs	sdv_mod/std_obs	Correlation	Threshold 20%	Threshold 30%	
1990	11,25	0,96	0,74	0,30	0,43	
1991	11,71	0,99	0,70	0,30	0,43	
1992	11,72	0,98	0,75	0,30	0,44	
1993	10,78	0,91	0,74	0,34	0,47	
1994	10,78	1,06	0,76	0,36	0,50	
1995	10,05	1,01	0,74	0,39	0,52	
1996	10,63	0,99	0,72	0,37	0,51	
1997	9,59	0,92	0,73	0,41	0,54	
1998	9,62	1,02	0,69	0,42	0,56	
1999	8,98	1,02	0,72	0,46	0,60	
2000	9,25	1,03	0,72	0,44	0,58	
TM4	bias_abs	sdv_mod/std_obs	Correlation	Threshold 20%	Threshold 30%	
1990	12,08	1,13	0,78	0,23	0,36	
1991	12,13	1,13	0,73	0,25	0,37	
1992	13,09	1,12	0,82	0,21	0,34	
1993	12,16	1,11	0,78	0,26	0,40	
1994	12,77	1,20	0,80	0,24	0,38	
1995	12,78	1,22	0,76	0,25	0,38	
1996	12,07	1,17	0,75	0,29	0,42	
1997	11,46	1,23	0,77	0,30	0,45	
1998	10,83	1,34	0,73	0,34	0,49	
1999	10,36	1,23	0,74	0,38	0,53	
2000	10,91	1,19	0,73	0,35	0,49	

These results show that the models reproduce the European 3 daytime filtered ozone with an absolute bias (one year average) ranging between 6.7 and 16 ppbv with the lowest bias obtained with UiO. For all models, except UiO, this corresponds to a positive bias due to overestimation of the ozone mixing ratio. Regarding the standard deviation ratio ($\sigma_{\text{mod}}/\sigma_{\text{obs}}$), showing the ability of the model to reproduce the amplitude of ozone variations, p-tomcat, TM4 and ECHAM5-MOZ overestimate this ratio whereas UiO and LMDz-INCA show an averaged ratio closed to one but resulting in a lesser extent from error compensations. The correlations lie between 0.53 for TOMCAT and 0.76 for TM4 (0.73=LMDz-INCA=0.73; UiO=0.71; ECHAM5-MOZ=0.70).

A3. Comparison with O₃ sondes

The scores of the models (using V1 emissions) compared with ozone sonde data were investigated in the D3.2 report.

Figure A6 (performed by C. Ordonez) depicts the ozone trends computed at Zugspitze and Jungfraujoch using ozone sonde measurement in the one hand and model results in the other hand. At Zugspitze, the interannual variability seems to be well captured by the three models (TM4, LMDzINCA, ECHAM5-MOZ). It is also the case at Junfraujoch except in 1991 where the negative anomaly is not reproduced by TM4 and LMDz-INCA. Regarding the trends, negative trends are deduced at both sites when using the model outputs whereas measurements at Zugspitze show a negative but closed to zero slope and measurements at Jungfraujoch show a positive trend. However, the uncertainties associated with these slope are of the same magnitude as the slopes themselves leading to difficulties to conclude on these tendencies.

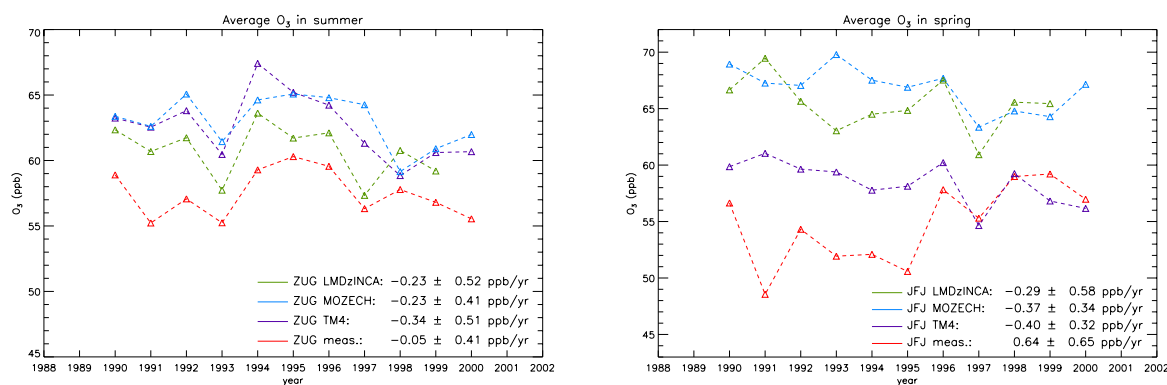


Figure A6: Ozone trends from sonde data and model results at Zugspitze (2960m) and Jungfraujoch (3580m) respectively for summer and spring

A4. Comparison with CO measurements

In order to assess simulated CO concentrations, the team from university of Cambridge performed comparisons with CMDL plus WOUDC data. The MQO score and Taylor analysis were applied to the model simulations of the time period 1997 to 2000.

Table A2 shows the model scores for various statistics averaged over all stations and 1997-2000 for carbon monoxide. All models have a negative bias which indicates either too large

OH concentrations in the models or emissions of CO which are too low. Given that the methane lifetime of the models are similar to those found in previous studies (or in the case of p-TOMCAT towards the upper end of the range) it seems likely that this indicates that the emissions of CO in the inventory are too low. TM4 has the highest MQO and LMDz-INCA the highest correlation coefficient.

Table A2: Model statistics for CMDL CO data averaged over all stations and years

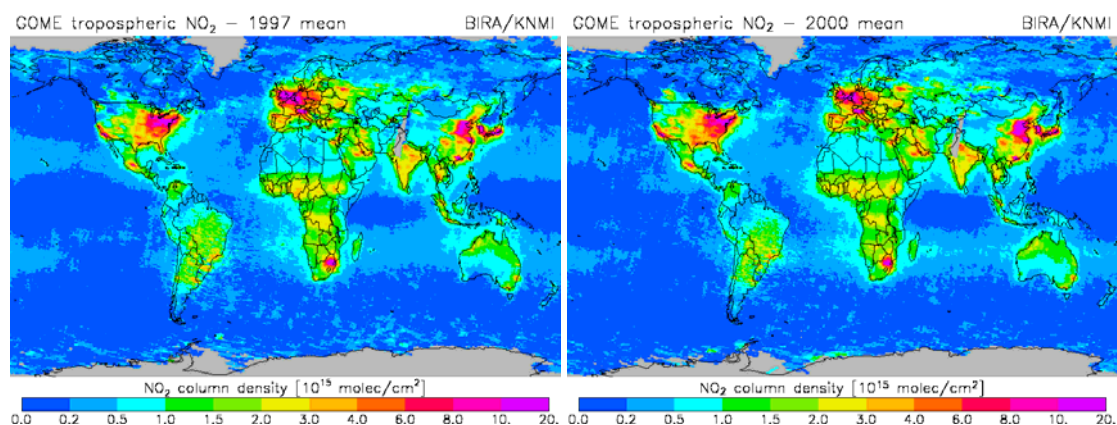
	PTOMCAT	LMDz INCA	ECHAM5-MOZ	UiO	TM	model mean
MQO 20%	0.44	0.41	0.35	0.31	0.58	0.41
Correlation coefficient	0.68	0.72	0.65	0.59	0.69	0.67
Bias (%)	-15.86	-22.12	-21.55	-20.33	-4.06	-16.79

A5. Comparison with satellite data

The GOME satellite data were used to evaluate the model simulations by comparing the NO₂ tropospheric column with the model ensemble results the years 1996-2000 in the one hand and by comparing the HCHO column simulated by LMDz-INCA and its interannual variability in the other hand.

NO₂ tropospheric columns

KNMI has performed an analysis based on the GOME NO₂ retrieval by BIRA/KNMI to investigate the extent and causes of variability of NO₂ concentrations during the 1990s. To systematically evaluate the models with the retrieval, the modelled 10:30 local time NO₂ columns are sampled at the time and place of the observations. The method of comparison is described in detail by van Noije et al. (2006), who also present an intercomparison of different GOME retrieval products for the year 2000. In Figure we present maps of the annual mean tropospheric NO₂ column densities for 1997 and 2000, comparing the BIRA/KNMI retrieval with the ensemble mean of the RETRO models (LMDz-INCA, ECHAM5-MOZ, p-TOMCAT, TM4, and UiO-CTM2). The spatial patterns of pollution are qualitatively similar with high NO₂ amounts over major industrial regions and over regions affected by biomass burning, and low values over the oceans. In the retrievals there is an apparent increase over China between 1997 and 2000, which is not captured in the models. However, the regional analysis presented below indicates that the wintertime values retrieved over Eastern China show an anomalous enhancement during the year 2000.



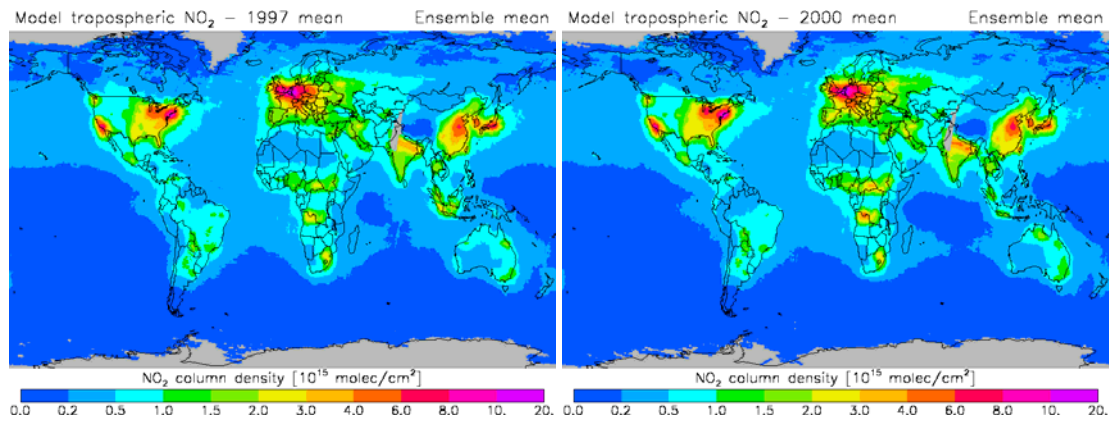


Figure A7: Retrieved and modelled annual mean tropospheric NO₂ column densities for 1997 and 2000. The annual means are constructed by equal weighting of all scenes retrieved during the year.

Figure A8 shows the corresponding maps for September 1997 compared with 1998. Enhanced levels from the 1997 El Niño wildfires in Indonesia are observed in both retrieval and models. A weaker interannual difference is observed over the biomass burning regions of South America and Southern Africa.

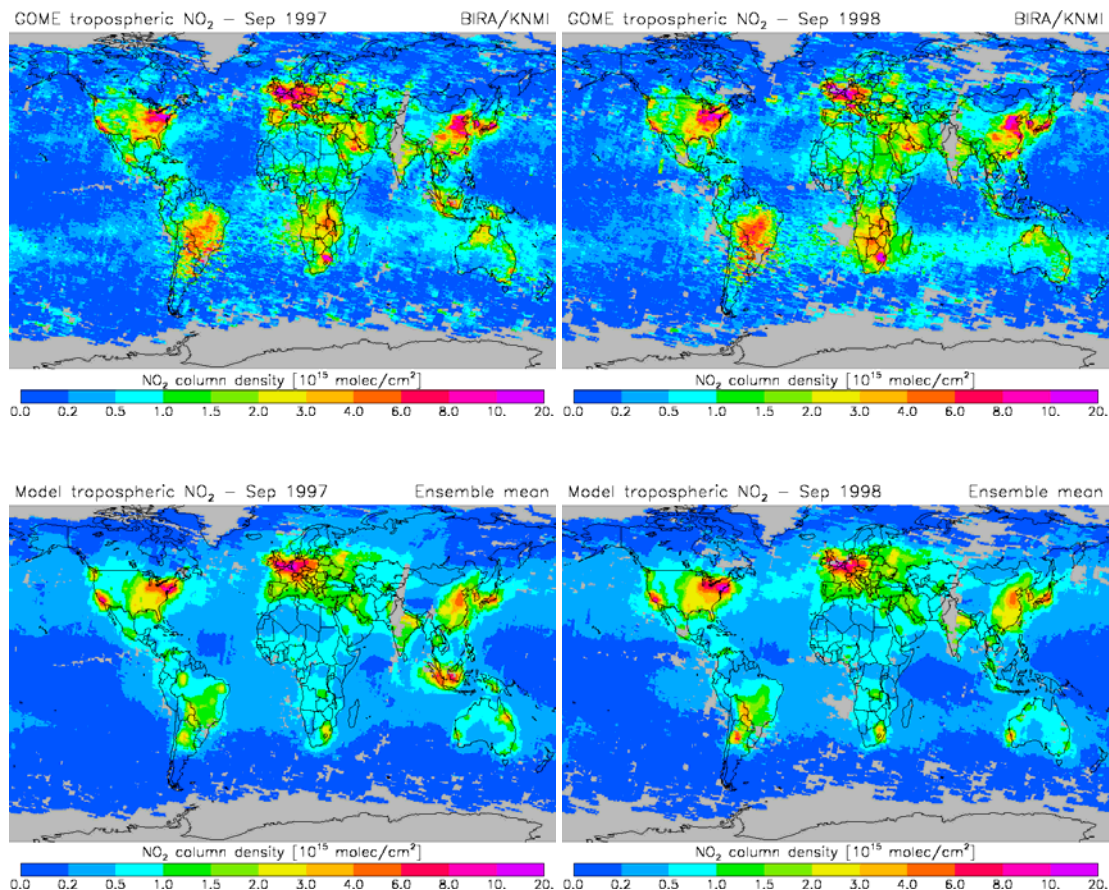


Figure A8: Retrieved and modelled tropospheric NO₂ column densities for September 1997 and 1998.

The seasonal and interannual variability has been analyzed for the regions shown in Figure A9. The resulting time series are presented in Figure A10. Over the Highveld region of South Africa the models give far too low NO₂ compared to the retrieval. This is most likely related to an underestimated of the emissions in this regions. Van Noije et al. (2006) came to the same conclusion based on a recent emission inventory from the International Institute for Applied Systems Analysis (IIASA). Over Eastern China the models generally underestimate the retrieval, especially in wintertime. Only ECHAM5-MOZ and p-TOMCAT come

reasonably close to the retrieved values for some years. For the interpretation of the differences it should be emphasized that there is also a large spread among the different retrieval products (van Noije et al., 2006). Over China the retrievals from BIRA/KNMI and from the University of Bremen give significantly higher wintertime values than the retrieval from Dalhousie University, at least for the year 2000 for which the different retrievals have been compared. Over the eastern United States ECHAM5-MOZ and p-TOMCAT are also in fair agreement with the observations. Over Europe, on the other hand, these two models seem to overestimate the retrieval during winter. Here UiO-CTM2 gives the best agreement, while LMDz-INCA and TM4 systematically underestimate the observations. The spread among the models over industrial regions is to large extent related to differences in the parameterization of the vertical mixing from the boundary layer into the free troposphere. Our results indicate that this mixing may be too fast in LMDz-INCA, TM4, and UiO-CTM2.

For the regions dominated by biomass burning the models behave quite differently. An additional cause for these differences is the fact that some models (ECHAM5-MOZ, TM4, and UiO-CTM2) apply a specified height distribution to the emissions from wildfires. This generally leads to a reduction of the tropospheric NO₂ columns. Because the vertical emission profile is not given for each emission location, in some instances the wildfire emissions are removed by applying the height distribution. This might explain why TM4 and ECHAM5-MOZ give much lower values during the El Niño wildfires in Indonesia than for instance LMDz-INCA and UiO-Oslo (which releases the emissions at the surface if the profile is not given). This doesn't seem to be the case over Africa, where TM4 and UiO-Oslo give similar values, somewhat higher than LMDz-INCA. In general the models underestimate the NO₂ columns from biomass burning. An exception to the rule is the Indonesian fire event of August–October 1997, where three models (LMDz-INCA, p-TOMCAT and UiO-Oslo) overestimate the retrieval, indicating that the emissions for this event are too high. The NO₂ columns are neither underestimated by p-TOMCAT during the dry seasons in Central Africa. Also ECHAM5-MOZ gives realistic values over South America during 1997 and 2000 and over Northern and Central Africa during 2000. However, for these regions the interannual variability simulated by ECHAM5-MOZ is much stronger than observed and the column amounts for the other years are strongly underestimated.

Regions of interest

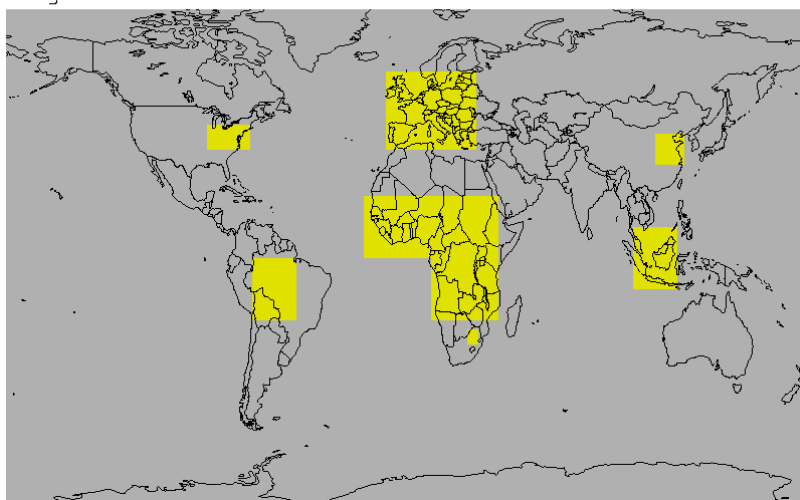
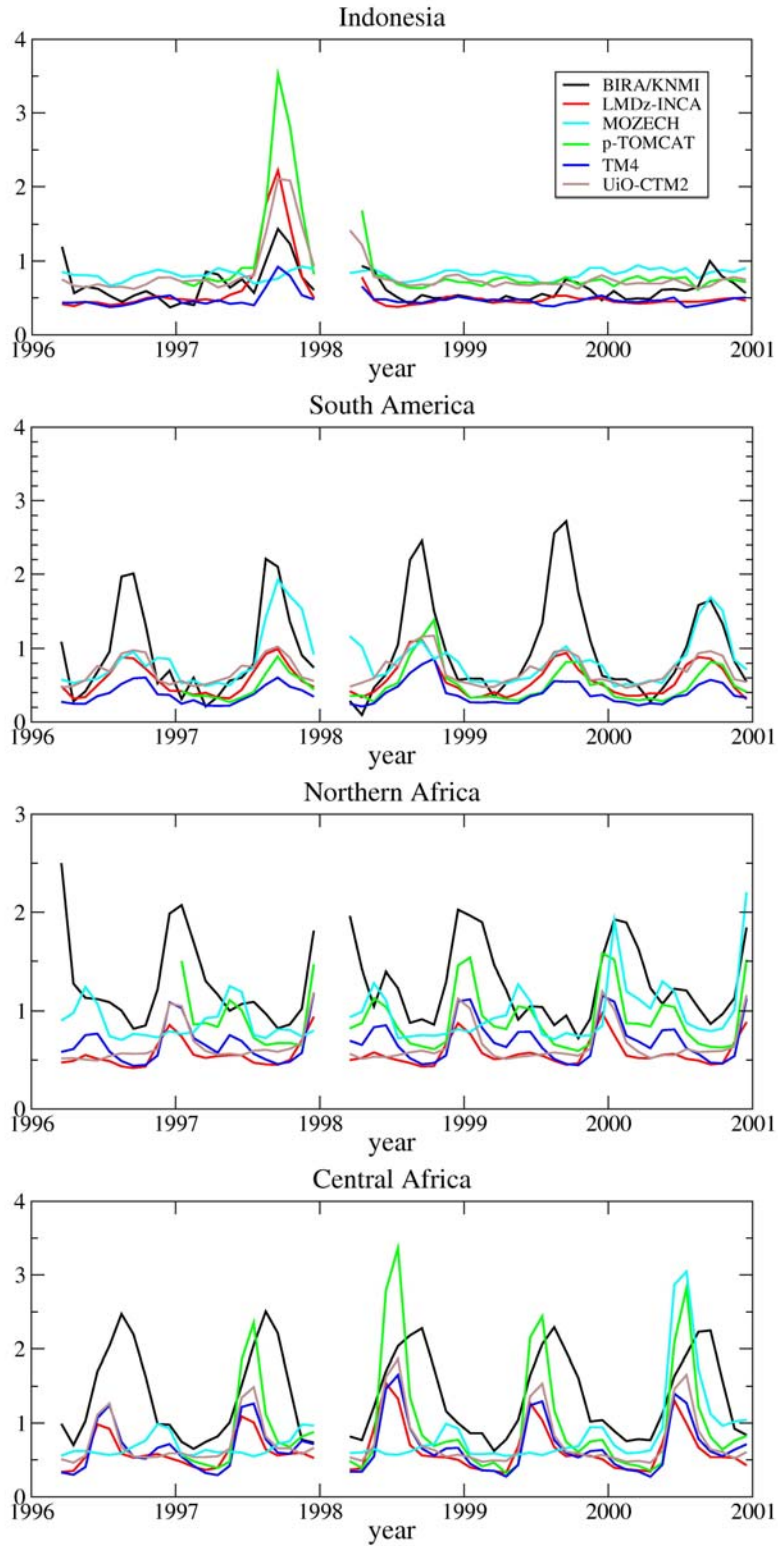


Figure A9: Definition of the regions used in this study.



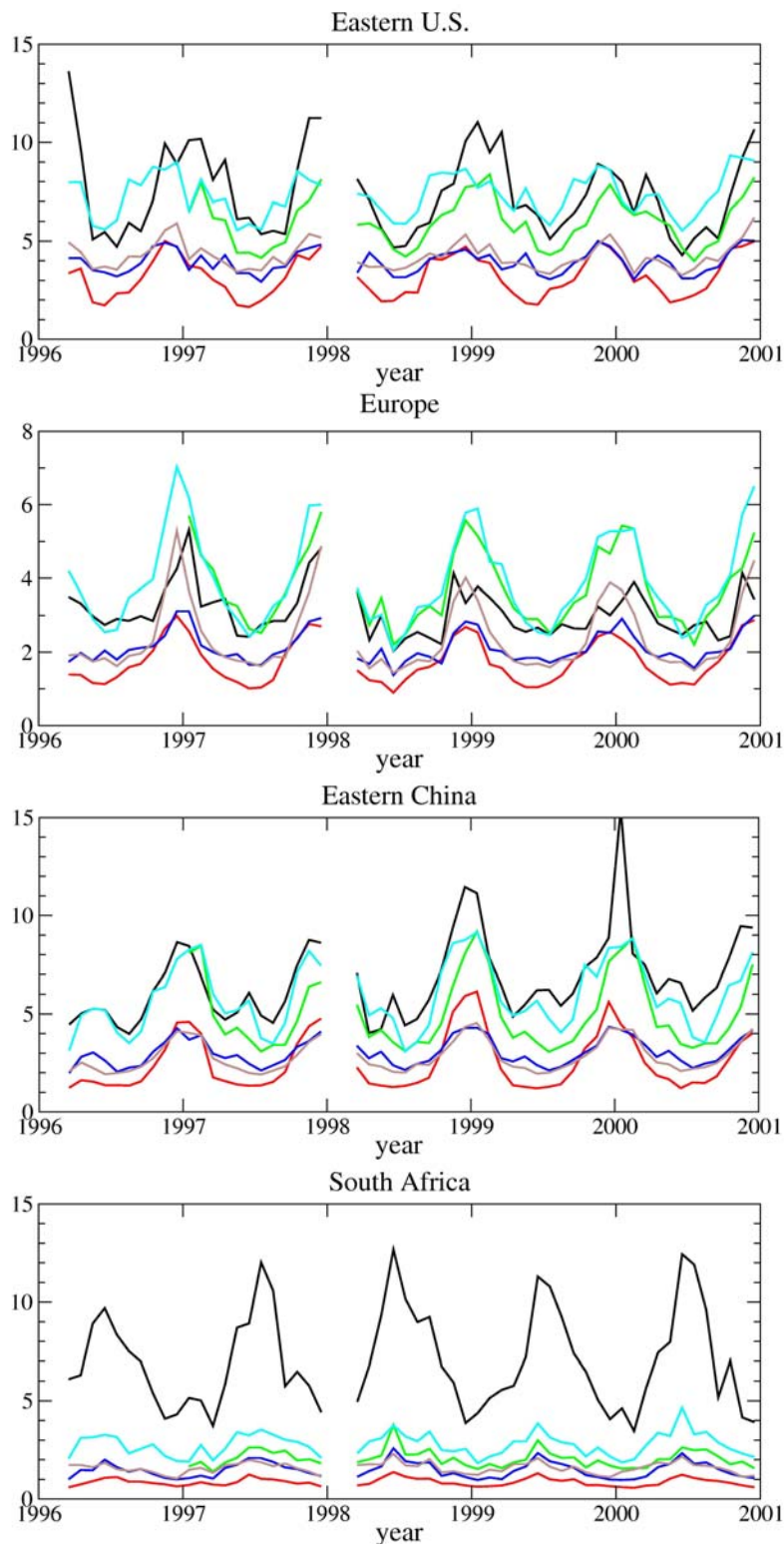


Figure A10: Retrieved and modelled monthly tropospheric NO₂ column densities (10^{15} molec/cm²) over the regions shown in Figure for the period March 1996–December 2000.

HCHO tropospheric columns

The team from the university of Bremen has performed comparisons of GOME satellite measurements with LMDz-INCA model outputs for formaldehyde

A comparison of HCHO columns obtained from the GOME instrument using the algorithms developed within this project is presented. This comparison comprises the years 1997 to 2001

and is the first study, where long-term global observations of HCHO are compared to model output. All GOME data presented here were gridded on the spatial resolution of the model ($3.75^\circ \times 2.5^\circ$). Further adaptations were not applied (e.g. using model data for a reference sector).

Figure A11 shows the mean formaldehyde columns from GOME but with a resolution adapted from the model. The corresponding model results for the same time period from 1997 to 2001 are illustrated in Figure A12. Obviously, the coarse grid of the model introduces some errors at mountain ranges: Although the outline of the Himalayas seems to be captured well, there are problems in the Andes which have only a very small extent in longitudinal direction.

In general, over land, the model retrieves larger columns of formaldehyde than those observed by GOME, particularly above South America. However, the pattern of the main source regions of formaldehyde in the tropics as well as the general latitudinal distribution are in good agreement.

In contrast, the formaldehyde over the oceans evident in the measurements is not reproduced by the model. The scatter plot of Figure A13 illustrates the correlation between the measurement and the model: While the correlation coefficient for measurement and model is high (overall 0.81) and also for land and ocean separately (0.89 and 0.83, respectively), the model systematically overestimates the formaldehyde over land and underestimates HCHO over most parts of the oceans.

As mentioned before, transport of isoprene and formaldehyde seems to be an unlikely explanation of the high columns observed over some oceanic regions due to their short lifetime of up to a few hours only. Transport over distances of about 50 to 150 km is feasible, but not long-range transport as would be necessary to explain the high values e.g. west of Africa. Two other explanations are possible: *In situ* production of HCHO from other more long-lived precursors or an oceanic source.

In particular, biomass burning plumes are known to contain high concentrations of other hydrocarbons, and little is known on the atmospheric chemistry and fate of these substances, which are not included in the INCA model run. Similarly, biogenic emissions from forests are not limited to isoprenes and monoterpenes, and potentially other molecules which are correlated to isoprene emissions could act as HCHO precursors. In addition, recycling mechanisms within an aging plume are conceivable, but at this point mere speculation.

As oceanic source, biogenic emissions are again a possibility, and algae are known to be a source of carbohydrates.

A very prominent difference between model and measurements are the lower HCHO columns measured over Australia and the southern part of South America. While the overall hemispherical gradient agrees between measurement and model, there is very little evidence for HCHO over Australia in the measurements in particular in the southern hemispheric winter with the exception of the far north, an area of intense burning activity. This is particularly surprising as eucalyptus is known to be an efficient isoprene emitter as discussed above.

In order to identify more distinctively the deviations between model and GOME observations several regions on the globe were picked to create time series of formaldehyde from 1997 to 2001 for both, GOME and model. This has been presented in Wittrock, 2006 and will be submitted to ACPD quite soon.

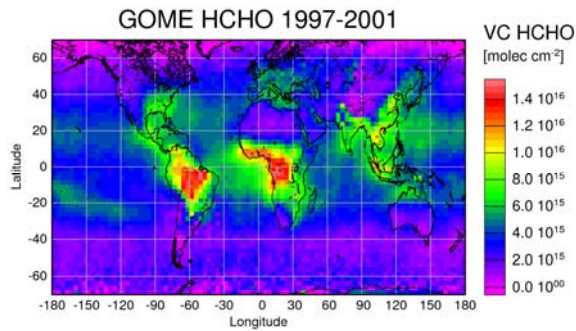


Figure A11: Mean values from GOME on model resolution ($2.5^\circ \times 3.75^\circ$) derived from monthly means from January 1997 to December 2001

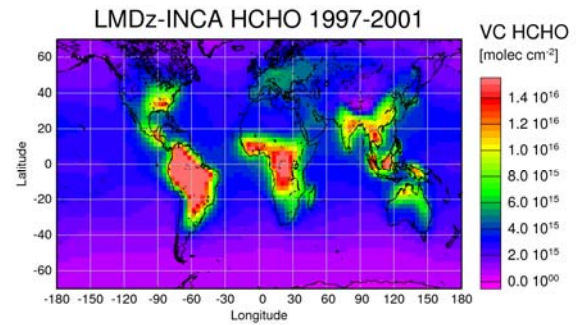


Figure A12: Mean values from model – here, the run taking into account the annual variability of biomass burning was utilised

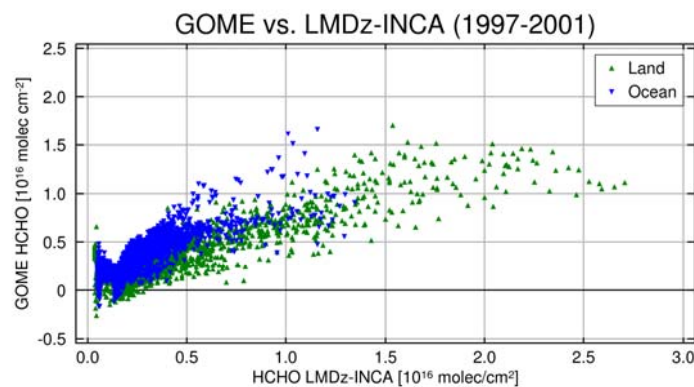


Figure A13: This scatter plot shows the correlation between GOME observation and the Model results. The correlation coefficient is 0.81 overall, while it is for the continents 0.89 and the oceans 0.83, respectively. The slope is 0.64 for the continents and 1.05 for the ocean.

A6. Budgets and Lifetimes

From the long-term simulations we have analyzed budgets and lifetimes of ozone and methane. In these calculations we adopted a chemical tropopause defined as the 150-ppbv level of ozone. For each month a mean tropopause was assumed based on the monthly mean ozone mixing ratio. Figure A14 shows the evolution of the corresponding tropospheric ozone burden for the different models.

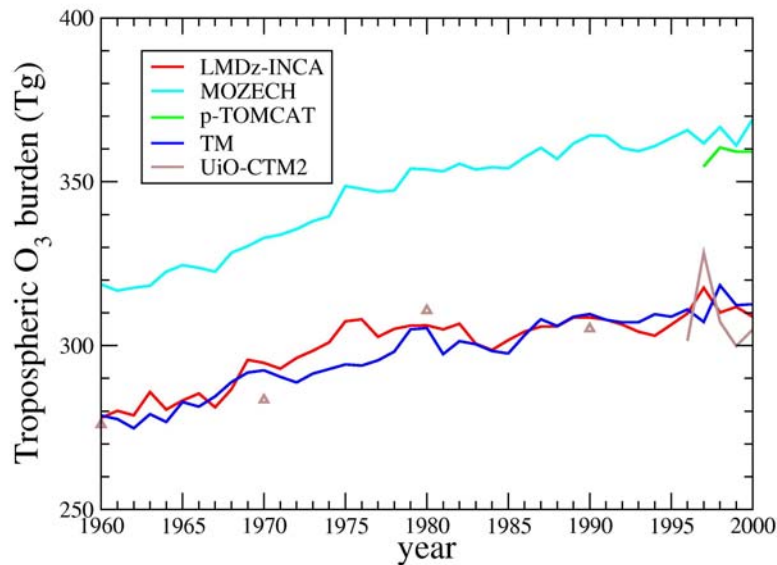


Figure A14: Evolution of the tropospheric ozone burden as calculated by the different models in the long-term simulations.

Different methods were used to calculate the stratosphere-troposphere exchange (STE) flux of ozone. For p-TOMCAT this flux was calculated directly from the net transport diagnostics in the model; for TM it is derived by closing the tropospheric ozone budget on a monthly basis taking into account the ozone burden changes; for LMDz-INCA, ECHAM5-MOZ and UiO-Oslo the STE flux is estimated by closing the budget on a yearly basis under the assumption that the annual burden changes are negligible. The resulting STE fluxes are shown in Figure A15. It should be realized that the differences introduced by the different methods for diagnosing the STE flux are relatively small and that the main differences between the models are related to differences in vertical transport and in the treatment of the stratospheric ozone boundary condition. The offline chemistry transport models p-TOMCAT, TM and UiO-CTM2, which use the ERA-40 wind fields directly in their advection schemes, are more sensitive to biases in the Brewer-Dobson circulation [van Noije et al., 2004, 2006] than LMDz-INCA and ECHAM5-MOZ, which use the ERA-40 wind (and temperature) fields only for nudging the internal dynamics.

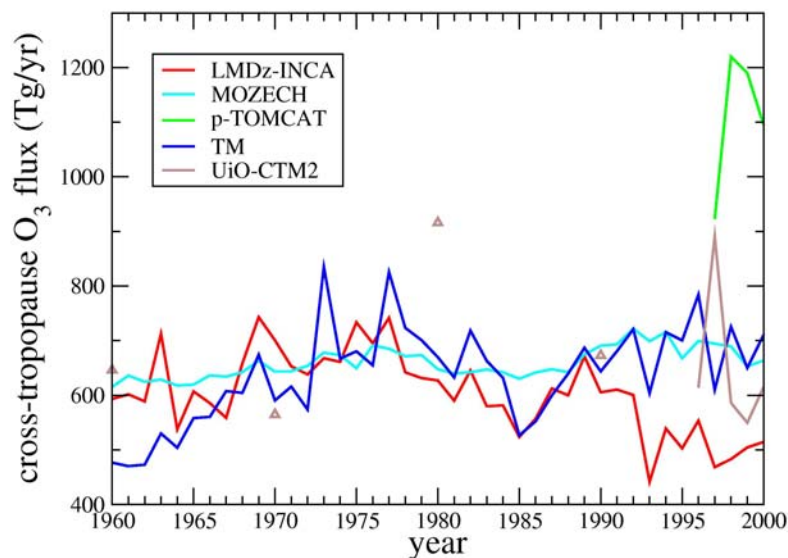


Figure A15: Time series of the ozone STE flux for the different models.

The ozone lifetime was calculated on an annual basis as the ratio of the tropospheric burden and the ozone loss due to chemical destruction and dry deposition. As shown in Figure A16, the models agree on the fact that the ozone lifetime has decreased over the period 1960-2000. The offline models generally show stronger interannual fluctuations than LMDz-INCA and ECHAM5-MOZ. Part of this variability may be related to spurious temporal inhomogeneities in the ERA-40 reanalysis, in particular in the vertical transport induced by the Brewer-Dobson circulation [van Noije et al., 2006] and in the water vapour abundance.

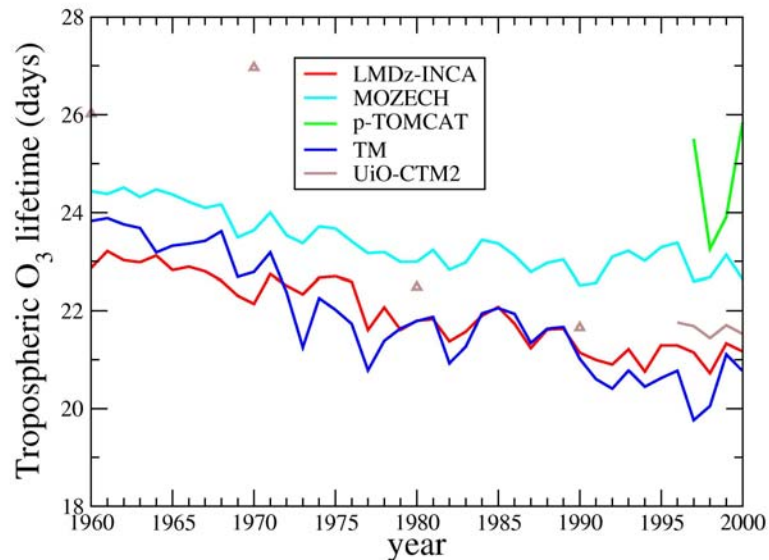


Figure A16. Evolution of the lifetime of tropospheric ozone as calculated by the different models in the long-term simulations.

Three models also provided the tropospheric OH concentration as a mass-weighted average over the tropospheric region. The continuous time series for the period 1960-2000 has so far only been provided by the TM model. This model shows a strong interannual variability and much weaker decadal or multi-decadal changes. Again the interannual variability simulated with an offline model such as TM may partly be due to spurious changes in the water vapour abundance in ERA-40. This issue is currently under further investigation by KNMI.

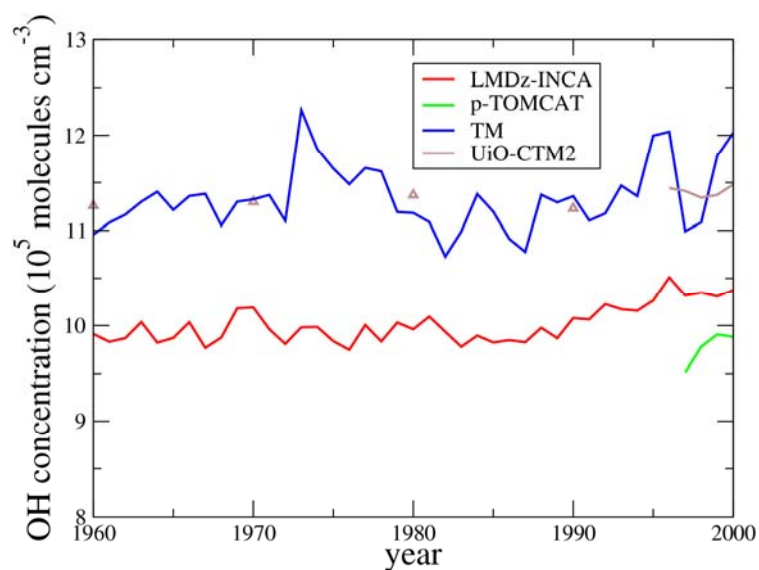


Figure A17. The mass-weighted tropospheric OH concentration calculated by the models LMDz-INCA, p-TOMCAT, TM and UiO-CTM2.

The corresponding methane chemical lifetime was calculated on an annual basis as the atmospheric methane burden divided by the chemical destruction due to reaction with OH in the troposphere. The result is shown in Figure A18.

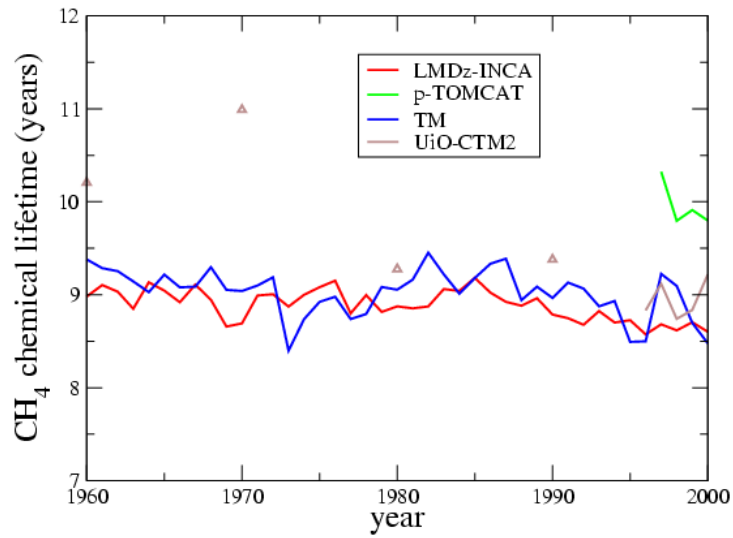


Figure A18. The chemical lifetime of methane for LMDz-INCA, p-TOMCAT, TM and UiO-CTM2.